Damping of Electromechanical Oscillations in Power Systems using Wide Area Control

Von der Fakultät Ingenieurwissenschaften der
Universität Duisburg-Essen
zur Erlangung des akademischen Grades eines

Doktor der Ingenieurwissenschaften (Dr. -Ing.)

genehmigte Dissertation

von

Ashfaque Ahmed Hashmani

aus
Matiari, Pakistan

Referent: Prof. Dr.-Ing. habil. István Erlich
Korreferent: Prof. Dr.-Ing. S. X. Ding
Tag der mündlichen Prüfung: 15.07.2010

Acknowledgment

I am grateful to my supervisor Prof. Dr.-Ing. habil. István Erlich for his support and invaluable suggestions throughout my Ph.D. study. He treats all his students equally. This gave me courage to work here, away from my homeland.

I would also like to thank all the members of the Institute, for their corporation.

Finally, I would like to thank the Deutscher Akademischer Austausch Dienst (DAAD) and Higher Education Commission (HEC), Pakistan for sponsoring my Ph.D. study at the Institute of Electrical Power Systems, University of Duisburg-Essen, Germany.

Last, but not least, my gratitude goes to my wife, mother and father. Without their encouragements and continuous support this Ph.D. study could not have come to a satisfactory conclusion.

Abstract

The design of a local H_∞-based power system stabilizer (PSS) controllers, which uses wide-area or global signals as additional measuring information from suitable remote network locations, where oscillations are well observable, is developed in this dissertation. The controllers, placed at suitably selected generators, provide control signals to the automatic voltage regulators (AVRs) to damp out inter-area oscillations through the machines' excitation systems.

A long time delay introduced by remote signal transmission and processing in wide area measurement system (WAMS), may be harmful to system stability and may degrade system robustness. Three methods for dealing with the effects of time delay are presented in this dissertation. First, time delay compensation method using lead/lag compensation along with gain scheduling for compensating effects of constant delay is presented. In the second method, Pade approximation approach is used to model time delay. The time delay model is then merged into delay-free power system model to obtain the delayed power system model. Delay compensation and Pade approximation methods deal with constant delays and are not robust regarding variable time delays. Time delay uncertainty is, therefore, taken into account using linear fractional transformation (LFT) method.

The design of local decentralized PSS controllers, using selected suitable remote signals as supplementary inputs, for a separate better damping of specific inter-area modes is also presented in this dissertation. The suitable remote signals used by local PSS controllers are selected from the whole system. Each local PSS controller is designed separately for each of the inter-area modes of interest. The PSS controller uses only those local and remote input signals in which the assigned single inter-area mode is most observable and is

located at a generator which is most effective in controlling that mode. The local PSS controller, designed for a particular single inter-area mode, also works mainly in a frequency band given by the natural frequency of the assigned mode. The locations of the local PSS controllers are obtained based on the amplitude gains of the frequency responses of the best-suited measurement to the inputs of all generators in the interconnected system. For the selection of suitable local and supplementary remote input signals, the features or measurements from the whole system are pre-selected first by engineering judgment and then using a clustering feature selection technique. Final selection of local and remote input signals is based on the degree of observability of the considered single mode in them.

Finally, this dissertation presents the extension of the scheme, described in the above paragraph, to realistic large-scale multi-owner power systems. The suitable remote signals used by local PSS controllers are selected from the whole system. The approach uses system identification technique for deriving an equivalent lower order state-space linear model suitable for control design. An equivalent lower order system of the actual system is determined from time-domain simulation data of the latter. The time-domain response is obtained by applying a test probing signal (input signal), used to perturb the actual system, to the AVR of the excitation system of the actual system. The measured time-domain response is then transformed into frequency domain. An identification algorithm is then applied to the frequency response data to obtain a linear dynamic reduced order model which accurately represents the system. Lower-order equivalent models have been used for the final selection of suitable local and remote input signals for the PSS controllers, selection of suitable locations of the PSS controllers and design of the PSS controllers.

Contents

Chapter 1

Introduction

1.1 Motivation

Recently, the number of bulk power exchanges over long distances has increased as a consequence of deregulation of the electrical energy markets worldwide and the extensions of large interconnected power systems. Moreover, the power transfers have also become somewhat unpredictable as dictated by market price fluctuations. The integration of offshore wind generation plants into the existing network is also expected to have a significant impact on the power flow of system as well as the dynamic behavior of the network. The expansion of the transmission grids, on the other hand, is very little due to environmental and cost restrictions. The result is that the available transmission and generation facilities are highly utilized with large amounts of power interchanges taking place through tie-lines and geographical regions. The tie lines operate near their maximum capacity, especially those connected to the heavy load areas. As a result, the system operation can find itself close to or outside the secure operating limits under severe contingencies. Stressed operating conditions can increase the possibility of inter-area oscillations between different control areas and even breakup of the whole system [1].

Reliability and good performance are necessary in power system operation to ensure a safe and continuous energy supply with quality. However, weakly damped low frequency electromechanical oscillations (also called inter-area oscillations), inherent to large interconnected power systems during transient conditions, are not only dangerous for the reliability and performance of such

systems but also for the quality of the supplied energy. The power flows over certain network branches resulting from generator oscillations can take peak values that are dangerous from the point of view of secure system operation and lead to limitations in network control.

Inter-area oscillations may cause, in certain cases, operational limitations (due to the restrictions in the power transfers across the transmission lines) and/or interruption in the energy supply (due to loss of synchronism among the system generators). Also, the system operation may become difficult in the presence of these oscillations.

Even today, when voltage problems are by far, more important for network operators than damping control, large disturbances tend to induce wide-area low frequency oscillations in major grids throughout the world: at 0.6 Hz in the Hydro-Quebec system [2], [3], 0.2 Hz in the western North-American interconnection [4], [5], 0.15-0.25 Hz in Brazil [6] and 0.19-0.36 Hz in the UCTE/CENTREL interconnection in Europe [7]. The recent 2003 blackout in eastern Canada and US was equally accompanied by severe 0.4 Hz oscillations in several post-contingency stages [8]. The two famous WECC cases in the summers of 1996 and 2000 were both associated with poorly damped inter-area oscillations under conditions of high power transfer on long paths [5].

With the heavier power transfers ahead, the damping of inter-area oscillations will decrease unless new lines are built or other heavy and expensive high-voltage equipment such as series-compensation is added to the grid's substations. The construction of new lines, however, is restricted by environmental and cost factors. Therefore, achievement of maximum available transfer capability as well as a high level of power quality and security has become a major concern. This concern requires the need for a better system control, leading to damping improvement.

Most of the existing approaches for damping measures are initiated merely from the point of view of single subsystems, which are independent in their operation. The damping measures are not coordinated with other regions. In contrast to these measures of a local nature, the system as a whole should be considered.

It is found that if remote signals from one or more distant locations of the power system are applied to the controller design, the system dynamic performance can be enhanced for the inter-area oscillations [9]. The basic mechanism of damping remains as the production of damping torque in synchronous generators through the use of appropriate field excitation.

New distributed instrumentation technology using accurate phasor measurement units (PMUs) has developed in recent years to become a powerful source of wide-area dynamic information. The recent advances in wide area measurement system (WAMS) technologies using PMUs can deliver synchronous phasors and control signals at a high speed [2], [5]. PMUs are deployed at strategic locations on the grid and obtain a coherent picture of the entire network in real time [10]. PMUs measure positive sequence voltages and currents at different locations of the grid. Global Positioning System (GPS) technology ensures proper time synchronization among several global signals [10]. The measured global signals are then transmitted via modern telecommunication equipment to the controllers.

The signals from PMUs (PMUs located remote to the controllers) are referred to as remote stabilizing signals. The remote signals are often referred to as global signals to illustrate the fact that they contain information about overall network dynamics as opposed to local control signals which lack adequate observability of some of the significant inter-area modes [2]. For local modes, the largest residue is associated with a local signal, e.g., generator rotor speed

signal for PSS. But for inter-area modes, the local signals may not be the ones with maximum observability. The signal with maximum observability for a particular mode can be from a remote location or combined information from several locations.

Aboul-Ela and others [11] have proposed a two-level design of PSS and SVC controller using global signals. In [2], a decentralized/hierarchical structure is proposed. Wide-area signals based PSS is used to provide additional damping.

Simulation studies have shown a high sensitivity of inter-area oscillations to generator voltage controller and hydro turbine governor settings [12]. Therefore, and because of the relatively low cost, measures to alleviate inter-area oscillations should be focused on power system controllers. The use of a supplementary control added to the Automatic Voltage Regulator (AVR) is a practical and economic way to supply additional damping to electromechanical oscillations. The first supplementary control for such task was proposed at the end of 1960's [13], and is usually known as Power System Stabilizer (PSS). PSS units have long been regarded as an effective way to enhance the damping of electromechanical oscillations in power system [13]. The PSS provides supplementary control action through the excitation system of generators and thus aids in damping the oscillations of synchronous machine rotors via modulation of the generator excitation. The supplemental damping is provided by an electric torque, applied to the rotor, which is in phase with the speed variation. The action of PSS, in this way, extends the angular stability limits of a power system.

For damping of local generator swings, PSSs have been established in the past [14], [1]. To enable damping of inter-area oscillations likewise with PSS, special control structures with additional signal inputs and well adapted pa-

rameter tunings are necessary. Since the first proposal of PSS at the end of 1960's, various control methods have been proposed for PSS design to improve overall system performance. Among the classical methods used are the phase-compensation method and the root-locus method. Among these, conventional PSS of the lead-lag compensation type [13], [15], [16] has been adopted by most utility companies because of its simple structure, flexibility and ease of implementation. Since power systems are highly nonlinear, conventional fixed-parameter PSSs cannot cope with changes in the operating conditions during normal operation and the system often tends to be unstable. Proper design of any control system that takes into account the continual changes in the structure of the network is, therefore, necessary to guarantee robustness over wide operating conditions in the system.

Robust control provides an effective approach to stabilize a power system over a wide range of operating conditions. Robust control approach deals with uncertainties introduced by variations of operating conditions and in this way, it guarantees system robustness to disturbances under various operating conditions. If the damping controller design is based on the robustness principle, minor errors in modeling will be alleviated and the closed-loop system will maintain satisfactory performance level.

Since last four decades, new PSS design methodologies based on robust control are proposed. Among many techniques available in the control literature, H_∞ has received considerable attention in the design of PSSs. The H_∞ controller is characterized by the feature that the order of the controller is always equal to the order of the generalized plant model, i.e., equal to the order of original plant plus the order of the weighting functions [17]. Higher order controllers may be too complex regarding practical implementation. Implementation of higher order controllers will lead to high cost, difficulty in com-

missioning, poor reliability and potential problems in maintenance. Higher order controllers when implemented in real time configurations can create undesirable effects such as time delays. Therefore, lower order controllers having simpler designs are sought. In this study, balanced residualization technique [18] is used to reduce the order of controllers.

This research mainly focuses on the problem of improving the performance of conventional PSS, for a better damping of inter-area oscillations, by using instantaneous measurements from remote locations of the grid as its supplementary inputs.

1.2 Objectives

The concept presented in this study consists of the assumption that the PSS inputs are formed by measured variables coming from the whole system, i.e., particularly also from remote generators [19]. In this way, each PSS receives more complete measuring information about the inter-area oscillations to be damped. It is possible to use any of the variables from the generators, e.g., generator rotor speeds or angles or variables not assigned to generators, e.g. selected tie-line power flows as remote input signals to the controller. In general, the PSS controllers to be designed in this study are each of the multi-input, single-output (MISO) type. From the view point of power system engineering, the proposed PSS controller concept can be interpreted as a system of second level PSSs using additionally global measuring information. In this way design of PSS controllers is carried out for attaining a damping behavior which is in favor to the entire power system and not only to certain subsystems.

Figure 1.1 describes the basic architecture used in this work. It consists of a set of *n* PSSs located at specially selected generators G_1,...,G_n together with *m* PMUs which are remote to the PSSs. The PSSs are acting on the reference inputs of the voltage regulators. In the context of wide-area stabilizing control of bulk power systems, the architecture shown in Figure 1.1 has higher operational flexibility and reliability, especially when some remote signals are lost. Under such circumstances, the controlled power system is still viable (although with a reduced performance level), owing to the fact that a fully autonomous and decentralized layer without any communication link is always present to maintain a standard performance level. As the global information is required only for some oscillatory modes, only a few PSS sites with the highest controllability of these modes need be involved in the supplementary global-signal-based actions.

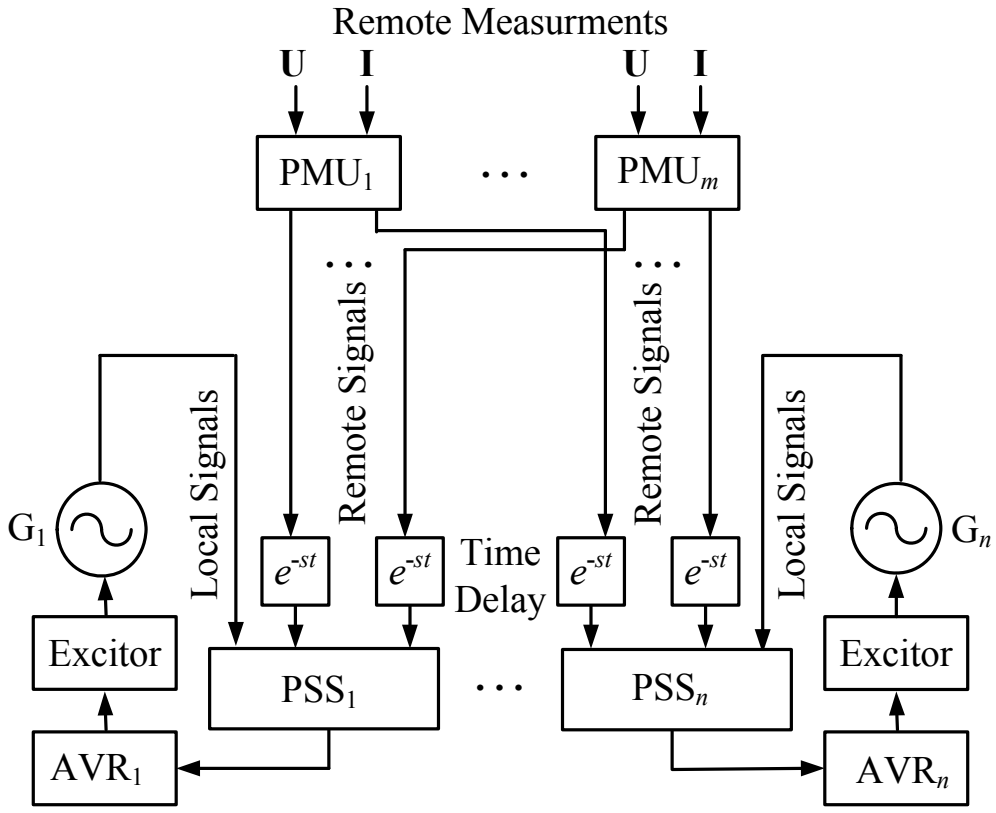

Figure 1.1 Multi-machine power system with PSS using WAMs

The main contribution of this thesis is to improve the performance of conventional PSS by using instantaneous measurements from remote locations of the grid. The research described herein will address the following objectives:

(i) The design of a local H_∞-based PSS controller which uses wide-area or global signals as additional measuring information from suitable remote network locations where the oscillations are well observable.

(ii) In the proposed approach, remote signals, which are used as supplementary inputs to the PSS controller, may arrive after a certain communication delay introduced by their transmission and processing in WAMS. Therefore, it is necessary to investigate the impact of time delay, in the remote input signal of the PSS controller, on the proposed approach. Also, the methods for dealing with the effects of time delay need to be investigated.

(iii) The design of local decentralized PSS controllers, using selected suitable remote signals as supplementary inputs, for a separate better damping of specific inter-area modes. Each local PSS controller is designed separately for each of the inter-area modes of interest. The PSS controller uses only those local and remote input signals in which the assigned single inter-area mode is most observable and is located at a generator which is most effective in controlling that mode. The local PSS controller, designed for a particular single inter-area mode, also works mainly in a frequency band given by the natural frequency of the assigned mode.

(iv) The design of controllers is usually carried out on small systems. The power system, in practical, is large in size. The large-scale power systems models, consisting of thousands of states, are impractical for

control design without extensive order reduction. The mode selective damping approach, described in (iii), is extended to realistic large-scale power systems by using system identification technique for deriving lower order state-space models suitable for control design. The complete, large-scale multi-input, multi-output (MIMO) power system is used directly as the basis for building the required lower-order state-space or transfer function equivalent model. The lower-order model is identified by probing the network in open loop with low-energy pulses or random signals. The identification technique is then applied to signal responses, generated by time-domain simulations of the large-scale model, to obtain reduced-order model. Lower-order equivalent models, thus obtained, are used for the final selection of suitable local and remote input signals for PSS controllers, for the selection of suitable locations of PSS controllers and for the design of PSS controllers.

1.3 Outline

The subsequent chapters of this dissertation are organized as follows:

Chapter 2 provides a general description of the power system stability phenomena including fundamental concepts, classification, and definitions of associated terms.

Chapter 3 presents the modeling and analysis of large power system dynamics.

Chapter 4 describes the development of a robust H_∞-based dynamic output feedback PSS controller using both local and remote signals. An ARE ap-

proach used for the design of full order controller is also described in this chapter. The full order controller is then reduced to a first order one using model reduction techniques. The effectiveness of the designed PSS controller is demonstrated through digital simulation studies on a test power system.

Chapter 5 presents the impact of time delay, introduced by remote signal transmission and processing in WAMS, on the performance of an H_∞-based PSS controller, designed in chapter 4. Three methods for dealing with the effects of time delay are presented. This chapter then describes the design of PSS controllers, using wide area or global signals as additional measuring information, considering time delay in the remote signals. Digital simulation studies on a two-machine power system are conducted to investigate effectiveness of the proposed controller during system disturbances.

Chapter 6 deals with the design of local decentralized robust H_∞-based PSS controllers using remote signals as supplementary inputs, for a better damping of inter-area oscillations, in a manner that each decentralized PSS controller is designed separately for each of the inter-area modes of interest. The effectiveness of the resulting PSS controllers is demonstrated through digital simulation studies conducted on a test three-machine, three-area power system.

Chapter 7 presents the extension of the approach described in Chapter 6 to large-scale power systems. Application of system identification technique for deriving lower-order state-space models from large-scale models is also presented in this chapter. The proposed approach is applied to a test sixteen-machine, three-area power system to show the effectiveness of the designed PSS controllers for a better damping of inter-area oscillations.

Chapter 8 summarizes the work presented in this dissertation. The main contributions of this dissertation are highlighted.

Chapter 2

Power System Stability

2.1 Introduction

Power system stability has been recognized as an important problem for secure system operation since the 1920s [20], [21]. Many major blackouts caused by power system instability have illustrated the importance of this phenomenon [22]. Historically, transient instability has been the dominant stability problem on most systems, and has been the focus of much of the industry's attention concerning system stability. As power systems have evolved through continuing growth in interconnections, use of new technologies and controls, and the increased operation in highly stressed conditions, different forms of system instability have emerged. For the satisfactory design and operation of power systems, a clear understanding of different types of instability and relationship between them is necessary. Therefore, there is a need for the proper definition and classification of power system stability.

2.2 Definition and Classification of Power System Stability

Power system stability is the ability of an electric power system, for a given initial operating condition, to either regain a new state of operating equilibrium or return to the original operating condition (if no topological changes occurred in the system) after being subjected to a physical disturbance, with

most system variables bounded so that practically the entire system remains intact [23].

The power system is a highly nonlinear system that operates in a constantly changing environment. The loads, generator outputs and main operating parameters change continually. Power systems are subjected to a wide range of small and large disturbances. *Small disturbances* in the form of incremental changes in the system load or generation occur continually. *Large disturbances* are the disturbances of a severe nature, such as a short circuit on a transmission line or loss of a large generator. A large disturbance may lead to structural changes due to the isolation of the faulted elements. When subjected to a disturbance, the stability of the system depends on the initial operating condition as well as the nature of the disturbance.

Power system stability can be classified into different categories and subcategories as shown in Figure 2.1 [23], [1]. The descriptions of the corresponding forms of stability phenomena are given in the following subsections.

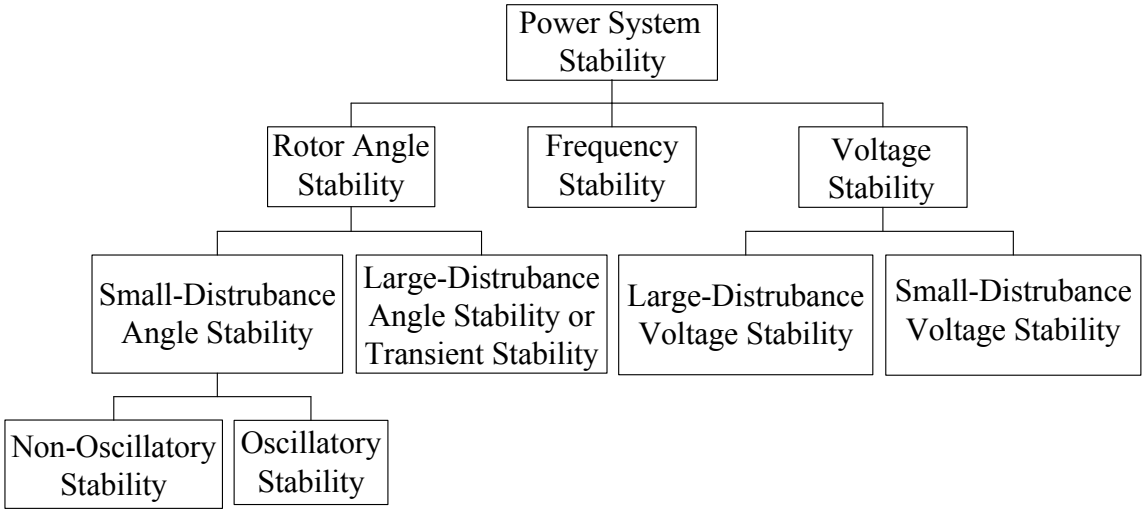

Figure 2.1 Classification of power system stability

2.2.1 Rotor Angle Stability

Rotor angle stability refers to the ability of synchronous machines of an interconnected power system to remain in synchronism after being subjected to a disturbance. It depends on the ability to maintain/restore equilibrium between electromagnetic torque (generator output) and mechanical torque (generator input) of each synchronous machine in the system. Instability that may result occurs in the form of increasing angular swings of some generators leading to their loss of synchronism with other generators.

The change in electromagnetic torque (ΔT_e) of a synchronous machine following a perturbation can be resolved into two components: (i) *Synchronizing torque component*, in phase with rotor angle deviation ($\Delta\delta$), and (ii) *Damping torque component*, in phase with the speed deviation ($\Delta\omega$). Mathematically, this can be expressed as follows:

$$\Delta T_e = T_s \Delta\delta + T_D \Delta\omega \tag{2.1}$$

where

$T_s\Delta\delta$ is the synchronizing torque component of torque change. T_s is the synchronizing torque coefficient.

$T_D\Delta\omega$ is the damping torque component of torque change. T_D is the damping torque coefficient.

System stability depends on the existence of both components of torque for each of the synchronous machines. Lack of sufficient synchronizing torque causes an increase in rotor angle through a nonoscillatory or aperiodic mode. This form of instability is known as *aperiodic* or *nonoscillatory instability*. Lack of damping torque causes rotor oscillations of increasing amplitude. This form of instability is known as *oscillatory instability*.

Rotor angle stability can be classified into the following two subcategories:

- Small-disturbance (or small-signal) rotor angle stability
- Large-disturbance rotor angle stability or transient stability

2.2.1.1 Small-Disturbance Rotor Angle Stability

Small-disturbance (or small-signal) rotor angle stability is concerned with the ability of the power system to maintain synchronism under small disturbances. The disturbances are considered to be sufficiently small that linearization of system equations is permissible for purposes of analysis [1], [24], [25] and the use of powerful analytical tools of linear systems is allowed to aid in the analysis of stability characteristics and in the design of corrective controls [24]. The results of the system response to small disturbances are usually given in terms of eigenvalues and eigenvectors.

In today's power systems, small-disturbance rotor angle stability problem is usually associated with insufficient damping of oscillations [23]. Small-disturbance rotor angle stability problems may be either local or global in nature. The descriptions of these problems are given below:

- Local problems involve a small part of the power system, and are usually associated with rotor angle oscillations (swinging) of a single power plant (units at a generating station) against the rest of the power system. Such oscillations are called *local plant mode oscillations*. The term local is used because the oscillations are localized at one station or a small part of the power system. Stability (damping) of these oscillations depends on the strength of the transmission system as seen by the power plant, generator excitation control systems and plant output [1]. When a generator is tied to a power system via a long radial line, it is susceptible to local mode oscillations [26].

- Global problems are caused by interactions among large groups of generators. They are associated with rotor angle oscillations (swinging) of a group of generators in one area of an interconnected power system against a group of generators in another area. Such oscillations are called *inter-area mode oscillations*.

The time frame of interest in small-disturbance stability studies is on the order of 10 to 20 seconds following a disturbance [23].

2.2.1.2 Large-Disturbance Rotor Angle Stability or Transient Stability

Large-disturbance rotor angle stability or transient stability is concerned with the ability of the power system to maintain synchronism when subjected to a severe disturbance, such as a short circuit on a transmission line. The resulting system response involves large excursions of generator rotor angles and is influenced by the nonlinear power-angle relationship.

Transient stability depends on both the initial operating state of the system and the severity of the disturbance. Usually, the system is altered so that the post-disturbance steady-state operation differs from that prior to the disturbance. Instability is usually in the form of aperiodic angular separation due to insufficient synchronizing torque, manifesting as *first swing instability* [23]. However, in large power systems, transient instability may not always occur as first swing instability associated with a single mode; it could be a result of superposition of a slow inter-area swing mode and a local-plant swing mode causing a large excursion of rotor angle beyond the first swing [1].

The time frame of interest in transient stability studies is usually 3 to 5 seconds following the disturbance. It may extend to 10–20 seconds for very large systems with dominant inter-area swings [23].

Small-disturbance rotor angle stability as well as transient stability is categorized as short term phenomena.

2.2.2 Voltage Stability

Voltage stability refers to the ability of a power system to maintain steady voltages at all buses in the system after being subjected to a disturbance from a given initial operating condition. It depends on the ability to maintain/restore equilibrium between load demand and load supply from the power system. Instability that may result occurs in the form of a progressive fall or rise of voltages of some buses. However, the most common form of voltage instability is the progressive drop in bus voltages. A possible outcome of voltage instability is loss of load in an area, or tripping of transmission lines and other elements by their protective systems leading to cascading outages. Loss of synchronism of some generators may result from these outages or from operating conditions that violate field current limit [27].

As in the case of rotor angle stability, voltage stability can also be classified into the following subcategories:

- *Small-disturbance voltage stability* refers to the system's ability to maintain steady voltages when subjected to small perturbations such as incremental changes in system load.
- *Large-disturbance voltage stability* refers to the system's ability to maintain steady voltages following large disturbances such as system faults, loss of generation, or circuit contingencies. The study period of interest may extend from a few seconds to tens of minutes.

As the time frame of interest for voltage stability problems may vary from a few seconds to tens of minutes, therefore, voltage stability may be either a short-term or a long-term phenomenon.

2.2.3 Frequency Stability

Frequency stability refers to the ability of a power system to maintain steady frequency within a nominal range following a severe system upset resulting in a significant imbalance between generation and load [23]. It depends on the ability to maintain/restore equilibrium between system generation and load, with minimum unintentional loss of load. Instability that may result occurs in the form of sustained frequency swings leading to tripping of generating units and/or loads.

Generally, frequency stability problems are associated with inadequacies in equipment responses, poor coordination of control and protection equipment, or insufficient generation reserve [28]-[31].

During frequency excursions, the characteristic times of the processes and devices that are activated will range from fraction of seconds, corresponding to the response of devices such as under-frequency load shedding and generator controls and protections, to several minutes, corresponding to the response of devices such as prime mover energy supply systems and load voltage regulators. Therefore, frequency stability may be a *short-term* phenomenon or a *long-term* phenomenon.

2.3 Small Signal Stability Assessment of Power Systems using Modal Analysis

A power system typically comprises a large number of components. Besides, the behavior of most of these components is described through differential-algebraic equations. Hence, in general, the dynamic behavior of a power system can be described by a set of *n* first order nonlinear ordinary differential equations, denominated as state equations, together with a set of algebraic equations, developed on the basis of the system model. Using vector-matrix notation, the set of differential-algebraic equations can be expressed as follows [1]:

$$\dot{\mathbf{x}} = \mathbf{f}(\mathbf{x}, \mathbf{u}) \tag{2.2}$$

$$\mathbf{y} = \mathbf{g}(\mathbf{x}, \mathbf{u}) \tag{2.3}$$

where

$\mathbf{x} = [x_1 \quad x_2 \quad \cdots \quad x_n]^{\mathrm{T}}$ is the vector of state variables, referred to as state vector,

$\mathbf{u} = [u_1 \quad u_2 \quad \cdots \quad u_r]^{\mathrm{T}}$ is the vector of input signals to the system, referred to as input vector,

$\mathbf{y} = [y_1 \quad y_2 \quad \cdots \quad y_m]^{\mathrm{T}}$ is the vector of system output variables, referred to as output vector,

$\mathbf{f} = [f_1 \quad f_2 \quad \cdots \quad f_n]^{\mathrm{T}}$ is the vector of nonlinear functions defining state variables in terms of state and input variables,

$\mathbf{g} = [g_1 \quad g_2 \quad \cdots \quad g_m]^{\mathrm{T}}$ is the vector of nonlinear functions defining state variables in terms of state and input variables,

where n is the order of the system, r is the number of inputs and m is the number of outputs. The input signals to the system (u_i) are the external signals that influence the performance of the system.

From the classification of power system stability, described in Section 2.2, the small signal stability is focused on small disturbances. Thus, to analyze the small signal stability of the system mathematically, the disturbances can be considered to be small in magnitude in order to linearize the equations that describe the dynamics of the system.

For small perturbation of the system from its initial operating point (the point around which small signal performance is to be investigated), (2.2) and (2.3) can be expressed in linearized form as follows [1]:

$$\Delta\dot{\mathbf{x}}(t) = \mathbf{A}\Delta\mathbf{x}(t) + \mathbf{B}\Delta\mathbf{u}(t) \tag{2.4}$$

$$\Delta\mathbf{y}(t) = \mathbf{C}\Delta\mathbf{x}(t) + \mathbf{D}\Delta\mathbf{u}(t) \tag{2.5}$$

where

Δ is the prefix which denotes a small deviation,

A is the state or plant matrix of size $n \times n$,

B is the control or input matrix of size $n \times r$,

C is the output matrix of size $m \times n$,

D is the (feed-forward) matrix which defines the proportion of input which appears directly in the output, size $m \times r$

The eigenvalues of the state matrix **A** determine the time domain response of the system to small perturbations and therefore provide valuable information regarding the stability characteristics of the system. The stability of the system is determined by the eigenvalues as follows:

(i) A *real eigenvalue* corresponds to a non-oscillatory mode. A negative real eigenvalue represents a decaying mode. A positive real eigenvalue represents aperiodic instability.

(ii) *Complex eigenvalues* occur in conjugate pairs, and each pair corresponds to an oscillatory mode. If all eigenvalues have a negative real part then all oscillatory modes decay with time and the system is said to be stable [24]. The critical eigenvalues are characterized by being complex (also denominated swing modes or oscillatory modes) and located near the imaginary axis of the complex plane [32]. For a complex pair of eigenvalues $\lambda = \sigma \pm j\omega$, the real component of the eigenvalues (σ) gives the damping, and the imaginary component (ω) gives the frequency of oscillation. A negative value of σ represents a damped oscillation whereas a positive value of σ represents oscillation of increasing amplitude. The frequency of oscillation in Hz is given by $f = \omega/2\pi$. The damping ratio (ζ) is given by:

$$\zeta = \frac{-\sigma}{\sqrt{\sigma^2 + \omega^2}} \tag{2.6}$$

For any eigenvalue λ, there are the corresponding vectors: right eigenvector, left eigenvector and the participation vector. The associated right eigenvector gives the *mode shape*, i.e., the relative activity of the state variables when a particular mode is excited [1]. The magnitudes of the elements of right eigenvector give the extents of the activities of the n state variables in the i^{th}-mode, and the angles of the elements give phase displacements of the state variables with regard to the mode [1]. The associated left eigenvector is referring to the initial conditions, since it has a direct effect on the amplitude of a mode excited by a specific input [24].

The participation vector combines the right and left eigenvectors. The element p_{ki} of the participation vector termed as the *participation factor* [33], is a measure of the relative participation of the k^{th} state variable in the i^{th}-mode, and vice versa. The participation factor p_{ki} measure the sensitivity of the i^{th}-eigenvalue to a change in the k^{th} diagonal element of the state matrix (a_{kk}), mathematically,

$$pf_{ki} = \partial\lambda_i / \partial a_{kk} \tag{2.7}$$

2.4 Summary

This chapter is focused on the issue of stability definition and classification in power systems from a fundamental as well as practical point of view. A precise definition of power system stability that is taking into consideration all forms is provided. The main focus of the chapter is to provide a systematic classification of power system stability, and the identification of different categories of stability behaviors that are important in power system stability analysis. The chapter also provides description of small signal stability assessment using modal analysis.

Chapter 3

Power System Modelling

3.1 Introduction

This chapter briefly reviews the issue of power system modeling that is useful for analysis and control design in later chapters. Power System Dynamics (PSD) software [34], used in this dissertation for simulation studies, is discussed in terms of sets of structural and functional subdivisions. These subdivisions precisely reveal the interrelations/interactions among the individual components as well as the computational structure for describing real large power systems. Further, the linearized dynamic model is decomposed as interconnected subsystems that could be used to design decentralized controllers for power system. Moreover, the problem of model reduction for large power systems is discussed by deriving a relatively low-order model which is necessary for applying controller design techniques.

3.2 Nonlinear Modelling and Simulation of Power Systems

Modern power systems are characterized by complex dynamic behaviors owing to their size and complexity. Power systems, even in their simplest form, exhibit nonlinear and time-varying behaviors. Moreover, there are numerous equipment found in today's power systems, namely: (i) synchronous generators; (ii) loads; (iii) reactive-power control devices like capacitor banks and shunt reactors; (iv) power electronically switched devices such as static Var

Compensators (SVCs), and currently developed flexible AC transmission systems (FACTS) devices; (v) series capacitors and other equipments. Precise modeling of these equipments plays important role for analysis and simulation studies of the whole system.

In order to obtain an appropriate model of power systems, each equipment or component of the power system should be described by appropriate algebraic and/or differential equations. Dynamic model of power systems is then obtained by combining the dynamic models of these individual components together with the associated algebraic constraints. In general, the dynamic model of power systems can be formulated by the nonlinear differential-algebraic equations given as follows:

$$\dot{\mathbf{x}}(t) = \mathbf{f}(\mathbf{x}, \mathbf{y}, \mathbf{u}, \mathbf{p}) \tag{3.1}$$

$$0 = \mathbf{g}(\mathbf{x}, \mathbf{y}, \mathbf{u}, \mathbf{p}) \tag{3.2}$$

where $\mathbf{x}(t)$, $\mathbf{y}(t)$ and $\mathbf{u}(t)$ are the state, output and input variables of the power system, respectively. $\mathbf{p}(t)$ represent parameters and/or effects of control at particular time in the system.

Modeling of power system is further discussed based on the PSD software that is used in this dissertation for power flow analysis, linearization of nonlinear differential-algebraic equations, calculation of eigenvalues and eigenvectors and nonlinear time-domain simulation of power systems. Figure 3.1 shows the main structural components and their interrelations that are functionally implemented in the PSD software environment. A brief explanation of the PSD is given as follows:

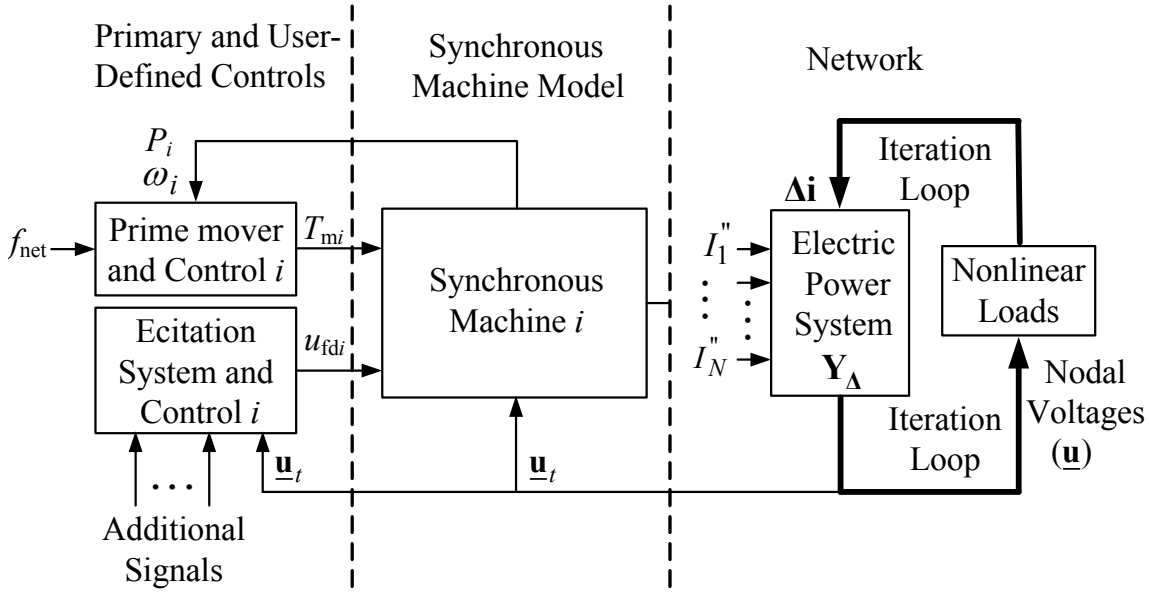

Figure 3.1 Integration of synchronous machine model into complete power system model

- The block in the middle of Figure 3.1 is used to describe the dynamics of synchronous machines. Synchronous machines have major influence on the overall dynamic performance of power systems due to their characteristics. A reduced 5th-order model, where stator transients (i.e., stator flux linkage derivatives $d\psi_d/dt$, $d\psi_q/dt$) are neglected [35], is used for all synchronous machines in this study. The model consists of a set of differential and a set of algebraic equations. Input variables to the models are the complex terminal voltage $\underline{u}_{ti}$, the field excitation voltage u_{fdi}, and the mechanical turbine torque T_{mi}. Moreover, the injected currents into the network, which depend on the corresponding state variables of the synchronous machines, are used as input to the algebraic network equations.

- The nodal voltages shown at the bottom of the right-side are computed by solving the algebraic network equations of the nodal admittance matrix. Nonlinear voltage dependent loads are incorporated in

the system where the solutions for updating injection currents are carried out iteratively.

- The blocks in the left of Figure 3.1 represent the voltage and governor controllers. The governor control block contains, in addition to the direct primary control of turbine torque (i.e., the governor mechanism), the mechanical dynamics of the equipment, such as the turbine or boiler that tie to the system dynamically through the governor control valve. Similarly, the voltage control block typically includes voltage regulators and exciters. Moreover, user-defined controller structures can be easily incorporated either through voltage or governor controller sides and such options give greater flexibility in analysis and simulation studies.

3.3 Modelling of Power Systems for Small-Signal Analysis

The starting model for small-signal analysis in power system is derived by linearizing the general nonlinear dynamic model of (3.1) and (3.2) around an operating (or equilibrium) point ($\mathbf{x}_0$, $\mathbf{y}_0$, $\mathbf{u}_0$, $\mathbf{p}_0$) and is given as follows:

$$\Delta\dot{\mathbf{x}}(t) = \mathbf{A}\Delta\mathbf{x}(t) + \mathbf{B}_1\Delta\mathbf{u}(t) + \mathbf{B}_2\Delta\mathbf{p}(t) \tag{3.3}$$

where $\Delta\mathbf{x}(t) = \mathbf{x}(t) - \mathbf{x}_0$, $\Delta\mathbf{u}(t) = \mathbf{u}(t) - \mathbf{u}_0$, and $\Delta\mathbf{p}(t) = \mathbf{p}(t) - \mathbf{p}_0$. $\mathbf{x}(t)$, $\mathbf{y}(t)$, $\mathbf{u}(t)$ and $\mathbf{p}(t)$ are the actual values of states, outputs, inputs and parameters respectively. Note that in considering the linear systems of the form (3.3), the symbol "Δ" will be omitted in the remaining part of this thesis.

Depending on how detailed the model in (3.1) and (3.2) is used, the resulting linearized model (3.3) may or may not be applicable to study particular

physical phenomena in power system. Any disturbance, acting on the system, affects all system states, and their exact changes are complex and can only be analyzed by using the full-order model. Despite this fact, in order to avoid unnecessary complexity, much effort has been devoted to the reduction of power system dynamic models. Moreover, model-reduction techniques have also another importance in power systems. In a large power system consisting of weakly connected subsystems, it is possible to derive a relatively low-order model relevant for understanding the interactions among the subsystems (inter-area dynamics), as well as detailed models relevant for understanding the dynamics inside each subsystem (intra-area dynamics) [34], [36]-[38]. The small-signal stability analysis of these developed models is then carried out. Basic analysis uses the elementary result that, given $\mathbf{u}(t) = 0$ and $\mathbf{p}(t) = 0$, the system of time-invariant linear differential equations (3.3) will have a stable response to initial conditions $\mathbf{x}(0) = 0$ when all eigenvalues of system matrix $\mathbf{A}$ are in the left-half plane. Moreover, the robustness of the system dynamics can be analyzed using the more involved sensitivity techniques with respect to parameter uncertainties [34], [36].

3.4 Summary

In this chapter, modeling and analysis of large power system dynamics are discussed. The chapter briefly discussed real large power systems representation with respect to the PSD software where the latter is used for analysis and simulation studies in this dissertation. Moreover, the model for the small-signal analysis in power system is also presented in this chapter.

Chapter 4

Robust PSS Controller Design using Supplementary Remote Signals

4.1 Introduction

This chapter presents the design of a local H_∞-based PSS controller which uses wide-area or global signals as additional measuring information from suitable remote network locations where the oscillations are well observable. The controller, placed at suitably selected generators, provide control signals to the AVRs to damp out inter-area oscillations through the machines' excitation systems. Electrical power outputs of generators have been used as input signals to the controller. To provide robust behavior, H_∞ control theory together with an algebraic Riccati equation (ARE) approach has been applied to design the proposed controller. Digital simulation studies are conducted on a test power system to investigate the effectiveness of the proposed controllers during system disturbances.

4.2 Robust H_∞ Output Feedback Controller Design for Power Systems

4.2.1 Problem Formulation

The general structure of the i^{th}-generator together with the PSS block in a multi-machine power system is shown in Figure 4.1. Local and remote input signals of washout filters are assumed to be electrical power outputs of generators. The outputs of washout filters are the inputs of the i^{th}-controller. The

washout filter prevents the controller from acting on the system during steady state.

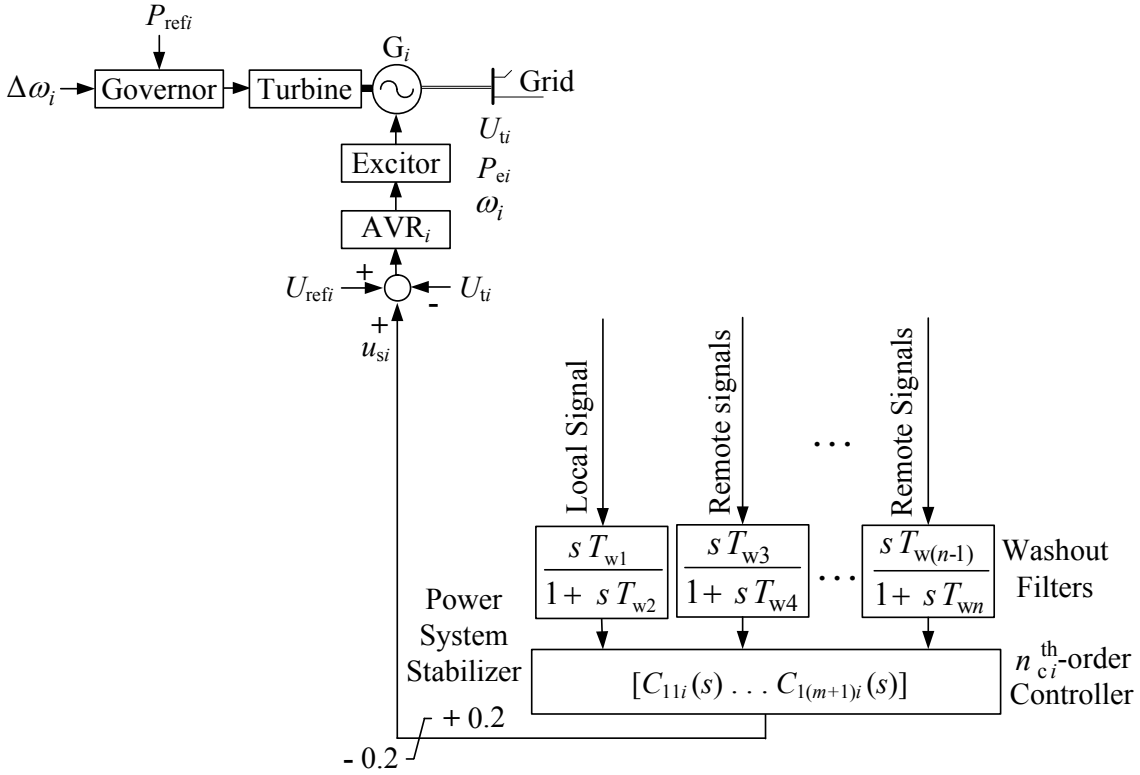

Figure 4.1 General structure of the i^{th}-generator together with the PSS in a multi-machine power system

After augmenting the washout stage in the system, the i^{th}-subsystem of the linear, time-invariant, continuous-time composite system which is composed of N subsystems, within the framework of H_∞ design, is described by the following state-space model [39], [40]:

$$\dot{\mathbf{x}}_i(t) = \mathbf{A}_{ii}\mathbf{x}_i(t) + \sum_{j=1, j\neq i}^{N} \mathbf{A}_{ij}\mathbf{x}_j(t) + \mathbf{B}_{1i}\mathbf{w}_i(t) + \mathbf{B}_{2i}\mathbf{u}_i(t) \tag{4.1}$$

$$\mathbf{z}_i(t) = \mathbf{C}_{1i}\mathbf{x}_i(t) + \mathbf{D}_{11i}\mathbf{w}_i(t) + \mathbf{D}_{12i}\mathbf{u}_i(t) \tag{4.2}$$

$$\mathbf{y}_i(t) = \mathbf{C}_{2i}\mathbf{x}_i(t) + \mathbf{D}_{21i}\mathbf{w}_i(t) + \mathbf{D}_{22i}\mathbf{u}_i(t)\ ,\ i = 1,\ldots, N \tag{4.3}$$

where

$\mathbf{x}_i(t) \in R^{n_i}$ is the state vector,

$\mathbf{u}_i(t) \in R^{m_i}$ is the vector of control input signals,

$\mathbf{y}_i(t) \in R^{p_i}$ is the vector of measured output signals available to the controller,

$\mathbf{z}_i(t) \in R^{q_i}$ is the vector of exogenous regulated output signals including all regulated or controlled signals and tracking errors,

$\mathbf{w}_i(t) \in R^{r_i}$ is the vector of exogenous input signals including noises, disturbances and reference or command signals for the i^{th}-subsystem, and

$\mathbf{A}_{ii}$, $\mathbf{A}_{ij}$, $\mathbf{B}_{1i}$, $\mathbf{B}_{2i}$, $\mathbf{C}_{1i}$, $\mathbf{C}_{2i}$, $\mathbf{D}_{11i}$, $\mathbf{D}_{12i}$, $\mathbf{D}_{21i}$ and $\mathbf{D}_{22i}$ are all constant matrices with appropriate dimensions.

Moreover, it is assumed that there is no unstable fixed mode [41] with respect to $\mathbf{C}_2 = \text{diag}\{\mathbf{C}_{21}, \mathbf{C}_{22}, \cdots, \mathbf{C}_{2N}\}$, $[\mathbf{A}_{ij}]_{N\times N}$ and $\mathbf{B}_2 = \text{diag}\{\mathbf{B}_{21}, \mathbf{B}_{22}, \cdots, \mathbf{B}_{2N}\}$.

The complete system can be equivalently described by the following composite equations:

$$\dot{\mathbf{x}}(t) = \mathbf{A}\mathbf{x}(t) + \mathbf{B}_1\mathbf{w}(t) + \mathbf{B}_2\mathbf{u}(t) \tag{4.4}$$

$$\mathbf{z}(t) = \mathbf{C}_1\mathbf{x}(t) + \mathbf{D}_{11}\mathbf{w}(t) + \mathbf{D}_{12}\mathbf{u}(t) \tag{4.5}$$

$$\mathbf{y}(t) = \mathbf{C}_2\mathbf{x}(t) + \mathbf{D}_{21}\mathbf{w}(t) + \mathbf{D}_{22}\mathbf{u}(t) \tag{4.6}$$

where,

$$\mathbf{x}(t) = \begin{bmatrix}\mathbf{x}_1^{\mathrm{T}}(t) & \mathbf{x}_2^{\mathrm{T}}(t) & \cdots & \mathbf{x}_N^{\mathrm{T}}(t)\end{bmatrix}^{\mathrm{T}},\ \mathbf{u}(t) = \begin{bmatrix}\mathbf{u}_1^{\mathrm{T}}(t) & \mathbf{u}_2^{\mathrm{T}}(t) & \cdots & \mathbf{u}_N^{\mathrm{T}}(t)\end{bmatrix}^{\mathrm{T}},$$

$$\mathbf{y}(t) = \begin{bmatrix}\mathbf{y}_1^{\mathrm{T}}(t) & \mathbf{y}_2^{\mathrm{T}}(t) & \cdots & \mathbf{y}_N^{\mathrm{T}}(t) & \mathbf{y}_{\mathrm{r}}^{\mathrm{T}}(t)\end{bmatrix}^{\mathrm{T}},$$

$$\mathbf{z}(t) = \begin{bmatrix}\mathbf{z}_1^{\mathrm{T}}(t) & \mathbf{z}_2^{\mathrm{T}}(t) & \cdots & \mathbf{z}_N^{\mathrm{T}}(t) & \mathbf{z}_{\mathrm{r}}^{\mathrm{T}}(t)\end{bmatrix}^{\mathrm{T}},$$

$$\mathbf{w}(t) = \begin{bmatrix}\mathbf{w}_1^{\mathrm{T}}(t) & \mathbf{w}_2^{\mathrm{T}}(t) & \cdots & \mathbf{w}_N^{\mathrm{T}}(t)\end{bmatrix}^{\mathrm{T}},$$

$$\mathbf{A} = \left[\mathbf{A}_{ij}\right]_{N\times N} = \begin{bmatrix} \mathbf{A}_{11} & \cdots & \mathbf{A}_{1N} \\ \vdots & \ddots & \vdots \\ \mathbf{A}_{N1} & \cdots & \mathbf{A}_{NN} \end{bmatrix}, \quad \mathbf{B}_1 = \text{diag}\{\mathbf{B}_{11}, \mathbf{B}_{12}, \cdots, \mathbf{B}_{1N}\},$$

$$\mathbf{B}_2 = \text{diag}\{\mathbf{B}_{21}, \mathbf{B}_{22}, \cdots, \mathbf{B}_{2N}\}, \quad \mathbf{C}_1 = \text{diag}\{\mathbf{C}_{11}, \mathbf{C}_{12}, \cdots, \mathbf{C}_{1N}\},$$

$$\mathbf{C}_2 = \text{diag}\{\mathbf{C}_{21}, \mathbf{C}_{22}, \cdots, \mathbf{C}_{2N}\}, \quad \mathbf{D}_{11} = \text{diag}\{\mathbf{D}_{111}, \mathbf{D}_{112}, \cdots, \mathbf{D}_{11N}\},$$

$$\mathbf{D}_{12} = \text{diag}\{\mathbf{D}_{121}, \mathbf{D}_{122}, \cdots, \mathbf{D}_{12N}\}, \quad \mathbf{D}_{21} = \text{diag}\{\mathbf{D}_{211}, \mathbf{D}_{212}, \cdots, \mathbf{D}_{21N}\}$$

where

$\mathbf{y}_\text{r}(t)$ is the vector of measured remote output signals available to the controller,

$\mathbf{z}_\text{r}(t)$ is the vector of exogenous regulated remote output signals

The following assumptions are imposed on the plant parameters:

(i) $(\mathbf{A}, \mathbf{B}_2)$ is stabilizable and $(\mathbf{A}, \mathbf{C}_2)$ is detectable;

(ii) $\mathbf{D}_{12}$ and $\mathbf{D}_{21}$ have full rank;

(iii) $\begin{bmatrix} \mathbf{A} - j\omega I & \mathbf{B}_2 \\ \mathbf{C}_1 & \mathbf{D}_{12} \end{bmatrix}$ has full column rank and $\begin{bmatrix} \mathbf{A} - j\omega I & \mathbf{B}_1 \\ \mathbf{C}_2 & \mathbf{D}_{21} \end{bmatrix}$ has full row rank for all ω

(iv) $\mathbf{D}_{11} = \mathbf{0}_{q\times r}$ and $\mathbf{D}_{22} = \mathbf{0}_{p\times m}$;

The dynamic output feedback controller considered for the system of (4.1)-(4.3) is given by:

$$\dot{\mathbf{x}}_{\text{c}i}(t) = \mathbf{A}_{\text{c}i}\mathbf{x}_{\text{c}i}(t) + \mathbf{B}_{\text{c}i}\mathbf{y}_{i\text{r}}(t) \tag{4.7}$$

$$\mathbf{u}_i(t) = \mathbf{C}_{\text{c}i}\mathbf{x}_{\text{c}i}(t) + \mathbf{D}_{\text{c}i}\mathbf{y}_{i\text{r}}(t) \tag{4.8}$$

where

$\mathbf{x}_{\text{c}i}(t) \in R^{n_{\text{c}i}}$ is the state vector of the i^{th}-local independent controller,

$n_{\text{c}i}$ is a specified dimension, $\mathbf{y}_{i\text{r}}(t) = \left[\mathbf{y}_i^{\text{T}}(t) \quad \mathbf{y}_\text{r}^{\text{T}}(t)\right]^{\text{T}}$ and

$\mathbf{A}_{ci}$, $\mathbf{B}_{ci}$, $\mathbf{C}_{ci}$, $\mathbf{D}_{ci}$, i =1, 2,…, N are constant matrices to be determined during the design.

In this study, the design procedure deals with nonzero $\mathbf{D}_{ci}$, however, it can be set equal to zero, i.e., $\mathbf{D}_{ci} = 0$, so that the i^{th}-local independent controller is strictly proper controller.

After augmenting the controller of (4.7) and (4.8) in the system of (4.1)-(4.3), the state space equation of i^{th}-extended subsystem will have the following form:

$$\dot{\widetilde{\mathbf{x}}}_i(t) = (\widetilde{\mathbf{A}}_{ii} + \widetilde{\mathbf{B}}_{2i}\mathbf{K}_i\widetilde{\mathbf{C}}_{2i})\widetilde{\mathbf{x}}_i(t) + (\widetilde{\mathbf{B}}_{1i} + \widetilde{\mathbf{B}}_{2i}\mathbf{K}_i\widetilde{\mathbf{C}}_{2i})\mathbf{w}_i(t) + \sum_{j=1, j\neq i}^{N} \widetilde{\mathbf{A}}_{ij}\widetilde{\mathbf{x}}_j(t) \quad (4.9)$$

$$\mathbf{z}_i(t) = (\widetilde{\mathbf{C}}_{1i} + \widetilde{\mathbf{D}}_{12i}\mathbf{K}_i\widetilde{\mathbf{C}}_{2i})\widetilde{\mathbf{x}}_i(t) + (\widetilde{\mathbf{D}}_{11i} + \widetilde{\mathbf{D}}_{12i}\mathbf{K}_i\widetilde{\mathbf{D}}_{21i})\mathbf{w}_i(t) \quad (4.10)$$

where $\widetilde{\mathbf{x}}_i(t) = \begin{bmatrix}\mathbf{x}_i^{\mathrm{T}}(t) & \mathbf{x}_{ci}^{\mathrm{T}}(t)\end{bmatrix}^{\mathrm{T}}$ is the augmented state vector for the i^{th}-subsystem and

$$\widetilde{\mathbf{A}}_{ij} = \begin{bmatrix}\mathbf{A}_{ij} & \mathbf{0}_{n_i\times n_{ci}} \\ \mathbf{0}_{n_{ci}\times n_i} & \mathbf{0}_{n_{ci}\times n_{ci}}\end{bmatrix}, \quad \widetilde{\mathbf{B}}_{1i} = \begin{bmatrix}\mathbf{B}_{1i} \\ \mathbf{0}_{n_i\times r_i}\end{bmatrix}, \quad \widetilde{\mathbf{B}}_{2i} = \begin{bmatrix}\mathbf{0}_{n_i\times n_{ci}} & \mathbf{B}_{2i} \\ \mathbf{I}_{n_{ci}} & \mathbf{0}_{n_{ci}\times n_{m_i}}\end{bmatrix},$$

$$\widetilde{\mathbf{C}}_{1i} = \begin{bmatrix}\mathbf{C}_{1i} & \mathbf{0}_{p_i\times n_{ci}}\end{bmatrix}, \quad \widetilde{\mathbf{C}}_{2i} = \begin{bmatrix}\mathbf{0}_{n_{ci}\times n_i} & \mathbf{I}_{n_{ci}\times n_{ci}} \\ \mathbf{C}_{2i} & \mathbf{0}_{q_i\times n_{ci}}\end{bmatrix}, \quad \widetilde{\mathbf{D}}_{11i} = \mathbf{D}_{11i},$$

$$\widetilde{\mathbf{D}}_{12i} = \begin{bmatrix}\mathbf{0}_{p_i\times n_{ci}} & \mathbf{D}_{12i}\end{bmatrix}, \quad \widetilde{\mathbf{D}}_{21i} = \begin{bmatrix}\mathbf{0}_{n_{ci}\times r_i} \\ \mathbf{D}_{21i}\end{bmatrix}, \quad \mathbf{K}_i = \begin{bmatrix}\mathbf{A}_{ci} & \mathbf{B}_{ci} \\ \mathbf{C}_{ci} & \mathbf{D}_{ci}\end{bmatrix}$$

Moreover, the overall extended system can be equivalently described by the following composite equations:

$$\dot{\widetilde{\mathbf{x}}}(t) = (\widetilde{\mathbf{A}} + \widetilde{\mathbf{B}}_2\mathbf{K}_{\mathrm{D}}\widetilde{\mathbf{C}}_2)\widetilde{\mathbf{x}}(t) + (\widetilde{\mathbf{B}}_1 + \widetilde{\mathbf{B}}_2\mathbf{K}_{\mathrm{D}}\widetilde{\mathbf{C}}_2)\mathbf{w}(t) \quad (4.11)$$

$$\mathbf{z}(t) = (\widetilde{\mathbf{C}}_1 + \widetilde{\mathbf{D}}_{12}\mathbf{K}_{\mathrm{D}}\widetilde{\mathbf{C}}_2)\widetilde{\mathbf{x}}(t) + (\widetilde{\mathbf{D}}_{11} + \widetilde{\mathbf{D}}_{12}\mathbf{K}_{\mathrm{D}}\widetilde{\mathbf{D}}_{21})\mathbf{w}(t) \quad (4.12)$$

where

$$\widetilde{\mathbf{A}} = \left[\widetilde{\mathbf{A}}_{ij}\right]_{N\times N}, \qquad \widetilde{\mathbf{B}}_1 = \mathrm{diag}\left\{\widetilde{\mathbf{B}}_{11}, \widetilde{\mathbf{B}}_{12}, \cdots, \widetilde{\mathbf{B}}_{1N}\right\},$$

$$\widetilde{\mathbf{B}}_2 = \mathrm{diag}\left\{\widetilde{\mathbf{B}}_{21}, \widetilde{\mathbf{B}}_{22}, \cdots, \widetilde{\mathbf{B}}_{2N}\right\}, \quad \widetilde{\mathbf{C}}_1 = \mathrm{diag}\left\{\widetilde{\mathbf{C}}_{11}, \widetilde{\mathbf{C}}_{12}, \cdots, \widetilde{\mathbf{C}}_{1N}\right\},$$

$$\widetilde{\mathbf{C}}_2 = \mathrm{diag}\left\{\widetilde{\mathbf{C}}_{21}, \widetilde{\mathbf{C}}_{22}, \cdots, \widetilde{\mathbf{C}}_{2N}\right\}, \quad \widetilde{\mathbf{D}}_{11} = \mathrm{diag}\left\{\widetilde{\mathbf{D}}_{111}, \widetilde{\mathbf{D}}_{112}, \cdots, \widetilde{\mathbf{D}}_{11N}\right\},$$

$$\widetilde{\mathbf{D}}_{12} = \mathrm{diag}\left\{\widetilde{\mathbf{D}}_{121}, \widetilde{\mathbf{D}}_{122}, \cdots, \widetilde{\mathbf{D}}_{12N}\right\}, \quad \widetilde{\mathbf{D}}_{21} = \mathrm{diag}\left\{\widetilde{\mathbf{D}}_{211}, \widetilde{\mathbf{D}}_{212}, \cdots, \widetilde{\mathbf{D}}_{21N}\right\},$$

$$\mathbf{K}_{\mathrm{D}} = \mathrm{diag}\left\{\mathbf{K}_1, \mathbf{K}_2, \cdots, \mathbf{K}_N\right\}$$

The overall extended system of (4.11) and (4.12) can be rewritten in a compact form as follows:

$$\dot{\widetilde{\mathbf{x}}}(t) = \mathbf{A}_{\mathrm{cl}}\widetilde{\mathbf{x}}(t) + \mathbf{B}_{\mathrm{cl}}\mathbf{w}(t) \tag{4.13}$$

$$\mathbf{z}(t) = \mathbf{C}_{\mathrm{cl}}\widetilde{\mathbf{x}}(t) + \mathbf{D}_{\mathrm{cl}}\mathbf{w}(t) \tag{4.14}$$

where

$$\mathbf{A}_{\mathrm{cl}} = \widetilde{\mathbf{A}} + \widetilde{\mathbf{B}}_2\mathbf{K}_{\mathrm{D}}\widetilde{\mathbf{C}}_2, \quad \mathbf{B}_{\mathrm{cl}} = \widetilde{\mathbf{B}}_1 + \widetilde{\mathbf{B}}_2\mathbf{K}_{\mathrm{D}}\widetilde{\mathbf{C}}_2,$$

$$\mathbf{C}_{\mathrm{cl}} = \widetilde{\mathbf{C}}_1 + \widetilde{\mathbf{D}}_{12}\mathbf{K}_{\mathrm{D}}\widetilde{\mathbf{C}}_2, \quad \mathbf{D}_{\mathrm{cl}} = \widetilde{\mathbf{D}}_{11} + \widetilde{\mathbf{D}}_{12}\mathbf{K}_{\mathrm{D}}\widetilde{\mathbf{D}}_{21}$$

4.2.2 H_∞ Controller Design using Riccati-based Approach

Any general system interconnection can be put in the general linear fractional transformation (LFT) framework shown in Figure 4.2, where **P**(*s*) is the generalized plant or interconnected system, **C**(*s*) is the controller.

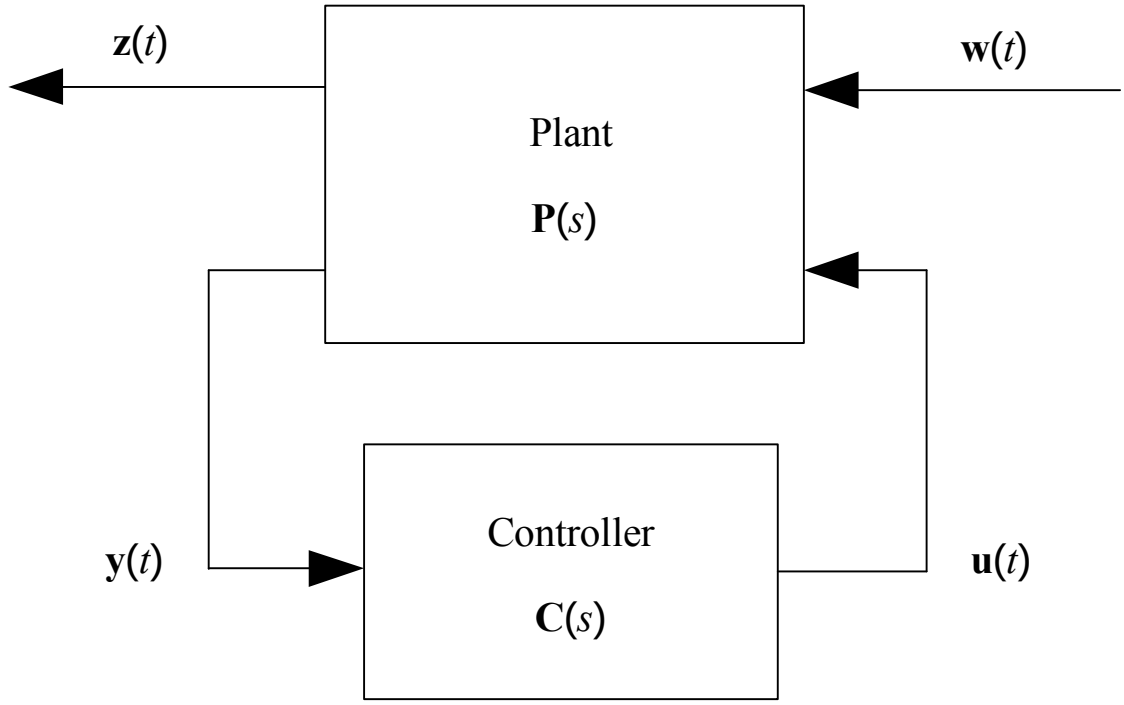

Figure 4.2 General LFT frame work representing general interconnected system

Designing an H_∞ output feedback controller for the system is equivalent to that of finding the matrix $\mathbf{K}_D$, in (4.13) and (4.14), that satisfies an H_∞ norm bound condition on the closed loop transfer function $\mathbf{T}_{\mathbf{zw}}(s) = \mathbf{C}_{\mathrm{cl}}(sI - \mathbf{A}_{\mathrm{cl}})^{-1}\mathbf{B}_{\mathrm{cl}} + \mathbf{D}_{\mathrm{cl}}$ from disturbance $\mathbf{w}(t)$ to the controlled outputs $\mathbf{z}(t)$ in Figure 4.2, i.e., $\left\|\mathbf{T}_{\mathbf{zw}}(s)\right\|_\infty < \gamma$ (for a given scalar constant $\gamma > 0$). Moreover, transfer functions $\mathbf{T}_{\mathbf{zw}}(s)$ must be stable [42]. An ARE approach [43] can be applied to establish the existence of control strategy of (4.7) and (4.8) that internally stabilizes the closed loop transfer function $\mathbf{T}_{\mathbf{zw}}(s)$ and satisfies a certain prescribed disturbance attenuation (or gain) level $\gamma > 0$ on $\mathbf{T}_{\mathbf{zw}}(s)$, i.e., $\left\|\mathbf{T}_{\mathbf{zw}}(s)\right\|_\infty < \gamma$. The matrices of dynamic output feedback control law of (4.7) and (4.8) are given by [43]:

$$\begin{aligned}\mathbf{N}\mathbf{A}_{ci}\mathbf{M}^{\mathrm{T}} = &\left\{\mathbf{A} + Y_{\infty}(\gamma^{-2}\mathbf{C}_1^{\mathrm{T}}\mathbf{C}_1 - \mathbf{C}_2^{\mathrm{T}}\mathbf{C}_2)\right\}(\gamma^{-2}Y_{\infty}X_{\infty} - \mathbf{I}) + \\ &\mathbf{B}_2(\mathbf{B}_2^{\mathrm{T}}X_{\infty} + \mathbf{D}_{ci}\mathbf{C}_2)\end{aligned} \tag{4.15}$$

$$\mathbf{N}\mathbf{B}_{ci} = -(Y_{\infty}\mathbf{C}_2^{\mathrm{T}} + \mathbf{B}_2\mathbf{D}_{ci}) \tag{4.16}$$

$$\mathbf{C}_{ci}\mathbf{M}^{\mathrm{T}} = -(\mathbf{B}_2^{\mathrm{T}}X_{\infty} + \mathbf{D}_{ci}\mathbf{C}_2) \tag{4.17}$$

where feedthrough gain $\mathbf{D}_{ci}$ is arbitrary provided that $\sigma_{\max}(\mathbf{D}_{ci}) \le \gamma$. X_{∞} and Y_{∞} are the stabilizing solutions of the following AREs:

$$\begin{aligned}&X\mathbf{A} + \mathbf{A}^{\mathrm{T}}X + X(\gamma^{-2}\mathbf{B}_1\mathbf{B}_1^{\mathrm{T}} - \mathbf{B}_2\mathbf{B}_2^{\mathrm{T}})X + \mathbf{C}_1^{\mathrm{T}}\mathbf{C}_1 + \\ &(X\mathbf{B}_2 + \mathbf{M}\mathbf{C}_{ci}^{\mathrm{T}} + \mathbf{C}_2^{\mathrm{T}}\mathrm{D}_{ci}^{\mathrm{T}})(\mathbf{I} - \gamma^{-2}\mathbf{D}_{ci}\mathrm{D}_{ci}^{\mathrm{T}})^{-1}(X\mathbf{B}_2 + \mathbf{M}\mathbf{C}_{ci}^{\mathrm{T}} + \mathbf{C}_2^{\mathrm{T}}\mathrm{D}_{ci}^{\mathrm{T}})^{\mathrm{T}} = 0\end{aligned} \tag{4.18}$$

$$\begin{aligned}&\mathbf{A}Y + Y\mathbf{A}^{\mathrm{T}} + Y(\gamma^{-2}\mathbf{C}_1^{\mathrm{T}}\mathbf{C}_1 - \mathbf{C}_2^{\mathrm{T}}\mathbf{C}_2)Y + \mathbf{B}_1\mathbf{B}_1^{\mathrm{T}} + \\ &(Y\mathbf{C}_2^{\mathrm{T}} + \mathbf{N}\mathbf{B}_{ci} + \mathbf{B}_2\mathbf{D}_{ci})(\mathbf{I} - \gamma^{-2}\mathrm{D}_{ci}^{\mathrm{T}}\mathbf{D}_{ci})^{-1}(Y\mathbf{C}_2^{\mathrm{T}} + \mathbf{N}\mathbf{B}_{ci} + \mathbf{B}_2\mathbf{D}_{ci})^{\mathrm{T}} = 0\end{aligned} \tag{4.19}$$

with the coupling condition $\mathbf{M}\mathbf{N}^{\mathrm{T}} = \gamma^{-2}XY - \mathbf{I}$.

The output feedback control law of (4.7) and (4.8) with (4.15)-(4.17) stabilizes the system of (4.4)-(4.6) and the closed-loop transfer function matrix $\mathbf{T}_{\mathbf{zw}}(s)$ satisfies $\left\|\mathbf{T}_{\mathbf{zw}}(s)\right\|_{\infty} < \gamma$.

4.3 Application Results

4.3.1 Power System Simulation Model

Figure 4.3 shows a test two-machine power system example that has been selected to apply the robust dynamic output feedback control design approach presented in the previous section and to illustrate the effectiveness of the proposed robust H_{∞}-based PSS controller for a better damping of system oscillations. The considered system has two identical synchronous generators, each

having a rating of 350 MVA and 15.75 kV. Both generators are equipped with identical IEEE standard exciters (IEEE type DC1A excitation system). Generator G2 is equipped with PSS. Load is represented as constant impedance and is connected to bus 5. The fault is located at bus 3. Detailed information about this test system including the controllers and their parameter values can be found in Appendix A. Moreover, for all simulation studies as well as for the PSS design, the structure of the i^{th}-generator together with an n_{ci}^{th}-order PSS controller in a multi-machine power system, presented in Section 4.2.1 (Figure 4.1), is considered.

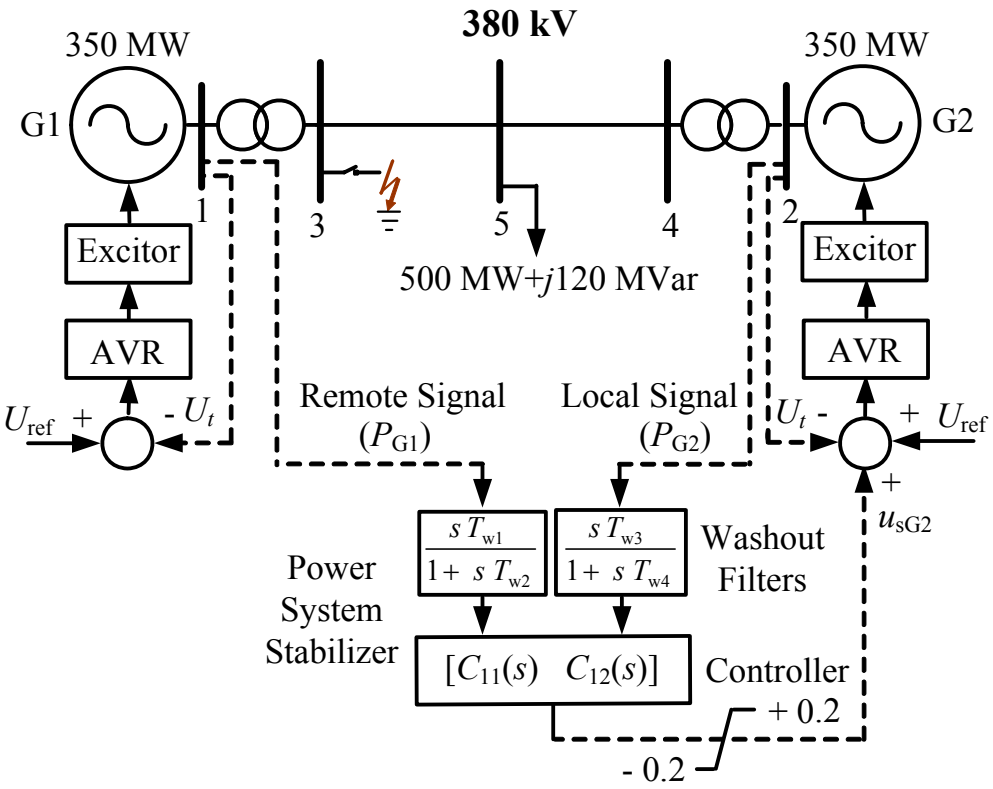

Figure 4.3 One line diagram of two-machine test power system together with the structure of generators and PSS (PSS located at generator G2)

4.3.2 Design Results

The base operating conditions for the two-machine power system example are listed in Appendix A. The linearized equations of the two-machine power system for the given parameter values can be expressed in the general form of (4.4)-(4.6). Therefore, the two-machine power system can be written in the form of system of (4.4)-(4.6) as follows:

$$\dot{\mathbf{x}}(t) = \mathbf{A}\mathbf{x}(t) + \mathbf{B}_1\mathbf{w}(t) + \mathbf{B}_2\mathbf{u}(t) \tag{4.20}$$

$$\mathbf{z}(t) = \mathbf{C}_1\mathbf{x}(t) + \mathbf{D}_{11}\mathbf{w}(t) + \mathbf{D}_{12}\mathbf{u}(t) \tag{4.21}$$

$$\mathbf{y}(t) = \mathbf{C}_2\mathbf{x}(t) + \mathbf{D}_{21}\mathbf{w}(t) \tag{4.22}$$

where

$$\mathbf{x}(t) = \begin{bmatrix}\mathbf{x}_1^{\mathrm{T}}(t) & \mathbf{x}_2^{\mathrm{T}}(t)\end{bmatrix}^{\mathrm{T}}, \quad \mathbf{u}(t) = \begin{bmatrix}\mathbf{u}_1^{\mathrm{T}}(t) & \mathbf{u}_2^{\mathrm{T}}(t)\end{bmatrix}^{\mathrm{T}},$$

$$\mathbf{y}(t) = \begin{bmatrix}\mathbf{y}_1^{\mathrm{T}}(t) & \mathbf{y}_2^{\mathrm{T}}(t)\end{bmatrix}^{\mathrm{T}}, \quad \mathbf{z}(t) = \begin{bmatrix}\mathbf{z}_1^{\mathrm{T}}(t) & \mathbf{z}_2^{\mathrm{T}}(t)\end{bmatrix}^{\mathrm{T}},$$

$$\mathbf{w}(t) = \begin{bmatrix}\mathbf{w}_1^{\mathrm{T}}(t) & \mathbf{w}_2^{\mathrm{T}}(t)\end{bmatrix}^{\mathrm{T}},$$

$$\mathbf{A} = \begin{bmatrix}\mathbf{A}_{11} & \mathbf{A}_{12} \\ \mathbf{A}_{21} & \mathbf{A}_{22}\end{bmatrix}, \quad \mathbf{B}_1 = \mathrm{diag}\{\mathbf{B}_{11}, \mathbf{B}_{12}\},$$

$$\mathbf{B}_2 = \mathrm{diag}\{\mathbf{B}_{21}, \mathbf{B}_{22}\}, \quad \mathbf{C}_1 = \mathrm{diag}\{\mathbf{C}_{11}, \mathbf{C}_{12}\},$$

$$\mathbf{C}_2 = \mathrm{diag}\{\mathbf{C}_{21}, \mathbf{C}_{22}\}, \quad \mathbf{D}_{11} = \mathrm{diag}\{\mathbf{D}_{111}, \mathbf{D}_{112}\},$$

$$\mathbf{D}_{12} = \mathrm{diag}\{\mathbf{D}_{121}, \mathbf{D}_{122}\}, \quad \mathbf{D}_{21} = \mathrm{diag}\{\mathbf{D}_{211}, \mathbf{D}_{212}\}$$

$u_1(t)$ and $u_2(t)$ are control inputs to generators G1 and G2 respectively. As in the considered two-machine test power system, PSS is located at only generator G2, therefore, $u_1(t) = 0$ and $u_2(t) = u_{\mathrm{sG2}}(t)$. During the design of robust H_∞-based PSS controller, electrical power output signals from both generators are

used as its feedback input signals, i.e., $\mathbf{y}(t) = \begin{bmatrix} P_{G1}(t) & P_{G2}(t) \end{bmatrix}^T$. Electrical power output of generator G1 (P_{G1}) is the remote measured feedback signal to the PSS which is located at the generator G2 while electrical power output of generator G2 (P_{G2}) is the local measured feedback signal to the PSS. Electrical power output signals from both generators, the output of the PSS together with the terminal voltage error signals, which are the inputs to the regulator of the exciter, are used as regulated signals within this design framework, i.e., $\mathbf{z}(t) = \begin{bmatrix} P_{G1}(t) & P_{G2}(t) & u_{sG2}(t) \end{bmatrix}^T$.

It is easy to check that ($\mathbf{A}$, $\mathbf{B}_2$) is stabilizable and ($\mathbf{A}$, $\mathbf{C}_2$) is detectable. This system is an open loop oscillatory system. The design procedure described in Section 4.2.2 is used to design the dynamic controller of the form of (4.7) and (4.8) such that minimum disturbance attenuation (from $\mathbf{w}(t)$ to $\mathbf{z}(t)$) is achieved. Riccati equations (4.18) and (4.19) are solved for positive, semi-definitive stabilizing solutions X_∞ and Y_∞ and then H_∞ controller is found by using (4.15)-(4.17) together with (4.7) and (4.8) by using Matlab Robust Control Tool box. Balanced residualization technique [18] is used to reduce the order of controller. The H_∞-based PSS controller, thus, obtained is:

$$\mathbf{C}_{H_\infty}(s) = \left[11.714 \frac{1 + s\,0.004}{1 + s\,0.0501} \;\vdots\; 14.999 \frac{1 + s\,0.007}{1 + s\,0.0501} \right]$$

The performance of the proposed H_∞ based PSS controller will be compared with that of a classical PSS controller [1] for the considered two-machine test power system. The classical PSS is also located at generator G2. The parameters for the classical controller are found for the additional phase lead necessary to satisfy the relative stability requirements. Controller is then added to uncompensated open-loop system to satisfy phase margin requirement. Controller is retuned to meet the required specifications for the system.

The classical PSS controller has been tuned to a large extent in order to obtain its optimal performance. The classical controller obtained is as follows:

$$\mathbf{C}_{\text{classical}}(s) = \left[3.5\frac{1+s\,0.32}{1+s\,0.069} \;\vdots\; 10\frac{1+s\,0.26}{1+s\,0.086} \right]$$

It should be noted that both the H_∞-based and classical PSS controllers use the same electrical power output signals from both generators as their inputs.

4.3.3 Time-Domain Simulation Results

The proposed controller in this study is based on the linearized model of the system. However, in order to demonstrate the effectiveness of the proposed controller, extensive simulation studies are conducted. Thus, in the studies, system behavior under large disturbance and wide range of system operating conditions is investigated.

In order to simulate the system behavior under large disturbance conditions, a balanced three-phase fault is applied at bus 3 as shown in Figure 4.3. The fault sequence of the three-phase fault used in these simulations is as follows:

Stage 1: The system is in pre-fault steady-state.

Stage 2: A three-phase fault occurs at t = 1.0 s.

Stage 3: The fault is cleared at t = 1.1 s.

Stage 4: The system is in a post-fault state.

Simulation results showing the behaviors of deviation of electrical power output of generator G1 ($\Delta P_{\text{G1}}(t)$) without PSS controller, with H_∞-based and classical PSS controllers are shown in Figures 4.4 and 4.5. Figure 4.4 indicates that the behavior of $\Delta P_{\text{G1}}(t)$ is better damped with the proposed H_∞-based PSS controller as compared to that without PSS controller. The behav-

ior of $\Delta P_{G1}(t)$, shown in Figure 4.5, indicates that the proposed H_∞-based PSS controller is effective even when its remote input signal is lost but with the reduced performance level.

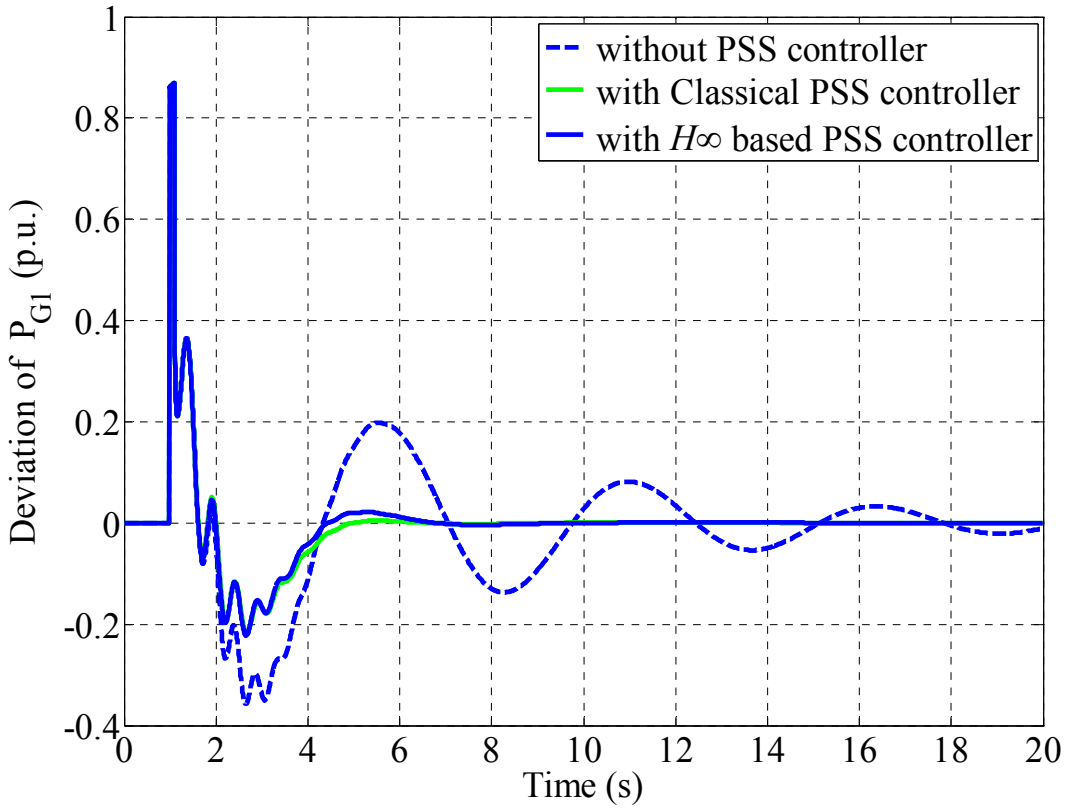

Figure 4.4 Deviation of P_{G1} following a three-phase fault with controllers using both local and remote signals as inputs

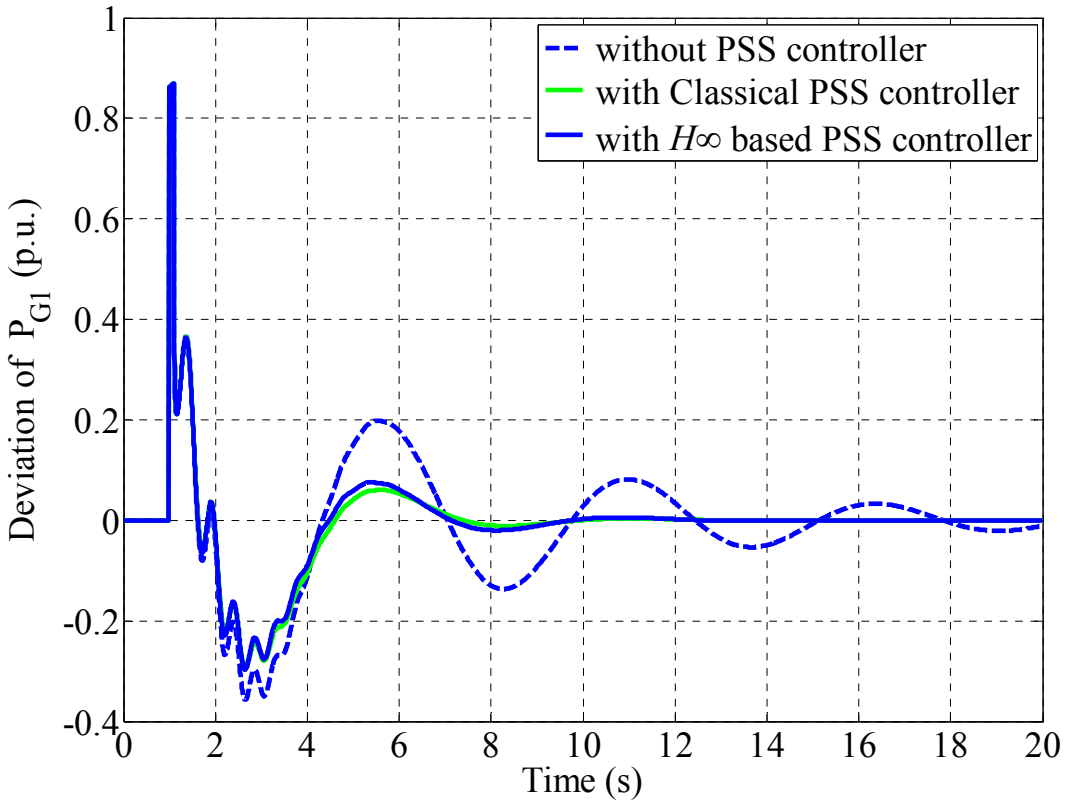

Figure 4.5 Deviation of P_{G1} following a three-phase fault with controllers using only local signal as input (remote signal is lost)

4.3.4 Robustness of Proposed Controller

To further assess the effectiveness of the proposed approach regarding robustness, the transient performance indices have been computed for different loading conditions at bus 5 in the considered two-machine test power system. The transient performance index (I) for electrical power output of the generator, following a three-phase short-circuit of 100 ms duration at bus 3 in the test system, is computed using the following equation:

$$I = \int_0^t \left| P_G(t) - P_{G0}(t) \right| \; dt \tag{4.23}$$

For comparison purpose, this index is normalized to the index for the base system operating condition for which the controller is designed. The normalized transient performance index (I_N) is given by:

$$I_{\mathrm{N}} = \frac{I_{\mathrm{DLC}}}{I_{\mathrm{BLC}}} \tag{4.24}$$

where I_{DLC} is the transient performance index for different loading conditions and I_{BLC} is the transient performance index for base loading condition. The normalized transient performance indices for the electrical power output of the generator for different loading conditions for the proposed H_∞-based and classical PSS controllers are shown in Figure 4.6. It can be seen from the figure that the normalized transient performance indices, for a wide range of system operating conditions, are more near to unity for the proposed H_∞-based PSS controller as compared to those for the classical PSS controller. This clearly indicates that, the transient responses of the generator with the proposed H_∞-based PSS controller, for different system operating conditions, are well damped as compared to those with the classical PSS controller and the system behavior exhibits robustness with the proposed H_∞-based PSS controller for all loading conditions.

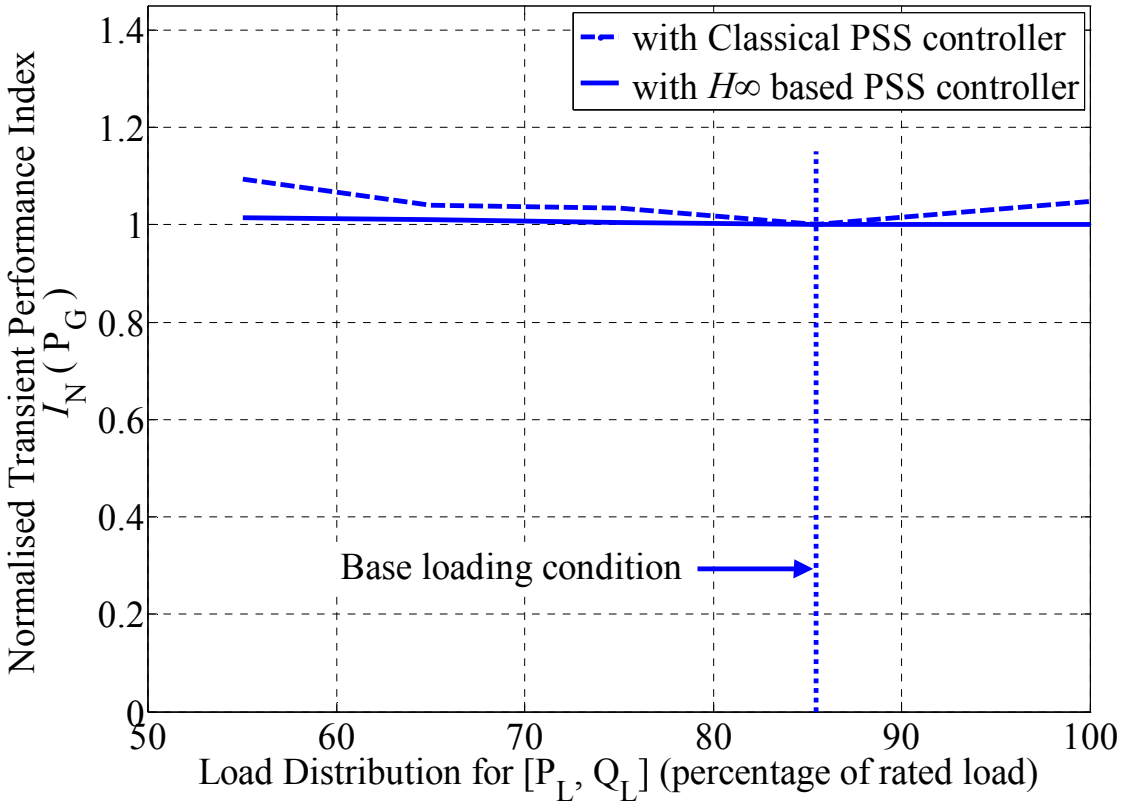

Figure 4.6 Normalized transient performance index for electrical power generated

4.4 Summary

An H_∞-based dynamic output feedback PSS controller, using both local and remote signals, has been developed. An ARE approach has been used for the design of controller. The effectiveness of the designed controller is demonstrated through digital simulation studies on a test power system. The nonlinear simulation results have shown that the proposed controller is effective and robust in suppressing system oscillations for a wide range of system operating conditions under large disturbances in the system studied. The results also show that the proposed controller is effective when its remote input signal is lost.

Chapter 5

Delayed-Input PSS

5.1 Introduction

The design of a local PSS controller using remote signals as supplementary inputs without considering time delay was presented in Chapter 4. Due to the transmission and processing of remote signals in WAMS, these may arrive after a certain communication delay. The time delays can invalidate many controllers that work well in no delayed-input systems and even cause disaster accidents [45]. It is found that a controller designed for the delay-free system if applied to the delayed-input system, the closed-loop system may lose stability. Time delay can make a control system to have less damping and there is a danger of losing synchronism. The design of a controller, therefore, must take into account this delay in order to provide a controller that is robust, not only for the range of operating conditions desired, but also for the uncertainty in delay [9].

This chapter considers a problem of improving the performance of local conventional PSS by using instantaneous measurements from remote locations of the grid considering time delay. A local H_∞-based PSS controller, which uses wide area or global signals as additional measuring information, is designed considering time delay in the remote signals. Three methods for dealing with the effects of time delay are presented in this chapter. First, time delay compensation method using lead/lag compensation along with gain scheduling for compensating effects of constant delay is presented. In the second method, Pade approximation approach is used to model time delay. The

time delay model is then merged into delay-free power system model to obtain the delayed power system model. Delay compensation and Pade approximation methods deal with constant delays and are not robust regarding time delays. Time delay uncertainty is, therefore, taken into account using LFT method.

To provide robust behavior, H_∞ control theory together with an ARE approach has been applied to design the proposed controller. Digital simulation studies are conducted on a test power system to investigate the effectiveness of the proposed controllers during system disturbances.

5.2 Time Delay in Power Systems

5.2.1 Design of Delay Compensator

Delay compensator consisting of lead/lag and gain modules is designed to diminish the effect of time delay. The effect of time delay on an oscillatory mode ($\sigma+j\omega$) is to introduce a phase lag with respect to angular frequency ω and gain amplification with respect to damping σ. The effect might derive eigenvalues of system matrix to undesirable places on complex plane and can make power system unstable. Phase lag φ due to delay τ is $\varphi = \omega\ \tau$ while the gain amplification γ_c due to delay τ is $\gamma_c = e^{-\sigma\tau}$.

Delay in time could be compensated in phase provided by lead/lag compensation block along with gain scheduling as shown in Figure 5.1. In Figure 5.1, output signals $\mathbf{Y}_{1df}$ of the delay-free system plant $\mathbf{P}(s)$ are the remote input signals of the PSS controller. The time delay, introduced by the remote input signals' transmission and processing in WAMS, therefore, occurs only in $\mathbf{Y}_{1df}$. In order to compensate the effect of this time delay on the system per-

formance, $\mathbf{Y}_{1df}$ are added to the delay compensator $H_c(s)$. The output signals $\mathbf{Y}_{1d}$ of delay compensator, therefore, represents the delayed remote input signals of the PSS controller $\mathbf{C}(s)$. The output signal Y_{2df} of delay-free system plant is the local input signal to the PSS controller and is, therefore, without time delay.

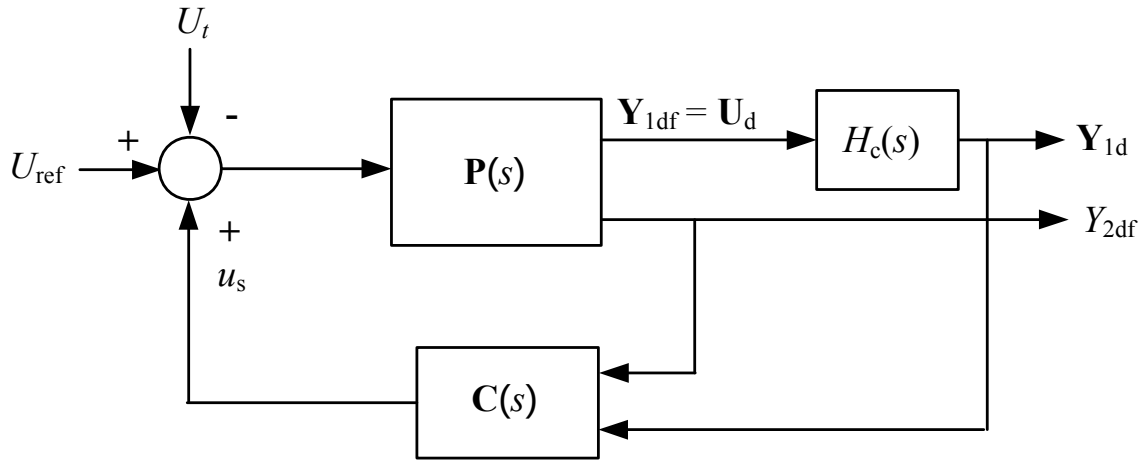

Figure 5.1 Frame work of wide area damping control

Transfer function of delay compensator is given as:

$$H_c(s) = K\left\{\frac{(1+s\,T_1)}{(1+\ s\ T_2)}\right\}^2 \tag{5.1}$$

where

$$T_1 = \frac{1}{\omega\sqrt{\alpha}}, \quad T_2 = \alpha T_1, \quad \alpha = \frac{1-\sin(\phi/2)}{1+\sin(\phi/2)}, \quad K = \beta e^{\sigma\tau}, \quad 0 \prec \beta \prec 1$$

Phase lead ($\varphi = \omega\ \tau$) provided by delay compensator balances the phase lag due to delay τ. Gain K provided by delay compensator reduces the gain amplification γ_c due to delay τ.

5.2.2 Pade Approximation Method for Constant Delay

In order to take into account the effect of time delay on the system performance, the remote input signals $\mathbf{Y}_{1df}$ of the PSS controller are added to the time delay block as shown in Figure 5.2. The output signals $\mathbf{Y}_{1d}$ of time delay block, therefore, represent the delayed remote input signals of the PSS controller.

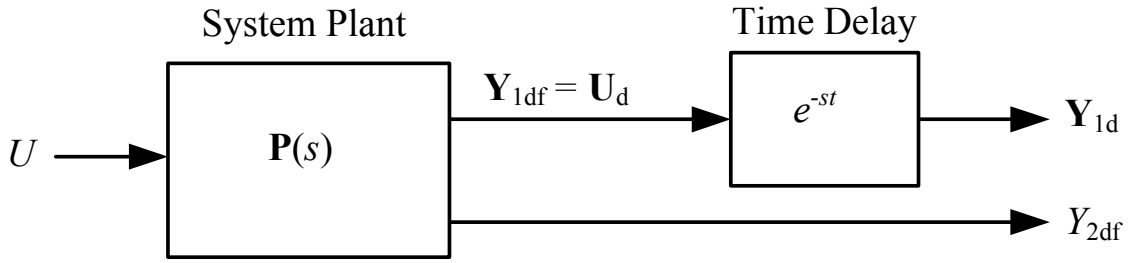

Figure 5.2 Delayed-input system

Time delay τ in a signal can be expressed as $e^{-s\tau}$. In order to design a controller and analyze the system performance, it is convenient to replace the exponential function by a rational polynomial transfer function. One popular rational approximation to $e^{-s\tau}$ is by Pade (reported in 1892). In control systems, time delay can be represented by the Pade approximation [44]. By using Pade approximation, the time delay $e^{-s\tau}$ in the remote input signals of the PSS controller can be expressed in state space form as follows [46]:

$$\dot{\mathbf{x}}_d(t) = \mathbf{A}_d\mathbf{x}_d(t) + \mathbf{B}_d\mathbf{u}_d(t) \tag{5.2}$$

$$\mathbf{y}_{1d}(t) = \mathbf{C}_d\mathbf{x}_d(t) + \mathbf{D}_d\mathbf{u}_d(t) \tag{5.3}$$

If same time delay is considered for each signal, then using 1st-order Pade approximation, constant matrices $\mathbf{A}_d$, $\mathbf{B}_d$, $\mathbf{C}_d$ and $\mathbf{D}_d$ can be written as follows:

$$\mathbf{A}_{\mathrm{d}}=\begin{bmatrix}\mathbf{a} & 0 & \cdots & 0\\ 0 & \mathbf{a} & & \vdots\\ \vdots & & \ddots & 0\\ 0 & \cdots & 0 & \mathbf{a}\end{bmatrix},\qquad \mathbf{B}_{\mathrm{d}}=\begin{bmatrix}\mathbf{b} & 0 & \cdots & 0\\ 0 & \mathbf{b} & & \vdots\\ \vdots & & \ddots & 0\\ 0 & \cdots & 0 & \mathbf{b}\end{bmatrix},$$

$$\mathbf{C}_{\mathrm{d}}=\begin{bmatrix}\mathbf{c} & 0 & \cdots & 0\\ 0 & \mathbf{c} & & \vdots\\ \vdots & & \ddots & 0\\ 0 & \cdots & 0 & \mathbf{c}\end{bmatrix},\qquad \mathbf{D}_{\mathrm{d}}=\begin{bmatrix}\mathbf{d} & 0 & \cdots & 0\\ 0 & \mathbf{d} & & \vdots\\ \vdots & & \ddots & 0\\ 0 & \cdots & 0 & \mathbf{d}\end{bmatrix}$$

Delay-free power system plant can be expressed as follows:

$$\dot{\mathbf{x}}_{\mathrm{df}}(t)=\mathbf{A}_{\mathrm{df}}\mathbf{x}_{\mathrm{df}}(t)+\mathbf{B}_{\mathrm{df}}\mathbf{u}(t) \tag{5.4}$$

$$\mathbf{y}_{\mathrm{df}}(t)=\mathbf{C}_{\mathrm{df}}\mathbf{x}_{\mathrm{df}}(t)+\mathbf{D}_{\mathrm{df}}\mathbf{u}(t) \tag{5.5}$$

where

$$\mathbf{y}_{\mathrm{df}}(t)=\begin{bmatrix}\mathbf{y}_{1\mathrm{df}} & y_{2df}\end{bmatrix}^{\mathrm{T}},\quad \mathbf{C}_{\mathrm{df}}=\begin{bmatrix}\mathbf{C}_{1\mathrm{df}} & \mathbf{C}_{2\mathrm{df}}\end{bmatrix}^{\mathrm{T}},\quad \mathbf{D}_{\mathrm{df}}=\begin{bmatrix}\mathbf{D}_{1\mathrm{df}} & \mathbf{D}_{2\mathrm{df}}\end{bmatrix}^{\mathrm{T}}$$

In the delayed-input system shown in Figure 5.2, since output signals $\mathbf{Y}_{1\mathrm{df}}$ of delay-free block are the inputs of time delay block, i-e., $\mathbf{Y}_{1\mathrm{df}} = \mathbf{U}_{\mathrm{d}}$, therefore, replacement of $\mathbf{u}_{\mathrm{d}}(t)$ by $\mathbf{y}_{1\mathrm{df}}(t)$ in (5.2) and (5.3) and then substitution of the value of $\mathbf{y}_{1\mathrm{df}}(t)$ from (5.5) into (5.2) and (5.3) yields:

$$\dot{\mathbf{x}}_{\mathrm{d}}(t)=\mathbf{A}_{\mathrm{d}}\mathbf{x}_{\mathrm{d}}(t)+\mathbf{B}_{\mathrm{d}}(\mathbf{C}_{1\mathrm{df}}\mathbf{x}_{\mathrm{df}}(t)+\mathbf{D}_{1\mathrm{df}}\mathbf{u}(t)) \tag{5.6}$$

$$\mathbf{y}_{1\mathrm{d}}(t)=\mathbf{C}_{\mathrm{d}}\mathbf{x}_{\mathrm{d}}(t)+\mathbf{D}_{\mathrm{d}}(\mathbf{C}_{1\mathrm{df}}\mathbf{x}_{\mathrm{df}}(t)+\mathbf{D}_{1\mathrm{df}}\mathbf{u}(t)) \tag{5.7}$$

Equations (5.4), (5.6) and (5.7), in matrix form, can be written as:

$$\begin{bmatrix}\dot{\mathbf{x}}_{\mathrm{df}}(t)\\ \dot{\mathbf{x}}_{\mathrm{d}}(t)\end{bmatrix}=\begin{bmatrix}\mathbf{A}_{\mathrm{df}} & 0\\ \mathbf{B}_{\mathrm{d}}\mathbf{C}_{1\mathrm{df}} & \mathbf{A}_{\mathrm{d}}\end{bmatrix}\begin{bmatrix}\mathbf{x}_{\mathrm{df}}(t)\\ \mathbf{x}_{\mathrm{d}}(t)\end{bmatrix}+\begin{bmatrix}\mathbf{B}_{\mathrm{df}}\\ \mathbf{B}_{\mathrm{d}}\mathbf{D}_{1\mathrm{df}}\end{bmatrix}\mathbf{u}(t) \tag{5.8}$$

$$\mathbf{y}_{1\mathrm{d}}(t)=\begin{bmatrix}\mathbf{D}_{\mathrm{d}}\mathbf{C}_{1\mathrm{df}} & \mathbf{C}_{\mathrm{d}}\end{bmatrix}\begin{bmatrix}\mathbf{x}_{\mathrm{df}}(t)\\ \mathbf{x}_{\mathrm{d}}(t)\end{bmatrix}+\mathbf{D}_{\mathrm{d}}\mathbf{D}_{1\mathrm{df}}\mathbf{u}(t) \tag{5.9}$$

Equation (5.8) is the state equation and (5.9) is the delayed output equation for the delayed-input system shown in Figure 5.2. As the system shown in Figure 5.2 also has a delay free output y_{2df}, therefore, output equation for the delayed-input system becomes:

$$\begin{bmatrix} \mathbf{y}_{1d}(t) \\ y_{2df}(t) \end{bmatrix} = \begin{bmatrix} \mathbf{D}_d\mathbf{C}_{1df} & \mathbf{C}_d \\ \mathbf{C}_{2df} & 0 \end{bmatrix} \begin{bmatrix} \mathbf{x}_{df}(t) \\ \mathbf{x}_d(t) \end{bmatrix} + \begin{bmatrix} \mathbf{D}_d\mathbf{D}_{1df} \\ \mathbf{D}_{2df} \end{bmatrix} \mathbf{u}(t) \tag{5.10}$$

From (5.8) and (5.10), the constant matrices **A**, **B**, **C** and **D** for the delayed-input system shown in Figure 5.2 are given as follows:

$$\mathbf{A} = \begin{bmatrix} \mathbf{A}_{df} & 0 \\ \mathbf{B}_d\mathbf{C}_{1df} & \mathbf{A}_d \end{bmatrix}, \qquad \mathbf{B} = \begin{bmatrix} \mathbf{B}_{df} \\ \mathbf{B}_d\mathbf{D}_{1df} \end{bmatrix},$$

$$\mathbf{C} = \begin{bmatrix} \mathbf{D}_d\mathbf{C}_{1df} & \mathbf{C}_d \\ \mathbf{C}_{2df} & 0 \end{bmatrix}, \qquad \mathbf{D} = \begin{bmatrix} \mathbf{D}_d\mathbf{D}_{1df} \\ \mathbf{D}_{2df} \end{bmatrix}$$

5.2.3 LFT Method for Time Delay Uncertainty

In LFT method, a time delay uncertainty can be described by an LFT [17]. Delay-free power system model is then cascaded with uncertain time delay model to obtain the uncertain delayed power system model as shown in Figure 5.3. Controller design based on LFT can keep the system stable over the delay uncertainty range.

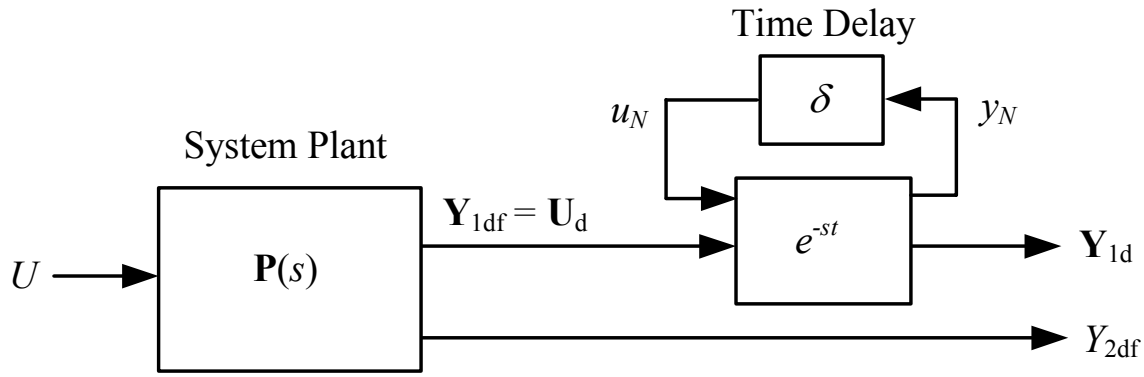

Figure 5.3 Delayed-input system with LFT included

By using 1st-order Pade approximation, delay $e^{-s\tau}$ in a signal can be represented by the following equations [46]:

$$\dot{x}_d(t) = -\frac{2}{\tau}x_d(t) + u_d(t) \tag{5.11}$$

$$y_d(t) = \frac{4}{\tau}x_d(t) - u_d(t) \tag{5.12}$$

By using (5.11) and (5.12), the block diagram of time delay $e^{-s\tau}$ can be drawn as shown in Figure 5.4. The block diagram shown in Figure 5.4 can be redrawn as shown in Figure 5.5.

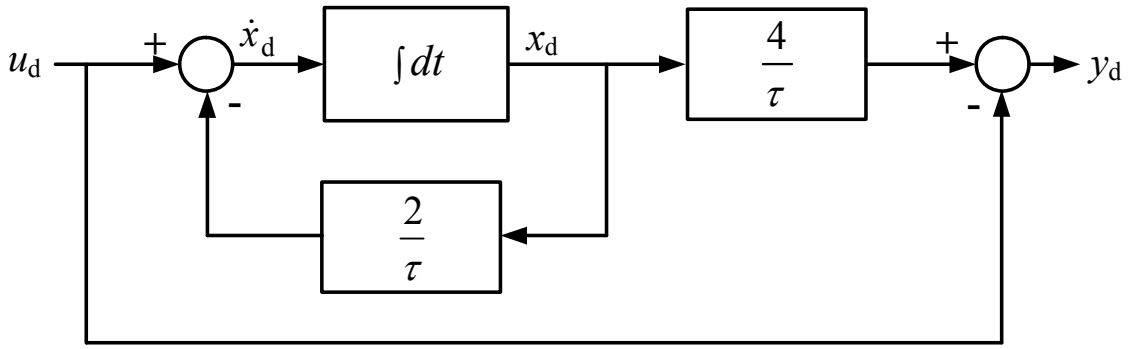

Figure 5.4 Block diagram of time delay $e^{-s\tau}$

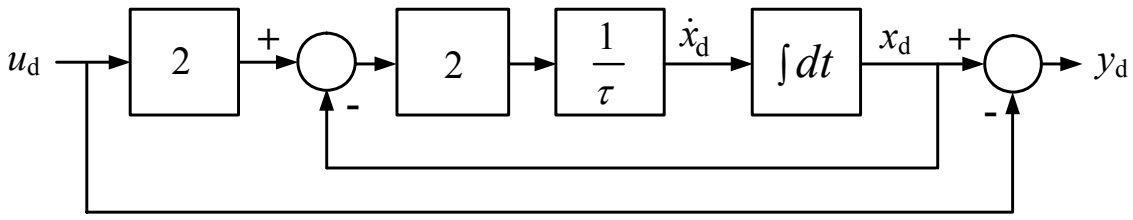

Figure 5.5 Block diagram of time delay $e^{-s\tau}$

The time delay parameter τ is not known exactly. However, it can be assumed that its value is within certain known interval, i.e.,

$$\tau = \bar{\tau}(1 + p_\tau \delta_\tau) \tag{5.13}$$

where, $\bar{\tau}$ is the nominal value of τ. p_τ and δ_τ represent the possible (relative) perturbations on τ. p_τ represents the boundary values within which the value of τ lies. Perturbation δ_τ is assumed to be unknown but lie in the interval [-1, 1].

The term $1/\tau$ in Figure 5.5 can be represented as an LFT in δ_τ, i.e., as a feedback interconnection of a constant matrix and an uncertainty matrix δ_τ, with dynamic parameters lying within interval [-1, 1], as follows:

$$\frac{1}{\tau} = \frac{1}{\bar{\tau}(1 + p_\tau \delta_\tau)} = \frac{1}{\bar{\tau}} - \frac{p_\tau}{\bar{\tau}} \delta_\tau (1 + p_\tau \delta_\tau)^{-1} = F_u(\mathbf{M}_\tau, \delta_\tau) \tag{5.14}$$

For a constant matrix,

$$\mathbf{M}_\tau = \begin{bmatrix} M_{11} & M_{12} \\ M_{21} & M_{22} \end{bmatrix} \tag{5.15}$$

$$F_u(\mathbf{M}_\tau, \delta) = M_{22} + M_{21}\delta(I - M_{11}\delta)^{-1} M_{12} \tag{5.16}$$

Substitution of values of M_{11}, M_{12}, M_{21}, M_{22}, obtained from comparison of (5.14) and (5.16), into (5.15), yields:

$$\mathbf{M}_\tau = \begin{bmatrix} -p_\tau & 1 \\ -\frac{p_\tau}{\bar{\tau}} & \frac{1}{\bar{\tau}} \end{bmatrix} \tag{5.17}$$

Equation (5.14) together with (5.17) represents LFT of the term 1/τ. The term 1/τ in Figure 5.5 is, therefore, replaced by its LFT with an associated matrix $\mathbf{M}_\tau$, as shown in Figure 5.6.

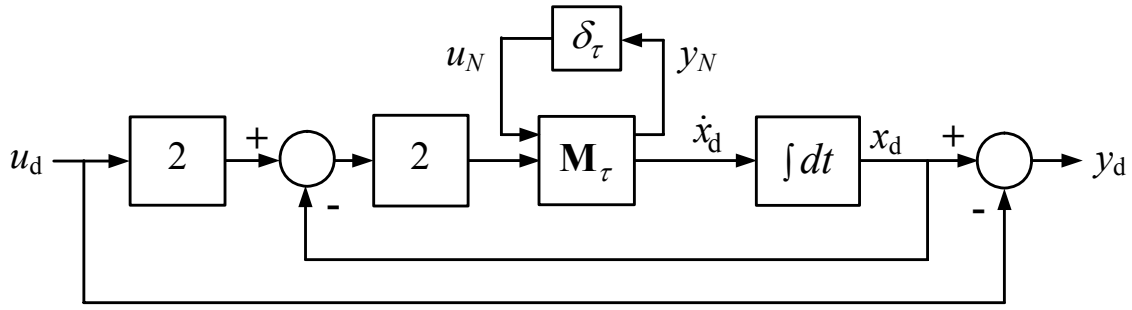

Figure 5.6 Block diagram representation of time delay $e^{-s\tau}$

The block diagram shown in Figure 5.6, representing time delay $e^{-s\tau}$ in a signal can be described by the following equations:

$$\begin{bmatrix} y_N \\ \dot{x}_d \end{bmatrix} = \begin{bmatrix} M_{11} & M_{12} \\ M_{21} & M_{22} \end{bmatrix} \begin{bmatrix} u_N \\ 4u_d - 2x_d \end{bmatrix} \tag{5.18}$$

$$u_N = \delta y_N \tag{5.19}$$

$$y_d = x_d - u_d \tag{5.20}$$

Equations (5.18) and (5.20) can be written in matrix form as follows:

$$\begin{bmatrix} \dot{x}_d \\ y_N \\ y_d \end{bmatrix} = \begin{bmatrix} -2M_{22} & M_{21} & 4M_{22} \\ -2M_{12} & M_{11} & 4M_{12} \\ 1 & 0 & -1 \end{bmatrix} \begin{bmatrix} x_d \\ u_N \\ u_d \end{bmatrix} \tag{5.21}$$

By substituting values of M_{11}, M_{12}, M_{21}, M_{22} from (5.17) into (5.21) gives:

$$\begin{bmatrix} \dot{x}_d \\ y_N \\ y_d \end{bmatrix} = \begin{bmatrix} \frac{-2}{\bar{\tau}} & -\frac{p_\tau}{\bar{\tau}} & \frac{4}{\bar{\tau}} \\ -2 & -p_\tau & 4 \\ 1 & 0 & -1 \end{bmatrix} \begin{bmatrix} x_d \\ u_N \\ u_d \end{bmatrix} \tag{5.22}$$

5.3 Application Results

5.3.1 Power System Simulation Model

A test two-machine power system example, presented in Chapter 4, Section 4.3.1 (Figure 4.3), is selected to apply the methods, for dealing with the effects of time delay, presented in Section 5.2 and to illustrate the effectiveness of the proposed robust H_∞-based PSS controller, for a better damping of system oscillations, in the presence of time delay in its remote input signal. Control design approach presented in the Chapter 4, Section 4.2 is used to design the controller. In order to take into account the effect of time delay on the performance of the considered test system, the remote input signal of the PSS controller ($P_{G1}(t)$) is added to the time delay block as shown in Figure 5.7. The output signal $P_{G1d}(t)$ of time delay block, therefore, represents the delayed remote input signal of the PSS controller. Detailed information about this test system including the controllers and their parameter values can be found in Appendix A. Moreover, for all simulation studies as well as for the PSS design, the structure of the i^{th}-generator together with an n_{ci}^{th}-order PSS controller in a multi-machine power system, presented in Chapter 4, Section 4.2.1 (Figure 4.1), is considered. In order to take into account the effect of time delay on the performance of i^{th}-generator, remote input signals of the PSS controller are added to their corresponding time delay blocks. The output signals of time delay blocks, therefore, represent the delayed remote input signals of the PSS controller.

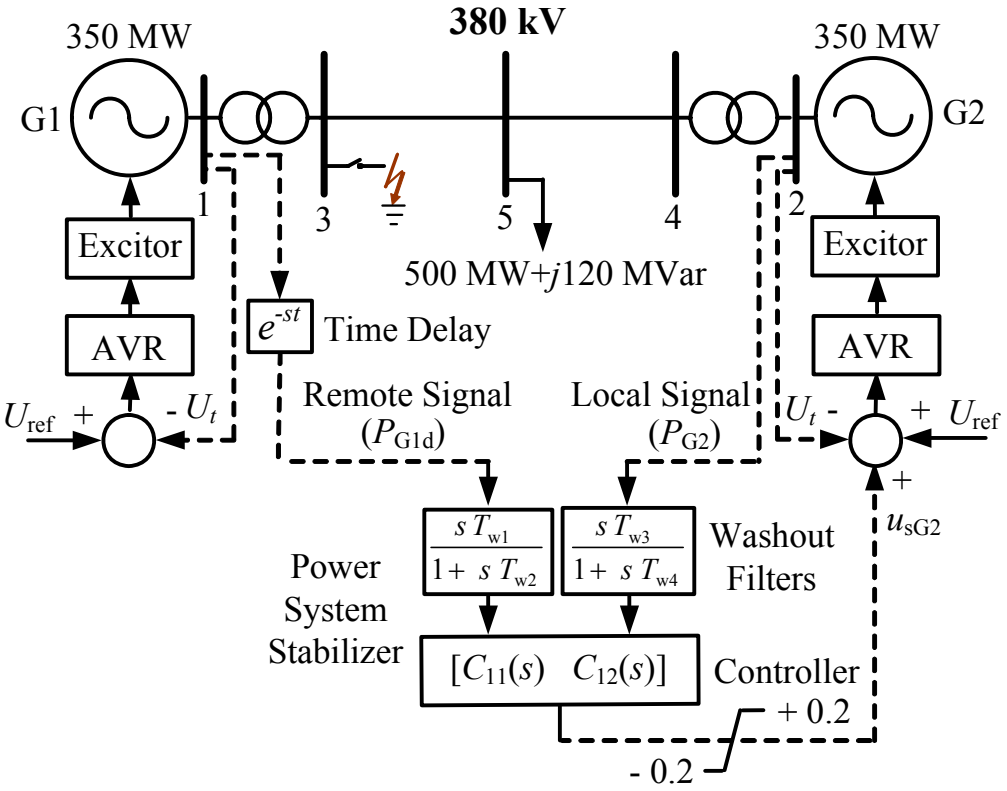

Figure 5.7 One line diagram of a test two-machine test power system together with the structure of generators and PSS

5.3.2 Design Results

The base operating conditions for the two-machine power system example, shown in Figure 5.7, are listed in Appendix A. The linearized equations for the considered test system, for the given parameter values, can be expressed in the general form of (4.4)-(4.6) as follows:

$$\dot{\mathbf{x}}(t) = \mathbf{A}\mathbf{x}(t) + \mathbf{B}_1\mathbf{w}(t) + \mathbf{B}_2\mathbf{u}(t) \tag{5.23}$$

$$\mathbf{z}(t) = \mathbf{C}_1\mathbf{x}(t) + \mathbf{D}_{11}\mathbf{w}(t) + \mathbf{D}_{12}\mathbf{u}(t) \tag{5.24}$$

$$\mathbf{y}(t) = \mathbf{C}_2\mathbf{x}(t) + \mathbf{D}_{21}\mathbf{w}(t) \tag{5.25}$$

where

$$\mathbf{x}(t) = \left[\mathbf{x}_{\mathrm{df}}^{\mathrm{T}}(t) \quad \mathbf{x}_{\mathrm{d}}^{\mathrm{T}}(t)\right]^{\mathrm{T}}, \qquad \mathbf{x}_{\mathrm{df}}(t) = \left[\mathbf{x}_{1}^{\mathrm{T}}(t) \quad \mathbf{x}_{2}^{\mathrm{T}}(t)\right]^{\mathrm{T}},$$

$$\mathbf{w}(t) = \left[\mathbf{w}_{1}^{\mathrm{T}}(t) \quad \mathbf{w}_{2}^{\mathrm{T}}(t)\right]^{\mathrm{T}}, \qquad \mathbf{u}(t) = \left[\mathbf{u}_{1}^{\mathrm{T}}(t) \quad \mathbf{u}_{2}^{\mathrm{T}}(t)\right]^{\mathrm{T}},$$

$$\mathbf{z}(t) = \left[\mathbf{z}_{1}^{\mathrm{T}}(t) \quad \mathbf{z}_{2}^{\mathrm{T}}(t)\right]^{\mathrm{T}}, \qquad \mathbf{y}(t) = \left[\mathbf{y}_{1\mathrm{d}}^{\mathrm{T}}(t) \quad \mathbf{y}_{2\mathrm{df}}^{\mathrm{T}}(t)\right]^{\mathrm{T}},$$

$$\mathbf{A} = \begin{bmatrix} \mathbf{A}_{\mathrm{df}} & \mathbf{0} \\ \mathbf{B}_{\mathrm{d}}\mathbf{C}_{21\mathrm{df}} & \mathbf{A}_{\mathrm{d}} \end{bmatrix}, \qquad \mathbf{A}_{\mathrm{df}} = \begin{bmatrix} \mathbf{A}_{11} & \mathbf{A}_{12} \\ \mathbf{A}_{21} & \mathbf{A}_{22} \end{bmatrix},$$

$$\mathbf{B}_1 = \mathrm{diag}\{\mathbf{B}_{11\mathrm{df}}, \mathbf{B}_{12\mathrm{df}}\}, \quad \mathbf{B}_2 = \mathrm{diag}\{\left[\mathbf{B}_{21\mathrm{df}} \quad \mathbf{B}_{\mathrm{d}}\mathbf{D}_{221\mathrm{df}}\right]^{\mathrm{T}}, \mathbf{B}_{22\mathrm{df}}\},$$

$$\mathbf{C}_1 = \mathrm{diag}\{\begin{bmatrix}\mathbf{D}_{\mathrm{d}}\mathbf{C}_{11\mathrm{df}} & \mathbf{C}_{\mathrm{d}}\end{bmatrix}, \mathbf{C}_{12\mathrm{df}}\}, \quad \mathbf{C}_2 = \mathrm{diag}\{\begin{bmatrix}\mathbf{D}_{\mathrm{d}}\mathbf{C}_{21\mathrm{df}} & \mathbf{C}_{\mathrm{d}}\end{bmatrix}, \mathbf{C}_{22\mathrm{df}}\},$$

$$\mathbf{D}_{11} = \mathrm{diag}\{\mathbf{D}_{111\mathrm{df}}, \mathbf{D}_{112\mathrm{df}}\}, \qquad \mathbf{D}_{12} = \mathrm{diag}\{\mathbf{D}_{\mathrm{d}}\mathbf{D}_{121\mathrm{df}}, \mathbf{D}_{122\mathrm{df}}\},$$

$$\mathbf{D}_{21} = \mathrm{diag}\{\mathbf{D}_{211\mathrm{df}}, \mathbf{D}_{212\mathrm{df}}\}$$

$u_1(t)$ and $u_2(t)$ are control inputs to generators G1 and G2 respectively. As in the considered two-machine power system of Figure 5.7, PSS is located at only generator G2, therefore, $u_1(t) = 0$ and $u_2(t) = u_{\mathrm{sG2}}(t)$. During the design of robust H_∞-based PSS controller, electrical power output signals from both generators are used as its feedback input signals, i.e., $\mathbf{y}(t) = [P_{\mathrm{G1d}}(t) \quad P_{\mathrm{G2}}(t)]^{\mathrm{T}}$. Electrical power output of generator G1 (P_{G1d}) is the remote measured feedback signal to the PSS which is located at the generator G2 while electrical power output of generator G2 (P_{G2}) is the local measured feedback signal to the PSS. Electrical power output signals from both generators, the output of the PSS together with the terminal voltage error signals, which are the inputs to the regulator of the exciter, are used as regulated signals within this design framework, i.e., $\mathbf{z}(t) = [P_{\mathrm{G1d}}(t) \quad P_{\mathrm{G2}}(t) \quad u_{\mathrm{sG2}}(t)]^{\mathrm{T}}$. $\mathbf{A}_{\mathrm{df}}$, $\mathbf{B}_{11\mathrm{df}}$, $\mathbf{B}_{12\mathrm{df}}$, $\mathbf{B}_{21\mathrm{df}}$, $\mathbf{B}_{22\mathrm{df}}$, $\mathbf{C}_{11\mathrm{df}}$, $\mathbf{C}_{12\mathrm{df}}$, $\mathbf{C}_{21\mathrm{df}}$, $\mathbf{C}_{22\mathrm{df}}$, $\mathbf{D}_{111\mathrm{df}}$, $\mathbf{D}_{112\mathrm{df}}$, $\mathbf{D}_{121\mathrm{df}}$, $\mathbf{D}_{122\mathrm{df}}$, $\mathbf{D}_{211\mathrm{df}}$, $\mathbf{D}_{212\mathrm{df}}$ are the constant matrices for the considered test system.

It is easy to check that ($\mathbf{A}$, $\mathbf{B}_2$) is stabilizable and ($\mathbf{A}$, $\mathbf{C}_2$) is detectable. This system is an open loop oscillatory system. The design procedure described in Chapter 4 (Section 4.2.2) is used to design the dynamic controller of the form of (4.7) and (4.8) such that minimum disturbance attenuation (from $\mathbf{w}(t)$ to $\mathbf{z}(t)$) is achieved. Riccati equations (4.18) and (4.19) are solved for positive, semi-definitive stabilizing solutions X_∞ and Y_∞ and then H_∞ controller is found by using (4.15)-(4.17) together with (4.7) and (4.8) by using Matlab Robust Control Tool box. Balanced residualization technique [18] is used to reduce the order of controllers at each of the stages of design.

5.3.2.1 Controller Design for Delay-Free System

Reduced-order H_∞-based PSS controller for delay-free (df) system, found in Chapter 4 (Section 4.3), is rewritten as follows:

$$\mathbf{C}_{\mathrm{df}}(s) = \left[11.714 \frac{1 + s\,0.004}{1 + s\,0.0501} \;\vdots\; 14.999 \frac{1 + s\,0.007}{1 + s\,0.0501} \right]$$

5.3.2.2 Design of Delay Compensator for Constant Delay System

By considering that the time delay in the remote input signal $P_{\mathrm{G1d}}(t)$ of the PSS controller is 700 ms and following the procedure described in Section 5.2.1, delay compensator designed is:

$$H_{\mathrm{c}}(s) = 0.1 \frac{(1 + s\,0.8469)}{(1 + s\,0.0749)}$$

5.3.2.3 Controller Design for Constant Delay System

By considering that the time delay in the remote input signal $P_{\mathrm{G1d}}(t)$ of the PSS controller is 700 ms and using 1$^{\mathrm{st}}$-order Pade approximation, the constant

matrices A_d, B_d, C_d, D_d for the time delay model of (5.2) and (5.3) are obtained as follows:

$$A_d = -\frac{2}{\tau} = -\frac{2}{0.7}, \quad B_d = 1, \quad C_d = \frac{4}{\tau} = \frac{4}{0.7}, \quad D_d = -1$$

The reduced-order H_∞-based PSS controller, obtained is:

$$\mathbf{C}_{cd}(s) = \left[4.613\frac{1+s\,14.71}{1+s\,28.59} \;\vdots\; 5.2983\frac{1+s\,11.85}{1+s\,28.59} \right]$$

In the above equation cd stands for constant delay.

5.3.2.4 Controller Design for Uncertain Delay System

By considering that the uncertainty in the time delay in the remote input signal $P_{G1d}(t)$ of the PSS controller ranges from 0 ms to 700 ms, (5.13) can be written as:

$$\tau = \bar{\tau} + \bar{\tau} p_\tau \delta_\tau = 0.35 + 0.35\delta_\tau$$

where, $\bar{\tau} = 0.35$ s, p_τ=1 and $\delta_\tau \in$ [-1, 1] . By substituting the values of $\bar{\tau}$ and p_τ into (5.22), the constant matrices A_d, B_d, C_d, D_d for the uncertain time delay model of (5.11) and (5.12), are obtained as follows:

$$A_d = \text{-}5.7142, \quad B_d = 11.4284, \quad C_d = 1, \quad D_d = \text{-}1$$

Reduced-order H_∞-based PSS controller obtained is:

$$\mathbf{C}_{ud}(s) = \left[32.19\frac{1+s0.031}{1+s\,3.264} \;\vdots\; 25.456\frac{1+s\,0.47}{1+s3.264} \right]$$

In the above equation ud stands for uncertain delay.

5.3.3 Time-Domain Simulation Results

In order to simulate the system behavior under large disturbance conditions, a balanced three-phase fault is applied at bus 3 as shown in Figure 5.7. The fault sequence of the three-phase fault used in these simulations is as follows:

Stage 1: The system is in pre-fault steady-state.

Stage 2: A three-phase fault occurs at t = 1.0 s.

Stage 3: The fault is cleared at t = 1.2 s.

Stage 4: The system is in a post-fault state.

5.3.3.1 Delay Compensator Case

The behaviors of deviation of electrical power output of generator G1 ($\Delta P_{G1}(t)$), with H_∞-based PSS controller designed without considering delay in its remote input signal, are shown in Figure 5.8. Figure 5.8 indicates that the response of $\Delta P_{G1}(t)$, with H_∞-based PSS controller designed without considering time delay, is better damped when no delay is included in the remote input signal of the controller during the simulation but becomes oscillatory when a constant delay of 700 ms is included in the remote input signal during the simulation. Figure 5.8 also indicates that for a constant delay of 700 ms included in the remote input signal during the simulation, the response of $\Delta P_{G1}(t)$ is better damped with the same PSS controller, designed without considering delay, when cascaded with the delay compensator designed for the delay of 700 ms.

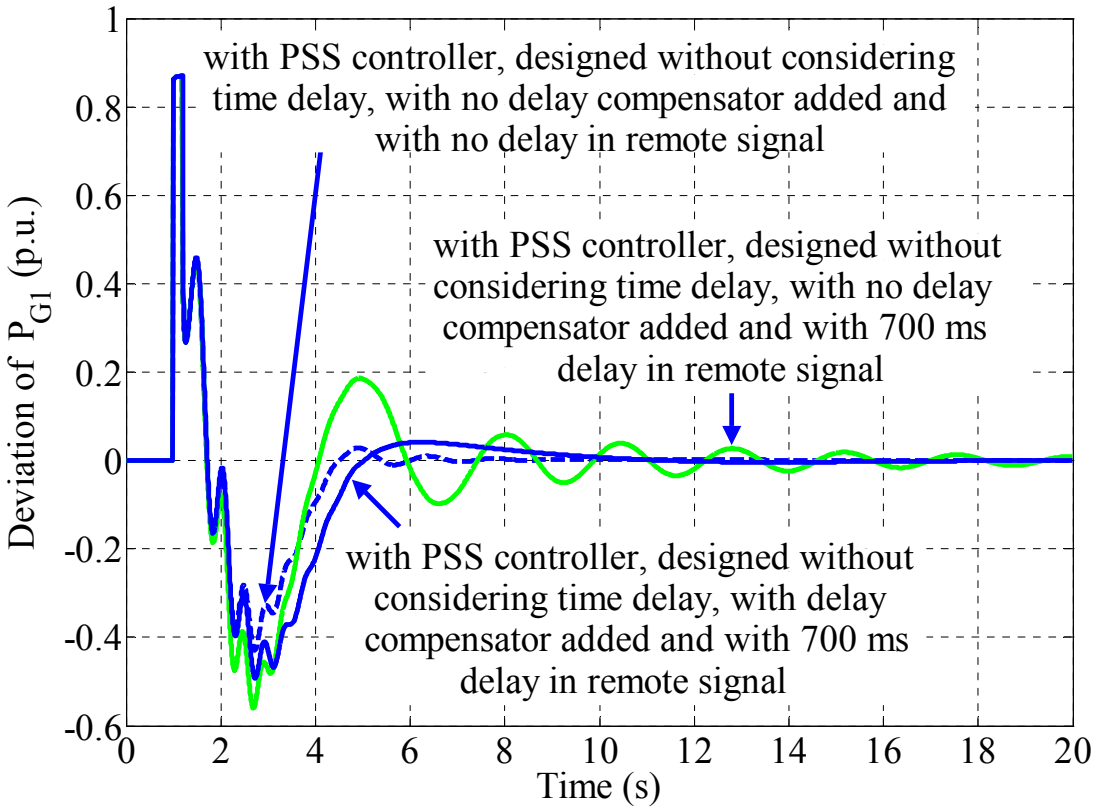

Figure 5.8 Deviations of P_{G1} following a three-phase fault with PSS controller, designed without considering time delay, with and without delay compensator added

5.3.3.2 Pade Approximation Method for Constant Delay Case

The behaviors of $\Delta P_{G1}(t)$, with H_∞-based PSS controllers designed without considering time delay and with considering constant time delay of 700 ms in their remote input signals, are shown in Figure 5.9. The figure shows that the response of $\Delta P_{G1}(t)$, with the H_∞-based PSS controller designed without considering time delay, is better damped when no time delay is included in the remote input signal during the simulation but becomes oscillatory when a constant delay of 700 ms is included in the remote input signal during the simulation. Figure 5.9 also indicates that for a constant delay of 700 ms included in the remote input signal during the simulation, the response of $\Delta P_{G1}(t)$, with PSS controller redesigned considering constant delay of 700 ms, is better

damped as compared to that with PSS controller designed without considering delay.

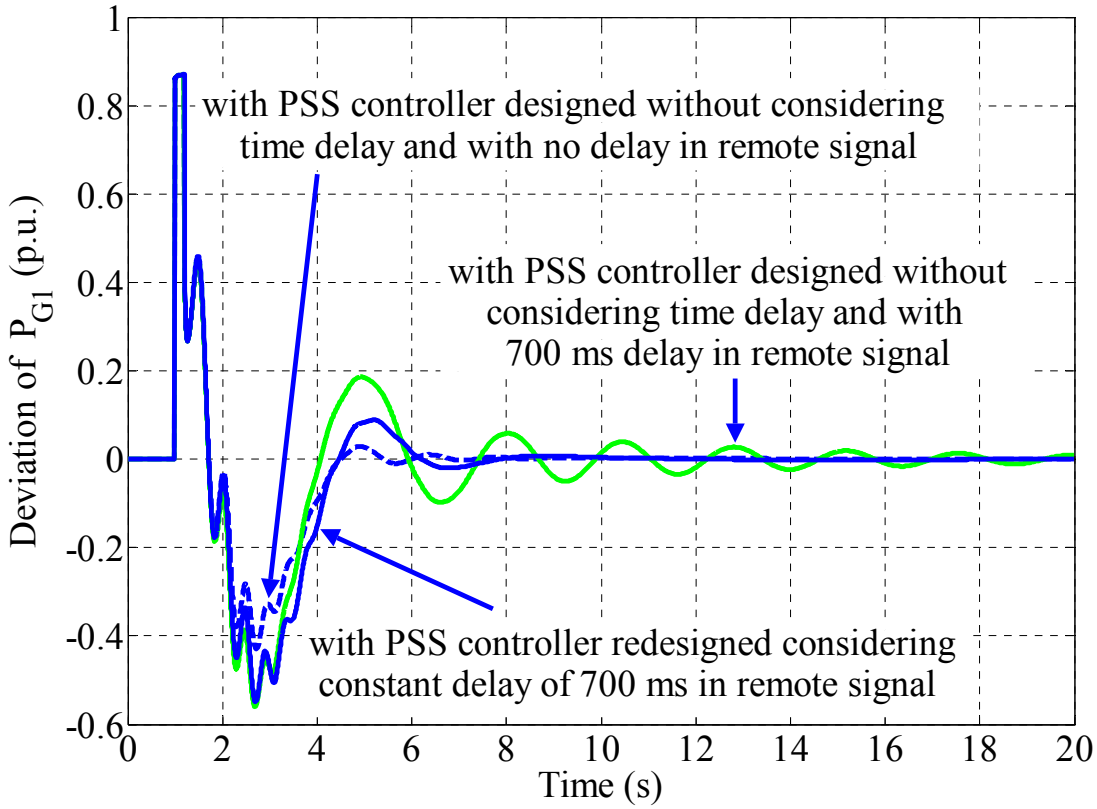

Figure 5.9 Deviations of P_{G1} following a three-phase fault with PSS controller designed without considering time delay and with PSS controller redesigned considering constant time delay

5.3.3.3 LFT Method for Time Delay Uncertainty Case

The behaviors of $\Delta P_{G1}(t)$, with H_∞-based PSS controllers designed without considering time delay and with considering uncertainty in the time delay in its remote input signal, are shown in Figure 5.10. Figure 5.10 indicates that for a time delay of 700 ms included in the remote input signal during the simulation, the response of $\Delta P_{G1}(t)$, with the PSS controller redesigned considering uncertainty in time delay, is better damped as compared to that with the PSS controller designed without considering delay.

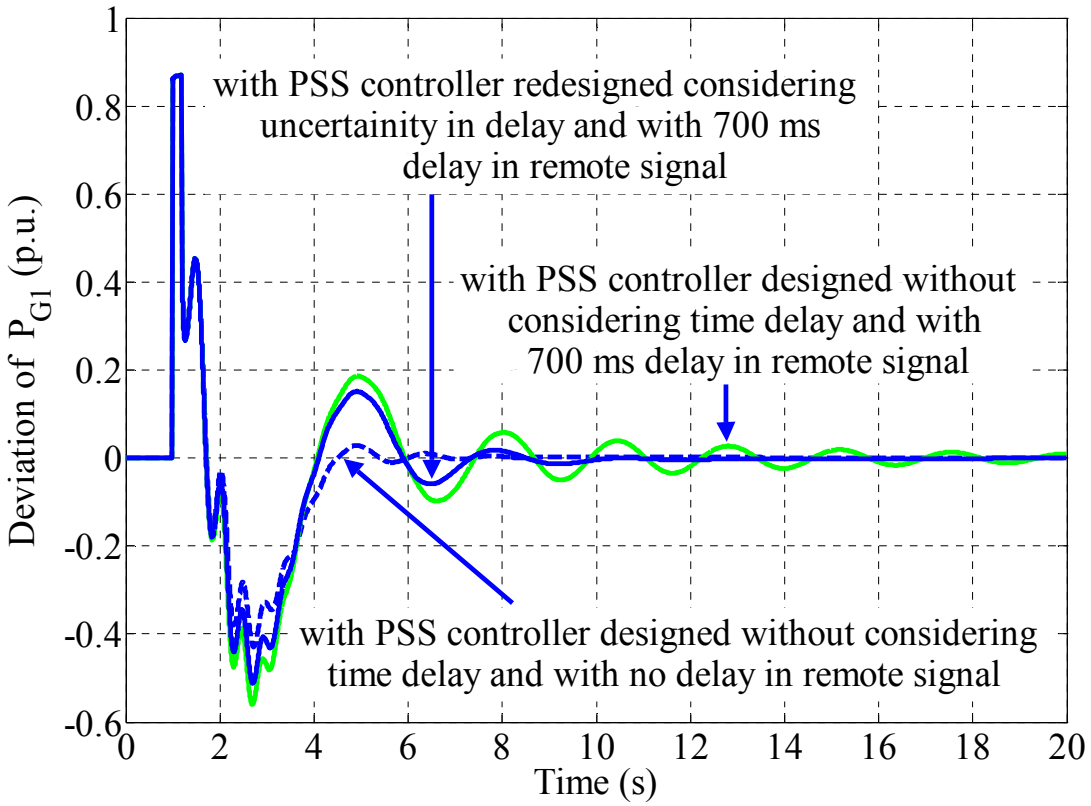

Figure 5.10 Deviations of P_{G1} following a three-phase fault with PSS controller designed without considering time delay and with PSS controller redesigned considering delay uncertainty

5.3.3.4 Robustness of Controller Regarding Time Delay

To further assess effectiveness of the proposed approach regarding robustness, transient performance indices are computed for different time delays. Transient performance index for electrical power output of the generator, following a three-phase short-circuit of 200 ms duration at bus 3 in Figure 5.7, is computed using the following equation:

$$I = \int_0^t \left| P_G(t) - P_{G0}(t) \right| \; dt \tag{5.26}$$

For comparison purpose, this index is normalized to the index for the mean value of delay range considered in the delay uncertainty case:

$$I_{\mathrm{N}} = \frac{I_{\mathrm{DD}}}{I_{\mathrm{MD}}} \tag{5.27}$$

where I_{N} is the normalized transient performance index, I_{DD} is transient performance index for different time delays and I_{MD} is transient performance index for the mean value of delay range considered in the delay uncertainty case.

The normalized transient performance indices for the electrical power output of the generator, for the time delays ranging from 0 to 700 ms, with the H_∞-based PSS controller, designed without considering delay, with the H_∞-based PSS controller designed without considering delay and cascaded with delay compensator, with the H_∞-based PSS controller designed considering constant delay, and with the H_∞-based PSS controller, designed considering uncertainty in delay are shown in Figure 5.11. It can be seen from the figure that the normalized transient performance indices for the PSS controller, designed considering uncertainty in delay, are more near to unity for the range of delays for which the controller is designed, as compared to those for the PSS controllers designed for the other three cases. This clearly indicates that, for different delays, the transient responses of the generator with the proposed PSS controller, designed considering delay uncertainty, are well damped as compared to those with the PSS controllers designed for the other three cases. This indicates that, the system behavior exhibits robustness with the proposed controller for the range of delays for which the controller is designed. This shows that the proposed PSS controller, designed considering delay uncertainty, is more robust regarding time delay uncertainty as compared to the PSS controllers designed for the other three cases.

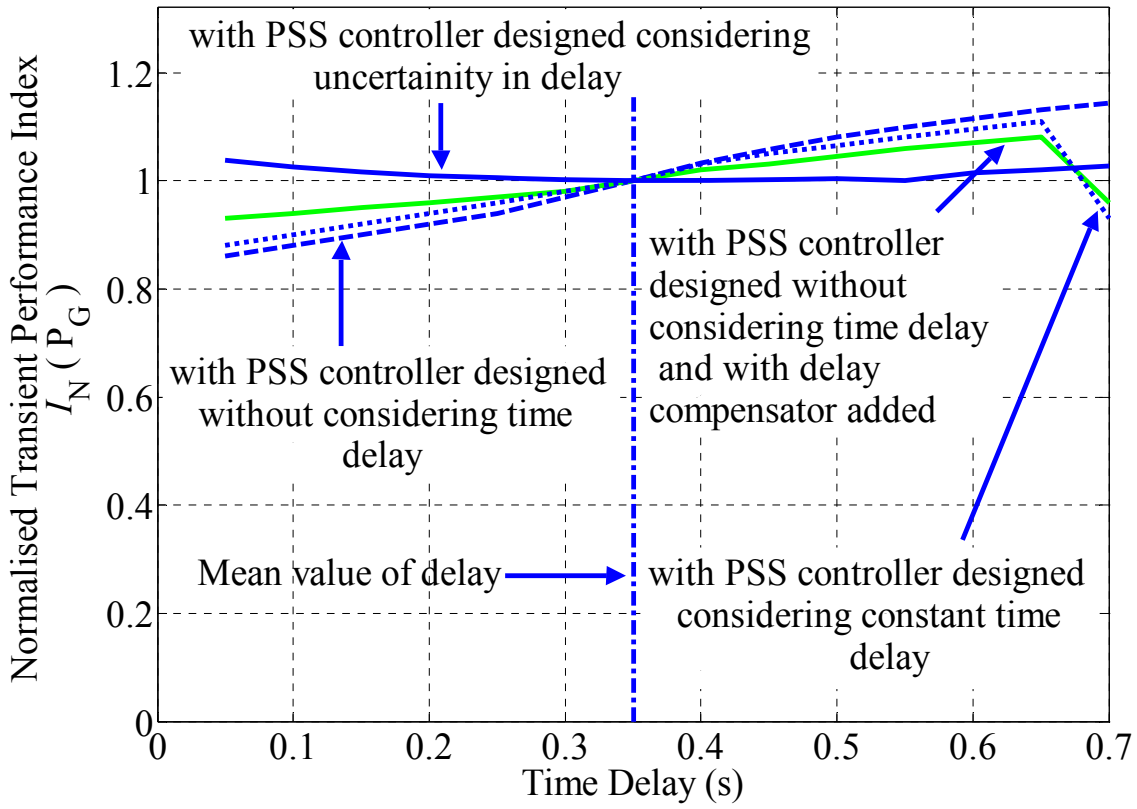

Figure 5.11 Normalized transient performance index (I_N) for electrical power generated (P_G)

5.4 Summary

An H_∞-based dynamic output feedback PSS controller design, using both local and remote signals as the feedback input signals, considering time delay in the remote signals, is developed in this chapter. Three methods for dealing with the effects of time delay are presented. In the first method, a delay compensator is designed and included with the controller, designed for the delay-free system, in the closed loop system in order to compensate the effects of considered constant time delay in the system. In the second method, the controller is redesigned for the delayed-input system considering constant delay in the system. In the third method, the controller is redesigned for the delayed-input system considering delay uncertainty in the system. The effectiveness of the

resulting controllers is demonstrated through digital simulation studies conducted on a test power system. The nonlinear simulations results have shown that the proposed controller is effective and robust in suppressing system oscillations despite the uncertainty in delay.

Chapter 6

Mode Selective Damping of Power System Electromechanical Oscillations

6.1 Introduction

This chapter presents the design of local decentralized H_∞-based PSS controllers, using selected suitable remote signals coming from the whole system, as supplementary inputs, for a separate better damping of specific inter-area modes. Each local PSS controller is designed separately for each of the inter-area modes of interest. The PSS controller uses only those local and remote input signals in which the assigned single inter-area mode is most observable and is located at a generator which is most effective in controlling that mode. The local PSS controller, designed for a particular single inter-area mode, also works mainly in a frequency band given by the natural frequency of the assigned mode. The locations of the local PSS controllers are obtained based on the amplitude gains of the frequency responses of the best-suited measurement to the inputs of all generators in the interconnected system. For the selection of suitable local and supplementary remote input signals, the features or measurements from the whole system are pre-selected first by engineering judgment and then using a clustering feature selection technique. Final selection of local and remote input signals is based on the degree of observability of the considered single mode in them. Digital simulation studies are conducted on a three-machine, three-area test power system to investigate the effectiveness of the proposed controllers during system disturbances.

6.2 Concept of Mode Selective Damping

The concept of mode selective damping is based on the following two-step decomposition strategy:

(i) The supplementary remote input signals to the PSS controllers, selected from the whole system, and the local input signals to the PSS controllers should contain maximum information of the assigned inter-area mode. Generators, chosen as PSS controllers' actuators, should act in each case on the assigned mode effectively;

(ii) Each of the local PSS controllers should work mainly in a frequency band given by the natural frequency of the assigned mode.

The decomposition strategy described above leads to a decentralized PSS controller structure in which each of the PSS controller systems, like the one in Figure 1.1, has to be established separately for each of the inter-area modes of interest. Each designed PSS controller uses local and supplementary remote input signals in which a particular single inter-area mode is most observable and the designed PSS controller is located at a generator which is most effective in controlling the same single inter-area mode. Therefore, the controller transfer function matrix $\mathbf{C}(s)$ attains a block diagonal structure:

$$\mathbf{C}(s) = \mathrm{diag}\{\mathbf{C}_{kk}(s)\} \tag{6.1}$$

Each of the PSS controllers belonging to a considered inter-area mode is to be interpreted as a central MIMO-type system, i.e., each controller sub-matrix $\mathbf{C}_{kk}$ is a full matrix.

6.3 Selection of Suitable Local and Remote Input Signals and Locations for PSS Controllers

6.3.1 Selection of Suitable Local and Remote Input Signals

The objective of mode selective damping, presented in Section 6.2, is to produce separate most effective damping of the inter-area modes of interest using local decentralized PSS controllers. The local and supplementary remote input signals to the local PSS controller should have maximum observability of the considered single inter-area mode in it. The entire data for the interconnected power system include features or measurements from power equipment such as the transmission lines, transformers, generators, and loads. Hence there is a large number of features in such an extensive power system. Therefore, before the selection of local and supplementary remote input signals based on the observability of considered single mode, the initial feature set is pre-selected first by engineering judgment and then using feature selection technique such as k-Means clustering algorithm.

6.3.1.1 Engineering Pre-Selection

First, a pre-selection is performed by engineering judgment, whereby only those features are used which are both available from the power utilities and measurable in the real power system. In this study, the selected features are:

- Real power outputs of generators
- Reactive power outputs of generators
- Real power over all transmission lines
- Reactive power over all transmission lines
- Real power transmitted between neighboring net groups/utilities
- Reactive power transmitted between neighboring net groups/utilities

- Bus voltages
- Bus voltage angles

The power flow between neighboring network groups is the sum of powers over all tie lines between them. The electrical power has been selected as a candidate for input to the controller. As electrical power includes the line current also, therefore, line current separately has not been selected as a candidate for input to the controller.

6.3.1.2 Feature Selection by k-Means Cluster Algorithm

The dimension of a pre-selected feature set can be reduced by eliminating the redundant features. Redundancy can be identified by a cluster algorithm. Using k-Means algorithm [47], the set of pre-selected features is divided into groups called clusters. A cluster consists of features that are similar statistically. Because of the similarity between the features within a cluster, one of them can be selected and the others can be treated as redundant information.

In clustering technique, first the distances between the feature vectors are computed. The features are then clustered according to the largest distance between any two clusters. If the feature vector $\mathbf{f}_g$ is the g^{th} object in cluster i and $\mathbf{f}_h$ is the h^{th} object in cluster k, then the distance between clusters i and k needs to be maximized, i.e., distance(i, k) = max(distance($\mathbf{f}_g$, $\mathbf{f}_h$)). After the completion of the process of clustering, one feature from each group is selected to form the new feature set. The k-Means cluster algorithm provides a feature ranking based on the distance between the cluster center and the features within the cluster. The feature that is closest to the center of its cluster is selected as the best feature in that cluster. As one feature is selected from one cluster, therefore, the total number of features selected from the entire data will be equal to the number of clusters.

In clustering algorithm described above, the features are selected based on the mathematical relationship only and does not include any physical or engineering intention. To include engineering knowledge in the selection process, the features inside the cluster are treated as physical measurements from the power system and judged by the criteria such as technical measurability, availability from the utilities, and expected usefulness for the oscillatory stability.

6.3.1.3 Final Selection of Local and Remote Feedback Input Signals

Final selection of local and remote signals can be carried out in a similar manner [48] based on the amplitude gains of the frequency responses of the features or measurements obtained using clustering technique. The resulting frequency response curves will exhibit resonance effects in the frequency bands of the selected modes. The signal best-suited as a local feedback input signal for a PSS controller is the one whose corresponding frequency response curve shows the maximum value out of frequency response curves for all other local measurements in the frequency band of the considered mode. Similarly, the most suitable supplementary remote feedback input signal for a local decentralized PSS controller is the signal with frequency response curve showing the maximum value out of frequency response curves for all other remote measurements in the frequency band of the considered mode.

6.3.2 Selection of Suitable Locations for PSS Controllers

According to [49], for a local mode, participation factor method gives correct results for predicting best PSS location. But for an inter-area mode this method may not give accurate prediction [49]. Participation factor method gives inaccurate or wrong predictions because this method does not take into

consideration PSS control effect information. Participation index include part information of modal controllability and observability [50]. The residue method is derived from the modal control theory of linear time-invariant systems.

In this study, the locations of local decentralized PSS controllers have been obtained in a similar manner [48] based on the amplitude gains of the frequency responses of the best-suited measurement to the inputs of all generators in the interconnected system. The resulting frequency response curves will exhibit resonance effects in the frequency bands of the selected modes. The generator best-suited as the location of a local decentralized PSS controller is the one for which the frequency response curve of the selected best-suited measurement shows the maximum value out of frequency response curves for all other generators in the frequency band of the considered mode. Note that, the best-suited measurement can be considered as the measurement whose corresponding frequency response curve shows the maximum value out of frequency response curves for all other final pre-selected measurements (measurements obtained after the application of clustering technique) in the frequency bands of all selected modes.

6.4 Design of Robust H_∞-based PSS Controllers for Power Systems

6.4.1 Problem Formulation

The overall extended system equations for the closed-loop system, developed in Chapter 4 (Section 4.2.1), are rewritten here as follows:

$$\dot{\tilde{\mathbf{x}}}(t) = \mathbf{A}_{\mathrm{cl}}\tilde{\mathbf{x}}(t) + \mathbf{B}_{\mathrm{cl}}\mathbf{w}(t) \tag{6.2}$$

$$\mathbf{z}(t) = \mathbf{C}_{\mathrm{cl}}\tilde{\mathbf{x}}(t) + \mathbf{D}_{\mathrm{cl}}\mathbf{w}(t) \tag{6.3}$$

where, $\tilde{\mathbf{x}}(t) = \left[\mathbf{x}^{\mathrm{T}}(t) \quad \mathbf{x}_{\mathrm{c}}^{\mathrm{T}}(t)\right]^{\mathrm{T}}$ is the augmented state vector for the closed-loop system, $\mathbf{x}(t)$ is the state vector of the open-loop system augmented by weighting functions, and $\mathbf{x}_{\mathrm{c}}(t)$ is the state vector of the controller.

The second decomposition step described in Section 6.2 can be realized by selecting the performance weighting functions in such a way that the PSS controller belonging to a particular assigned single mode works mainly in the frequency band of that mode. In this way, separate damping of each mode becomes possible. The design procedure described in Chapter 4 (Section 4.2.2) is used to design the dynamic controller of the form of (4.6) and (4.7) such that minimum disturbance attenuation (from $\mathbf{w}(t)$ to $\mathbf{z}(t)$) is achieved.

6.4.2 Sequential Design of Controllers

Decentralized control systems are systems with constraints on the structure of the control system. This chapter focuses on the decentralized control system with block diagonal structure. Standard optimal controller synthesis algorithms (e.g. H_∞ or H_2 synthesis) lead to multivariable (centralized) controllers and can not handle requirements for controllers with a specific structure [51]. It is logical and also practical, that not all PSSs are put into operation simultaneously, but one by one. Therefore, the design of PSS controllers should guarantee that the system is stable at least at each of the commissioning stages of PSSs [52]. In this study, therefore, sequential design [53], which is probably the most common and popular design method for decentralized control of real multivariable processes [51], is used to design the proposed PSS controllers.

In sequential design, one controller is designed at a time. The design of the first controller is carried out with all other control loops open. The first con-

trol loop is then closed in the design of the second controller and so on. Each local controller is, therefore, designed with the information of previously designed local controllers. Sequential design method, therefore, includes the dynamics of the interactions from the other controllers at each design stage.

6.5 Application Results

6.5.1 Power System Simulation Model

Three-machine, three-area power system example, shown in Figure 6.1, is selected to apply the robust dynamic output feedback control design approach presented in Section 6.4 and to illustrate the effectiveness of the proposed robust H_∞ controller for a separate better damping of specific inter-area modes. The considered test system has three equivalent synchronous generators each representing one of the three areas. All generators are equipped with identical IEEE standard exciters (IEEE type DC1A excitation system). Loads are connected to buses 4, 5, 6, and 7. Detailed information about this test system including the controllers and their parameter values can be found in Appendix B. The base operating conditions for the test system are also listed in Appendix B. Moreover, for all simulation studies as well as for the PSS design, the structure of the i^{th}-generator together with an n_{ci}^{th}-order PSS controller in a multi-machine power system, presented in Chapter 4, Section 4.2.1 (Figure 4.1), is considered. For illustrative purposes and from a sensitivity study, the damping ratio limit criterion for the test system, considered in this study, is defined as greater than 10% for all oscillatory modes and for all operating conditions including element outage. This is reasonable, since this system has a similar structure compared to some existing power systems, such as the Argentinean network which has a similar damping limit criterion [54].

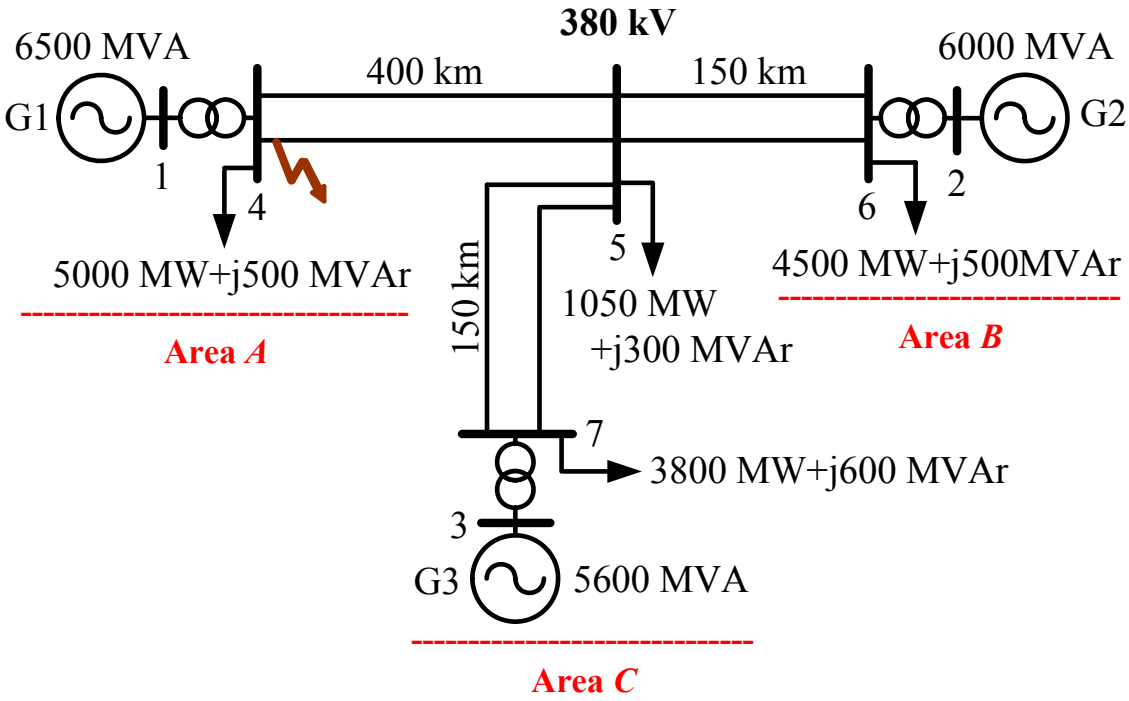

Figure 6.1 One line diagram of a test three-machine, three-area power system

The profile of two most weakly damped rotor angle low-frequency electromechanical inter-area modes of oscillation, for the nominal power flow solution of the test system, is provided in Table 6.1. As there are two weakly damped inter-area modes in the considered test system, therefore, the decomposition strategy described in Section 6.2 suggests that there will be two PSS controllers for the considered test system.

Table 6.1 Weakly damped inter-area modes of test system

Mode No.	Inter-area Modes	Damping Ratio (%)	Frequency (Hz)
1	-0.4070+4.2293	9.58	0.67
2	-0.3810+5.8765	6.47	0.92

6.5.2 Selection of Suitable Local and Remote Input Signals and Locations for PSS Controllers in the Test System

Following the procedure described in Section 6.3, the results for the selection of suitable local and supplementary remote signals and locations for the PSS controllers are given in the following sub-sections.

6.5.2.1 Engineering Pre-Selection of Features or Measurements

Following the procedure described in Section 6.3.1.1, the features selected are listed in Table 6.2.

Table 6.2 Features from the test system

#	Feature Description	Symbol	No.
1	Real power output of generators	P	03
2	Reactive power output of generators	Q	03
3	Real power over transmission lines	P	03
4	Reactive power over transmission lines	Q	03
5	Bus voltages	U	07
6	Bus voltage angles	θ_U	07
Total number of features			26

6.5.2.2 Feature Selection by k-Means Cluster Algorithm

The features selected by engineering judgment are reduced to a small set of features using k-Means cluster algorithm. The data set used for clustering is in the form of a feature matrix of dimension $p \times n$, where p represents the number of patterns and n represents the number of original feature vectors. In this study, the patterns represent the values of pre-selected features, at different

time instants in the time domain simulation. In practice, the fault can occur at any bus in the system. Therefore, it is necessary to carry out clustering of features, for fault at all buses in the system. The data set, in this study, is clustered into three clusters for a short-circuit fault of 100 ms duration on the transmission lines near buses 4, 5, 6, and 7, with the fault cleared by opening the circuit breakers of the faulty line, in the test system. Including engineering knowledge in the selection process, final pre-selected features obtained are as given in the Table 6.3. The amplitude gains of frequency responses of final pre-selected features or measurements, listed in Table 6.3, are shown in Figure 6.2. These frequency response curves exhibit resonance effects in the frequency bands of two weakly damped inter-area modes in the test system.

Table 6.3 Final pre-selected features

#	**Final Pre-selected Features**
1	Real power through line between nodes 5 and 6 (P_{56})
2	Voltage at node 2 (U_2)
3	Reactive power supplied by generator G3 (Q_{G3})
4	Voltage angle at node 1 (θ_{U1})
5	Voltage at node 5 (U_5)
6	Real power delivered by generator G2 (P_{G2})
7	Reactive power delivered by generator G2 (Q_{G2})
8	Real power through line between nodes 5 and 7 (P_{57})
9	Real power delivered by generator G3 (P_{G3})

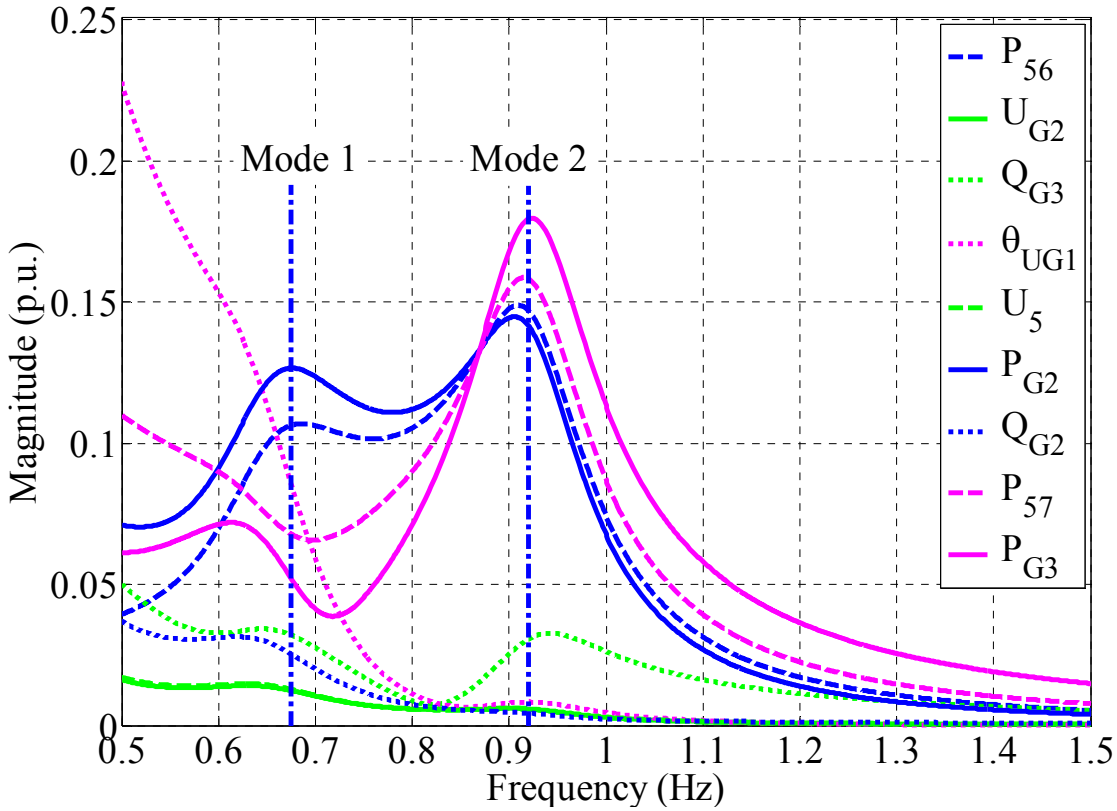

Figure 6.2 Frequency responses of pre-selected measurements

6.5.2.3 Selection of Suitable Locations for PSS Controllers in the Test System

The results shown in Figure 6.2 indicate that in the frequency bands of two most weakly damped inter-area modes in the test system, the frequency response curve for the electrical power output of generator G3 (P_{G3}) has maximum value out of frequency response curves for all other final pre-selected measurements (measurements obtained after the application of clustering technique). Therefore, according to the procedure described in Section 6.3.2, P_{G3} is considered as the best-suited measurement, whose frequency responses need to be obtained to the inputs at generators G1, G2, and G3 for finding the suitable locations of two local decentralized PSS controllers in the test system.

The frequency responses of P_{G3} to the inputs at generators G1, G2, and G3, with no PSS controller located in the test system, are shown in Figure 6.3. These frequency response curves exhibit resonance effects in the frequency bands of the two weakly damped inter-area modes in test system. It is clear from the Figure 6.3 that for the inter-area mode 1 having the frequency 0.67 Hz, the frequency response curve of P_{G3} for an input to generator G2 has maximum value out of frequency response curves for inputs to generators G1 and G3. This indicates that the generator G2 is highly effective and suitable as the location of PSS controller to be designed to damp the inter-area mode 1. Figure 6.3 also shows that for the inter-area mode 2 having the frequency 0.92 Hz, the frequency response curve of P_{G3} for an input to generator G3 has maximum value out of frequency response curves for inputs to generators G1 and G2. This indicates that the generator G3 is highly effective and suitable as the location of PSS controller to be designed to damp the inter-area mode 2.

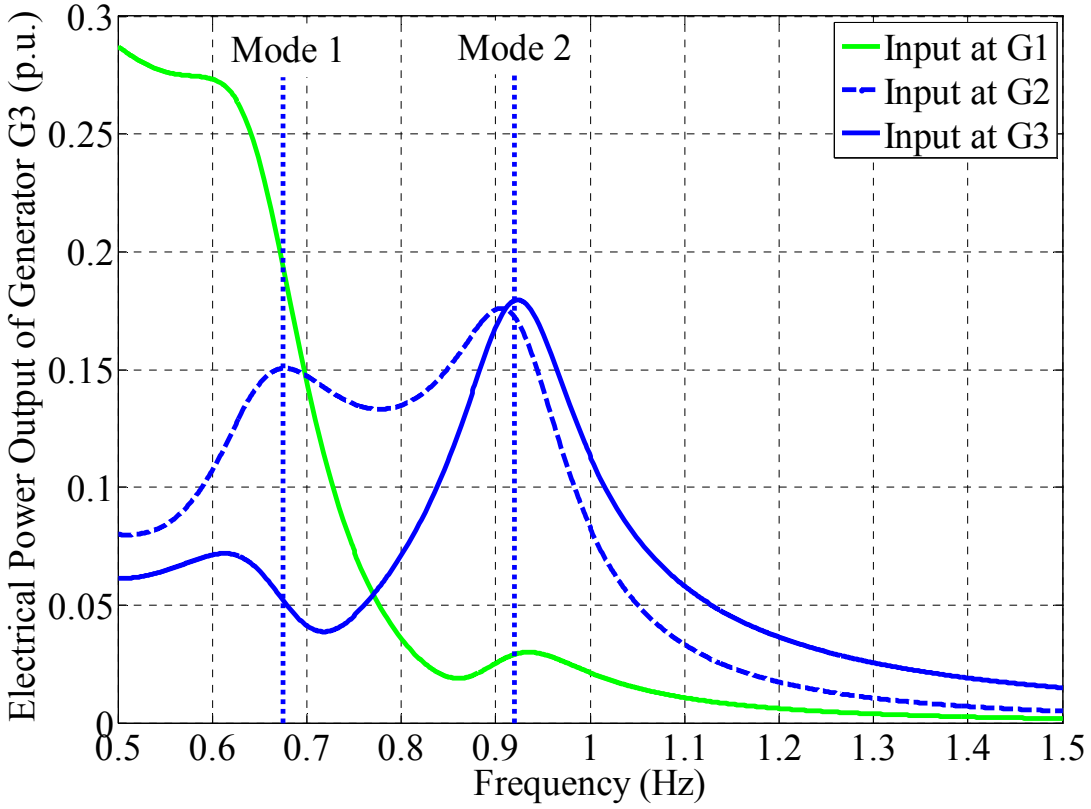

Figure 6.3 Frequency responses of P_{G3} for inputs at generators G1, G2, and G3 with no PSS controller located in the test system

6.5.2.4 Final Selection of Suitable Local and Remote Input Signals

Final selection of local and remote signals is carried out, as described in Section 6.3.1.3, on basis of the amplitude gains of the frequency responses (Figure 6.2) of the final pre-selected features or measurements, i.e., the measurements obtained after the application of clustering technique. Figure 6.2 indicates that for the PSS controller, to be designed for inter-area mode 1, having suitable location G2, local signals are P_{G2}, Q_{G2}, and U_{G2} whereas the others are remote signals. Similarly, for the PSS controller, to be designed for inter-area mode 2, having suitable location G3, local signals are P_{G3}, Q_{G3} whereas the others are remote signals.

The results shown in Figure 6.2 indicate that in the frequency band of the inter-area mode 1, the frequency response curve for the electrical power output of generator G2 (P_{G2}) has maximum value out of frequency response curves for all other local measurements and the frequency response curve for the real power through transmission line between buses 5 and 6 (P_{56}) has maximum value out of frequency response curves for all other remote measurements. This indicates that P_{G2} is suitable as a local feedback input signal and P_{56} is suitable as a supplementary remote feedback input signal for a local decentralized PSS controller to be designed to damp the inter-area mode 1. Figure 6.2 also shows that in the frequency band of the inter-area mode 2, the frequency response curve for P_{G3} has maximum value out of frequency response curves for all other local measurements and the frequency response curve for the real power through transmission line between buses 5 and 7 (P_{57}) has maximum value out of frequency response curves for all other remote measurements. This indicates that P_{G3} is suitable as a local feedback input signal and P_{57} is suitable as a supplementary remote feedback input signal for a local decentralized PSS controller to be designed to damp the inter-area

mode 2. Table 6.4 provides the results for the selection of suitable local and remote input signals and locations of local decentralized PSS controllers, to be designed to damp out the two most weakly damped inter-area modes in the considered test system.

Table 6.4 Selected suitable local and remote signals and locations for the PSS controllers

Mode No.	Local Signals to Controllers	Remote Signals to Controllers	Locations of Controllers to be Designed
1	P_{G2}	P_{56}	Generator G2
2	P_{G3}	P_{57}	Generator G3

6.5.3 Design Results

During the design of robust H_∞-based PSS controller for the inter-area mode 1, P_{G2} and P_{56} are used as its feedback input signals, i.e., $\mathbf{y}(t) = \begin{bmatrix} P_{G2}(t) & P_{56}(t) \end{bmatrix}^T$. The measured signals P_{G2} and P_{56}, the output of the PSS (u_{sG2}) together with the terminal voltage error signals, which are the inputs to the regulator of the exciter, are used as regulated signals within this design framework, i.e., $\mathbf{z}(t) = \begin{bmatrix} P_{G2}(t) & P_{56}(t) & u_{sG2}(t) \end{bmatrix}^T$. Similarly, during the design of robust H_∞-based PSS controller for the inter-area mode 2, P_{G3} and P_{57} are used as its feedback input signals, i.e., $\mathbf{y}(t) = \begin{bmatrix} P_{G3}(t) & P_{57}(t) \end{bmatrix}^T$. The measured signals P_{G3} and P_{57}, the output of the PSS (u_{sG3}) together with the terminal voltage error signals, which are the inputs to the regulator of the exciter, are used as regulated signals within this design framework, i.e., $\mathbf{z}(t) = \begin{bmatrix} P_{G3}(t) & P_{57}(t) & u_{sG3}(t) \end{bmatrix}^T$. The design procedure described in Chapter 4 (Section 4.2.2) is used to design the dynamic controllers of the form of (4.7)

and (4.8) such that minimum disturbance attenuation (from $\mathbf{w}(t)$ to $\mathbf{z}(t)$) is achieved. Balanced residualization technique [18] is used to reduce the order of controllers at each of the stages of design.

6.5.3.1 Sequential Design of PSS Controllers

As two PSS controllers need to be designed for the test system, the sequential design can, therefore, be performed in two different ways, depending on the sequence in which the controllers are designed. Table 6.5 provides description of the sequences for the design of controllers in the two possible sequential designs. Note that the first control loop consists of plant and the PSS controller, designed for inter-area mode 1, located at G2 and the second control loop consists of plant and the PSS controller, designed for inter-area mode 2, located at G3.

Table 6.5 Sequences for design of controllers in two possible sequential designs

Sequential Design No.	Sequences for the Design of Controllers
1	(i) PSS controller for the inter-area mode 1 is designed first with keeping the second control loop open. (ii) PSS controller for the inter-area mode 2 is then designed with keeping the first control loop closed, i.e., with the already designed PSS controller for the inter-area mode 1 located at generator G_2 in the test system.

2	(i) PSS controller for the inter-area mode 2 is designed first with keeping the first control loop open. (ii) PSS controller for the inter-area mode 1 is then designed with keeping the second control loop closed, i.e., with the already designed PSS controller for the inter-area mode 2 located at generator G_3 in the test system.

First Sequential Design

In the first sequential design, the PSS controller for the inter-area mode 1 is designed first with keeping the second control loop open in the test system. The H_∞-based PSS controller for the inter-area mode 1 obtained is:

$$\mathbf{C}_{11}(s) = \left[2.878 \frac{(1+s\,0.5814)(1+\,s1.8918)}{(1+s\,0.5984)(1+s\,1.7559)} \;\vdots\; 11.49 \frac{(1+s0.5459)(1+s\,7.000)}{(1+s\,0.5984)(1+s\,1.7559)} \right]$$

Table 6.6 provides the profile of two most weakly damped inter-area modes of the test system with controller designed for inter-area mode 1, with controller designed for inter-area mode 1 and controller designed for inter-area mode 2, and with controller redesigned for inter-area mode 1 and controller designed for inter-area mode 2. Figure 6.4 shows the frequency responses of P_{G3} to the inputs at generators G1, G2, and G3 with the controller designed for the inter-area mode 1 located at G_2 in the test system. The results given in Table 6.6 and Figure 6.4 indicate that the damping of inter-area modes 1 and 2 has increased slightly when the controller designed for mode 1 is incorporated in the test system.

Table 6.6 Weakly damped inter-area modes in test system

Mode No.	With Controller Designed for Mode 1			With Controllers Designed for Modes 1 and 2			With Controller Redesigned for Mode 1 and Controller Designed for Mode 2		
	Inter-area Modes	ξ (%)	Freq. (Hz)	Inter-area Modes	ξ (%)	Freq. (Hz)	Inter-area Modes	ξ (%)	Freq. (Hz)
1	-0.5964+4.1297	14.29	0.66	-0.7245+4.3765	16.33	0.70	-1.3874+4.3612	30.32	0.69
2	-0.5339+5.8101	9.15	0.92	-3.1923+6.7959	42.52	1.08	-3.2558+6.8934	42.71	1.10

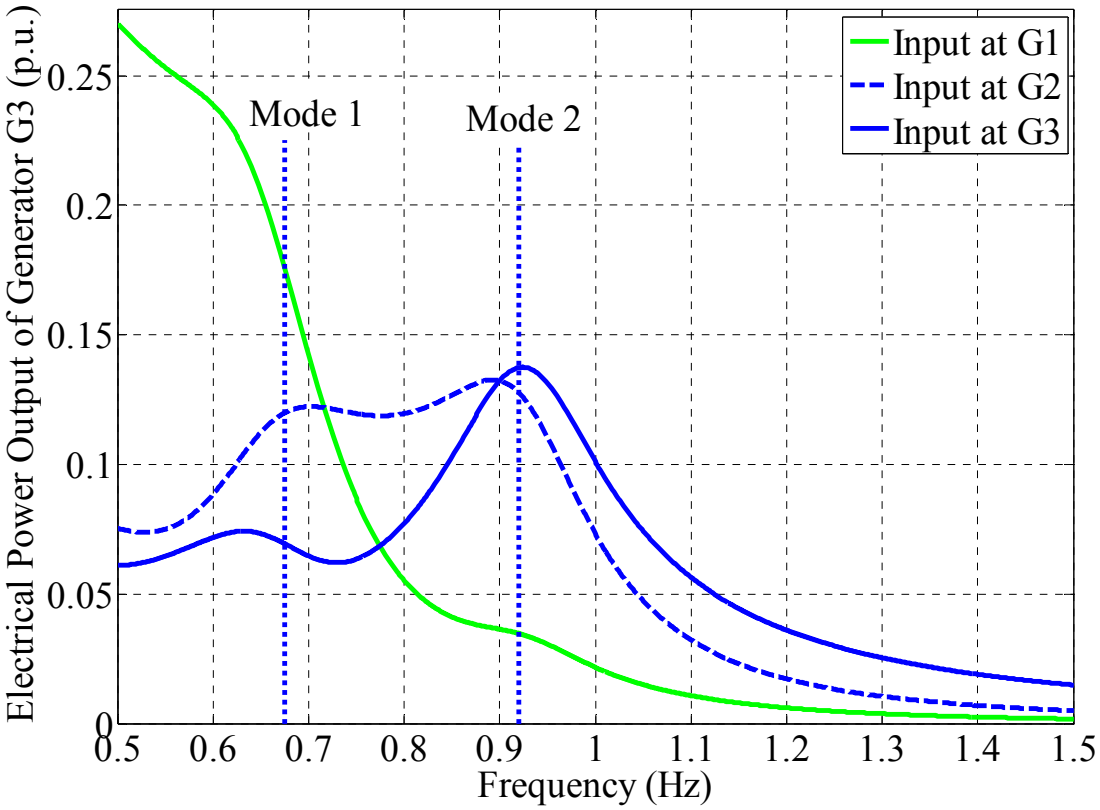

Figure 6.4 Frequency responses of P_{G3} for inputs at generators G1, G2, and G3 with the controller designed for inter-area mode 1 located in test system

The PSS controller for the inter-area mode 2 is now designed with keeping the first control loop closed, i.e., with the already designed controller for the inter-area mode 1 located at G2 in the test system. The H_∞-based PSS controller for the inter-area mode 2 obtained is:

$$\mathbf{C}_{22}(s)=\left[\,12.30\frac{(1+s\,0.2014)(1+s\,0.3014)}{(1+s\,0.5857)(1+s\;0.0185)}\;\vdots\;2.1\frac{(1+s\,0.91)(1+s\,0.85)}{(1+s\,0.5857)(1+s\;0.0185)}\,\right]$$

The frequency responses of P_{G3} to the inputs at generators G1, G2, and G3, with the controllers designed for the inter-area modes 1 and 2 located at G2 and G3 respectively in the test system, are shown in Figure 6.5. The results given in Table 6.6 and Figure 6.5 indicate that the damping of inter-area mode 2 has increased significantly whereas the damping of inter-area mode 1 has increased slightly when the controller designed for inter-area mode 2 is incorporated at G3 in the test system which has already controller for inter-area mode 1 located in it at G2. This indicates that the controller designed for inter-area mode 2 has contributed significantly to the damping of inter-area mode 2.

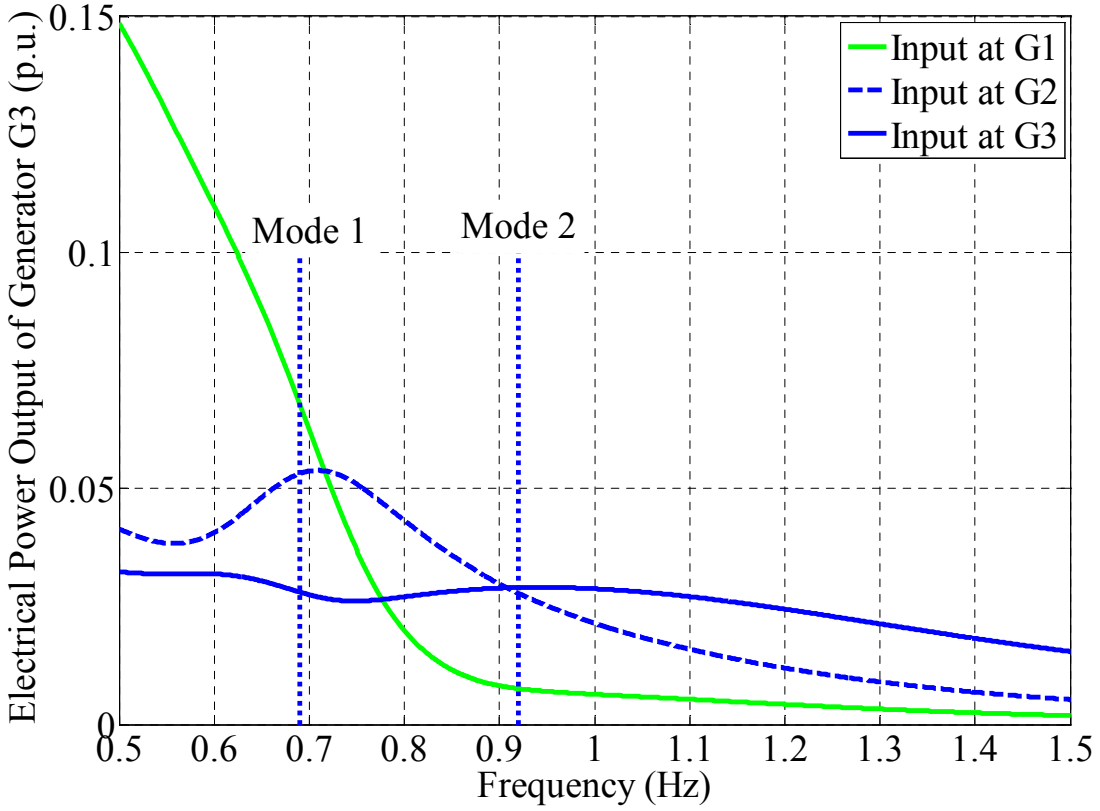

Figure 6.5 Frequency responses of P_{G3} for inputs at generators G1, G2, and G3 with the controllers designed for inter-area modes 1 and 2 located in the test system

The results given in Table 6.6 and Figure 6.5 indicate that the inter-area mode 1 still needs damping improvement. The controller for inter-area mode 1 is, therefore, designed again with keeping the second control loop closed, i.e., with the already designed controller for inter-area mode 2 located at G3 in the test system. The redesigned H_∞-based PSS controller for the inter-area mode 1 obtained is:

$$\mathbf{C}_{11}^{\text{new}}(s) = \left[12.158 \frac{(1+s\,2.0814)(1+\ s1.7218)}{(1+s\,0.5084)(1+s\,0.3559)} \;\vdots\; 10.19 \frac{(1+s0\,.5449)(1+s\,4.000)}{(1+s\,0.5084)(1+s\,0.3559)} \right]$$

The frequency responses of P_{G3} to the inputs at generators G1, G2, and G3, with the controller redesigned for the inter-area mode 1 located at G2 and the controller designed for the inter-area mode 2 located at G3 in the test system, are shown in Figure 6.6. The results given in Table 6.6 and Figure 6.6 show that the damping of inter-area mode 1 has increased significantly whereas the damping of inter-area mode 2 has increased only slightly when the controller redesigned for inter-area mode 1 is incorporated at G2 in the test system which has already controller for inter-area mode 2 located in it at G3. This indicates that the controller redesigned for inter-area mode 1 has contributed significantly to the damping of inter-area mode 1. Table 6.6 and Figure 6.6 also indicate that the damping of inter-area modes 1 and 2 has increased significantly when the two H_∞-based PSS controllers, designed for the two most weakly damped inter-area modes of the test system, are incorporated in the test system.

Note that in the first sequential design of PSS controllers, the controller for inter-area mode 1 is redesigned. This is the case only for the test system considered in this study. It is not necessary that the controller is redesigned in other test systems also.

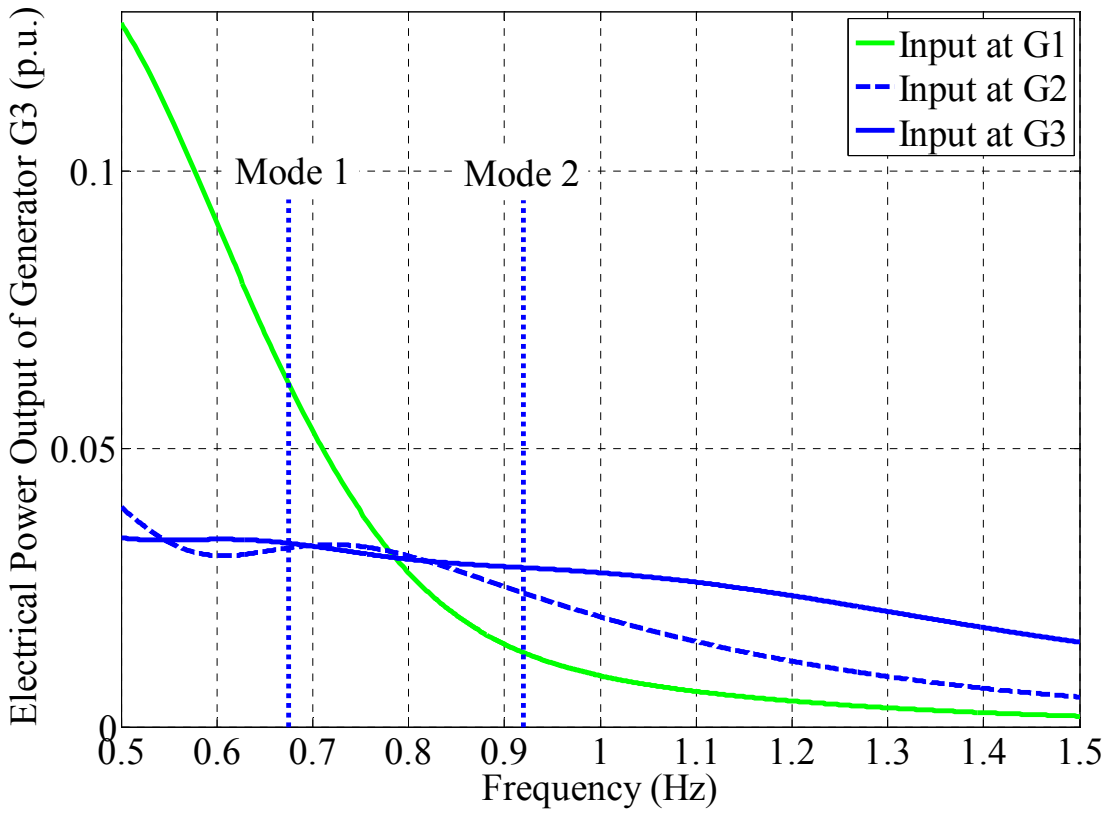

Figure 6.6 Frequency responses of P_{G3} for inputs at generators G1, G2, and G3 with the controller redesigned for inter-area mode 1 and the controller designed for inter-area mode 2 located in the test system

Second Sequential Design

In the second sequential design, the PSS controller for the inter-area mode 2 is designed first with keeping the fist control loop open in the test system. The H_∞-based PSS controller for the inter-area mode 2 obtained is:

$$\mathbf{C}_{22}(s) = \left[15.302 \frac{(1+s\,0.1591)(1+\,s0.6014)}{(1+s\,0.1857)(1+s\,0.0183)} \;\vdots\; 2.100 \frac{(1+s0.5000)(1+s\,0.7500)}{(1+s\,0.1857)(1+s\,0.0183)} \right]$$

Table 6.7 provides the profile of two most weakly damped inter-area modes of the test system with the controller designed for the inter-area mode 2 and with the controller designed for inter-area mode 2 and the controller designed for inter-area mode 1. Figure 6.7 shows the frequency responses of P_{G3} to the inputs at generators G1, G2, and G3 with the controller designed for the

inter-area mode 2 located at G_3 in the test system. The results given in Table 6.7 and Figure 6.7 indicate that damping of inter-area mode 2 has increased significantly whereas the damping of mode 1 has increased slightly when the controller designed for mode 2 is incorporated at G3 in the test system.

Table 6.7 Weakly damped inter-area modes in test system

Mode No.	With Controller Designed for Mode 2			With Controllers Designed for Modes 2 and 1		
	Inter-area Modes	ξ (%)	Freq. (Hz)	Inter-area Modes	ξ (%)	Freq. (Hz)
1	-0.5152+4.3498	11.76	0.69	-1.4108+3.9906	33.33	0.64
2	-2.0602+6.7564	29.17	1.08	-2.2634+6.8972	31.18	1.10

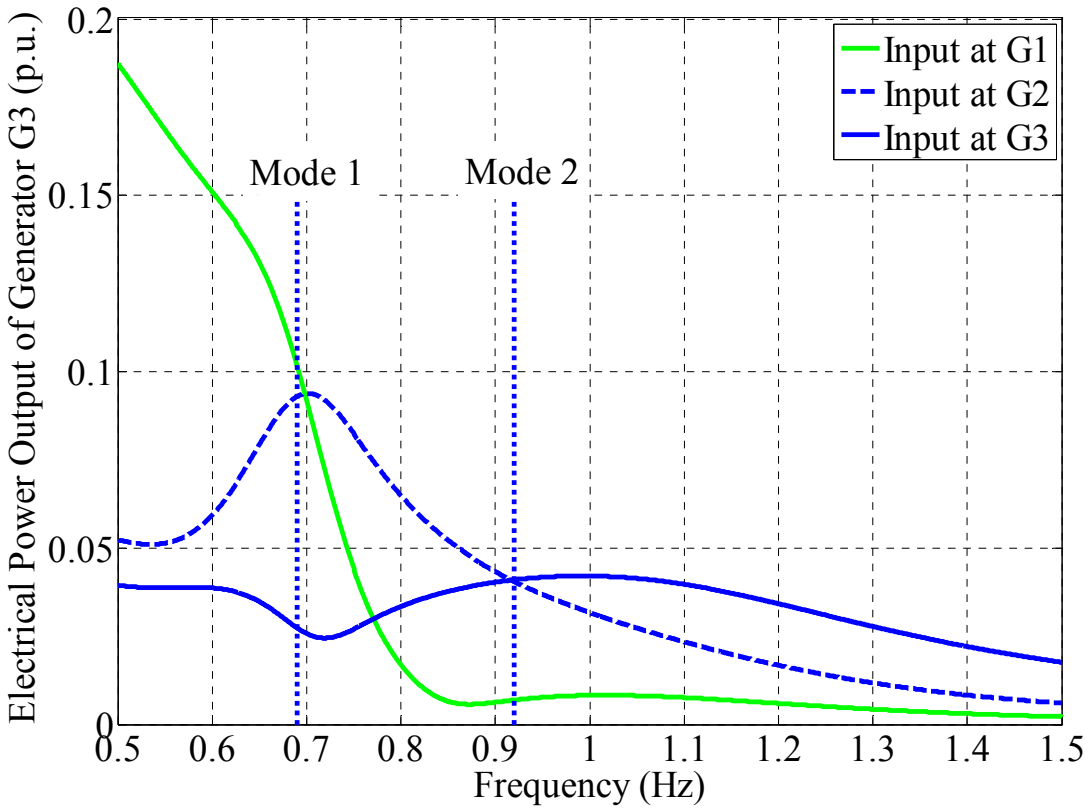

Figure 6.7 Frequency responses of P_{G3} for inputs at generators G1, G2, and G3 with the controller designed for inter-area mode 2 located in the test system

The PSS controller for the inter-area mode 1 is now designed with keeping the second control loop closed, i.e., with the already designed controller for the inter-area mode 2 located at G3 in the test system. The H_∞-based PSS controller for the inter-area mode 1 obtained is:

$$\mathbf{C}_{11}(s) = \left[30.878 \frac{(1+s\,0.6819)(1+s\,2.1918)}{(1+s\,0.5984)(1+s\,1.7559)} \;\vdots\; 3.49 \frac{(1+s\,5.1459)(1+s\,7.000)}{(1+s\,0.5984)(1+s\,1.7559)} \right]$$

The frequency responses of P_{G3} to the inputs at generators G1, G2, and G3, with the controllers designed for the inter-area modes 2 and 1 located at G3 and G2 respectively in the test system, are shown in Figure 6.8. The results given in Table 6.7 and Figure 6.8 show that the damping of inter-area mode 1 has increased significantly whereas the damping of inter-area mode 2 has increased slightly when the controller designed for mode 1 is incorporated at G2 in the test system which has already controller for inter-area mode 2 located in it at G3. This indicates that the controller designed for mode 1 has contributed significantly to the damping of inter-area mode 1. The results also indicate that the damping of inter-area modes 1 and 2 has increased significantly when the two H_∞-based PSS controllers, designed for the two most weakly damped inter-area modes of the test system, are incorporated in the test system.

Comparison of results for the first and second sequential designs indicate that the damping of inter-area mode 1 has increased slightly more in the second sequential design than that in the first sequential design whereas the damping of inter-area mode 2 has increased significantly more in the first sequential design than that in the second sequential design. Therefore, it is concluded that first sequential design is better than the second one.

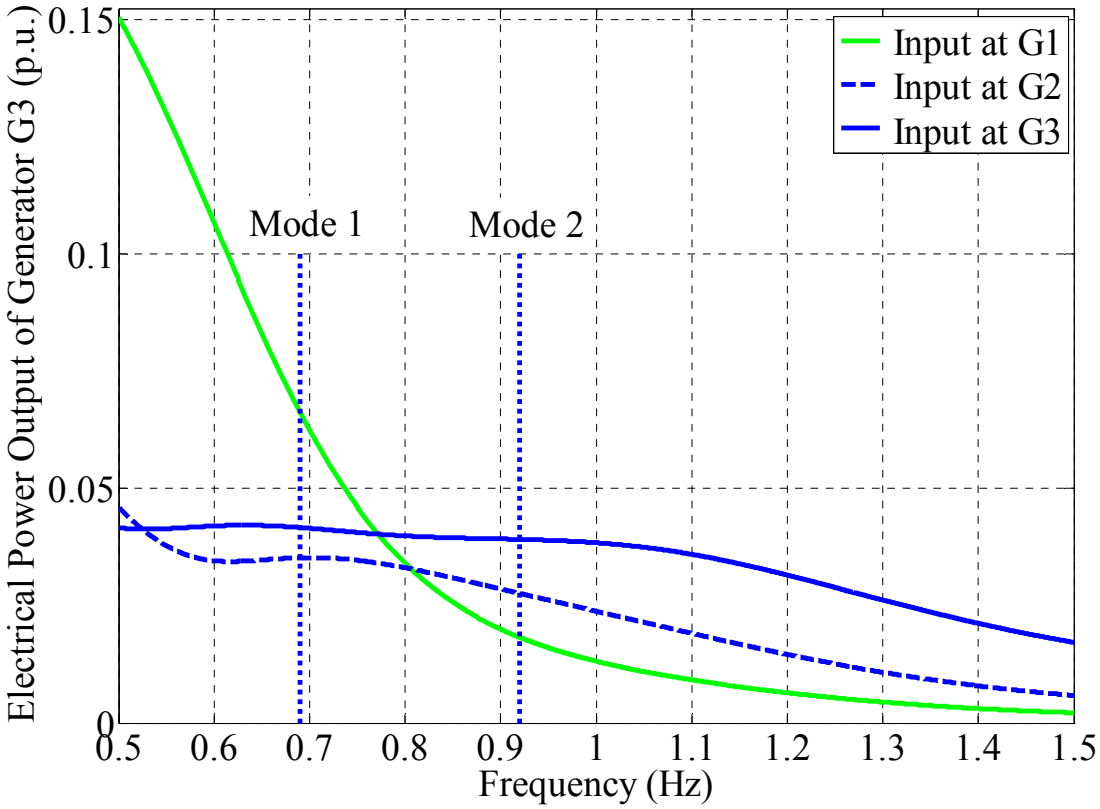

Figure 6.8 Frequency responses of P_{G3} for inputs at generators G1, G2, and G3 with the controllers designed for inter-area modes 1 and 2 in the test system

6.5.4 Time-Domain Simulation Results

In order to simulate the system behavior under large disturbance conditions, a balanced three-phase fault is applied at various transmission lines (T. Ls.) for the duration of 100 ms, with the fault cleared by opening the circuit breakers of the faulted circuit, in the test system. Different cases are given below:

6.5.4.1 First Sequential Design of PSS Controllers

Case 1: Three-phase fault at a point near bus 4, on one of T. Ls between buses 4 and 5, cleared by isolating the faulted line

The behavior of deviation of electrical power output of generator G1 ($\Delta P_{G1}(t)$) without PSS controllers, with the PSS controller designed for the inter-area

mode 1, with the PSS controller designed for inter-area mode 1 and the PSS controller designed for inter-area mode 2, and with the PSS controller redesigned for the inter-area mode 1 and the PSS controller for the inter-area mode 2 is shown in Figure 6.9. The simulation results shown in Figure 6.9 clearly indicate that the behavior of $\Delta P_{G1}(t)$ is better damped with the controller, designed for the inter-area mode 1, as compared to that without controllers. The results also indicate that the behavior of $\Delta P_{G1}(t)$ is better damped with the controllers, designed for the inter-area modes 1 and 2, as compared to that with the controller, designed for the inter-area mode 1. The results show that the behavior of $\Delta P_{G1}(t)$ becomes better damped with the controller, redesigned for the inter-area mode 1 and the controller for the inter-area mode 2 as compared to that with the controller, designed for the inter-area mode 1 first time and the controller for the inter-area mode 2.

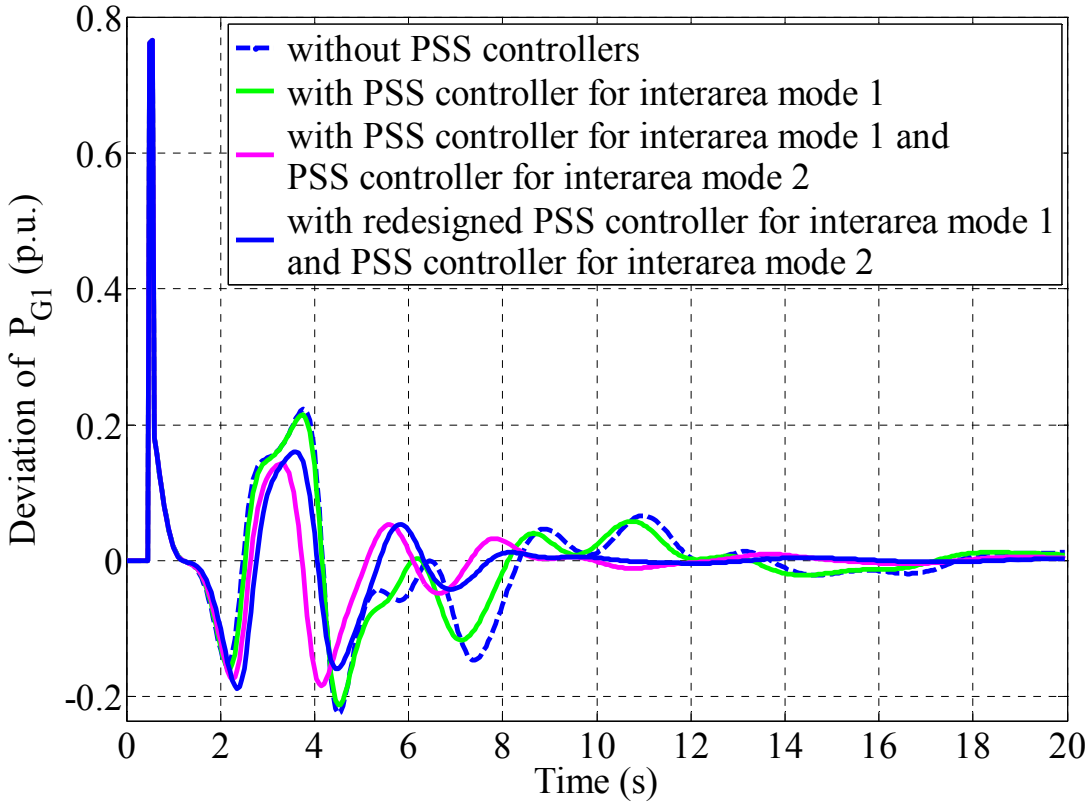

Figure 6.9 Deviation of $P_{G1}(t)$, following a three-phase fault near bus 4

Case 2: Three-phase fault at a point near bus 6, on one of T. Ls between buses 6 and 5, cleared by isolating the faulted line

The behavior of deviation of electrical power output of generator G2 ($\Delta P_{G2}(t)$) without PSS controllers, with the PSS controller designed for the inter-area mode 1, with the PSS controller designed for inter-area mode 1 and the PSS controller designed for inter-area mode 2, and with the PSS controller redesigned for the inter-area mode 1 and the PSS controller designed for the inter-area mode 2 is shown in Figure 6.10. The simulation results shown in Figure 6.10 clearly indicate that the behavior of $\Delta P_{G2}(t)$ is better damped with the controller, designed for the inter-area mode 1, as compared to that without controllers. The results also indicate that the behavior of $\Delta P_{G2}(t)$ is better damped with the controllers, designed for the inter-area modes 1 and 2, as compared to that with the controller, designed for the inter-area mode 1. The results show that the behavior of $\Delta P_{G2}(t)$ becomes better damped with the controller, redesigned for the inter-area mode 1 and the controller for the inter-area mode 2 as compared to that with the controller, designed for the inter-area mode 1 first time and the controller for the inter-area mode 2.

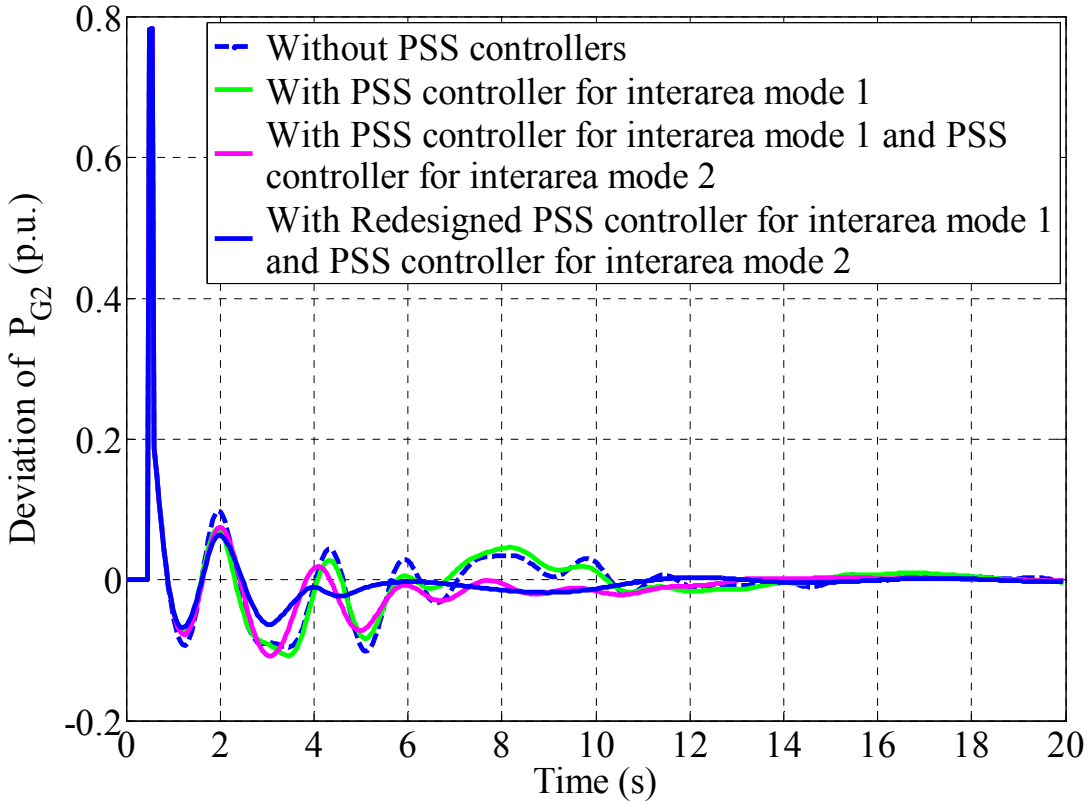

Figure 6.10 Deviation of $P_{G2}(t)$, following a three-phase fault near bus 6

Case 3: Three-phase fault at a point near bus 7, on one of T. Ls between buses 7 and 5, cleared by isolating the faulted line

The behavior of deviation of electrical power output of generator G3 ($\Delta P_{G3}(t)$) without PSS controllers, with the PSS controller designed for the inter-area mode 1, with the PSS controller designed for inter-area mode 1 and the PSS controller designed for inter-area mode 2, and with the PSS controller redesigned for the inter-area mode 1 and the PSS controller designed for the inter-area mode 2 is shown in Figure 6.11. The simulation results shown in Figure 6.11 clearly indicate that the behavior of $\Delta P_{G3}(t)$ is better damped with the controller, designed for the inter-area mode 1, as compared to that without controllers. The results also indicate that the behavior of $\Delta P_{G3}(t)$ is better damped with the controllers, designed for the inter-area modes 1 and 2, as compared to that with the controller, designed for the inter-area mode 1. The

results show that the behavior of $\Delta P_{G3}(t)$ becomes better damped with the controller, redesigned for the inter-area mode 1 and the controller for the inter-area mode 2 as compared to that with the controller, designed for the inter-area mode 1 first time and the controller for the inter-area mode 2.

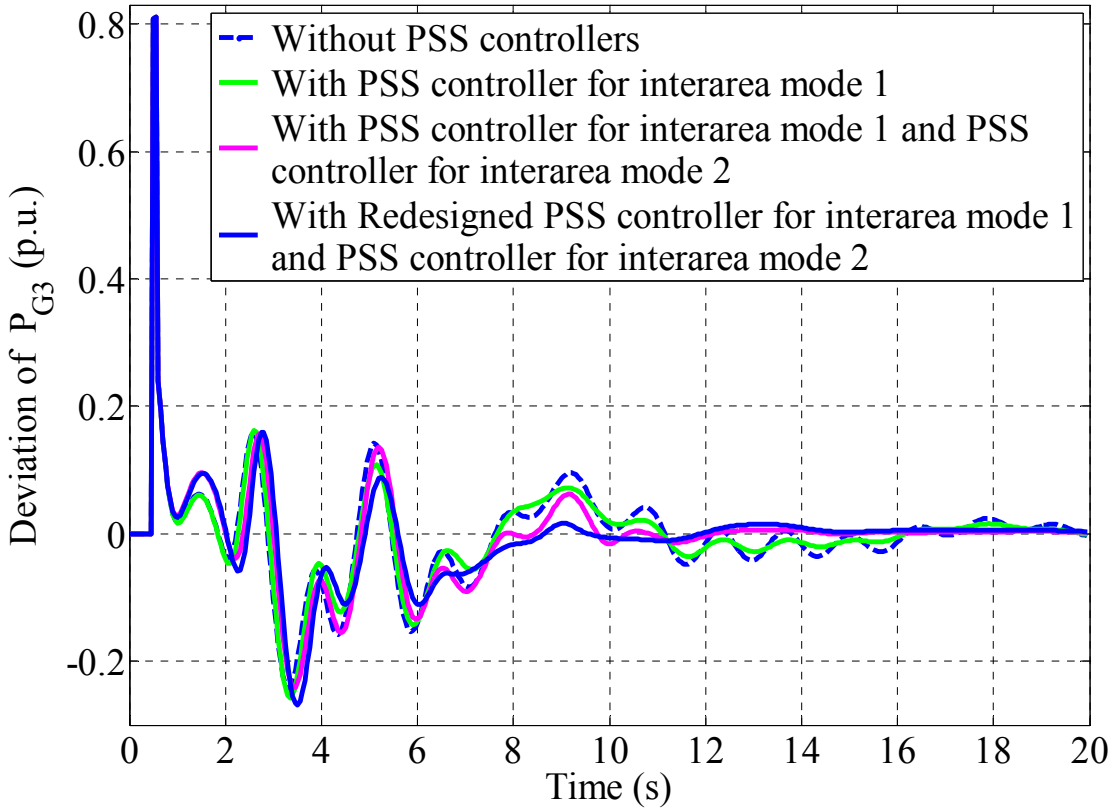

Figure 6.11 Deviation of $P_{G3}(t)$, following a three-phase fault near bus 7

6.6 Summary

The local decentralized control design approach, for the separate damping of inter-area modes of interest, proposed in this chapter, is applied on a three-machine, three-area test power system. The local PSS controllers, in the proposed approach, use selected suitable remote signals from the whole system, as supplementary feedback inputs, to damp their corresponding assigned inter-area modes only. Two local decentralized robust H_∞-based PSS controllers

have been designed for the two most weakly damped inter-area modes present in the test power system. Each of the two controllers, designed for the test power system, uses only those local and remote feedback input signals in which the assigned inter-area mode is highly observable and is located at a generator which is highly effective in controlling the same assigned inter-area mode. The two PSS controllers for the test power system are designed in such a way that each of them is effective only in a frequency band given by the natural frequency of the corresponding assigned mode. The two PSS controllers, therefore, damp only their corresponding assigned inter-area modes. The effectiveness of the resulting robust H_∞-based PSS controllers is demonstrated through digital simulation studies conducted on a three-machine, three-area test power system. The nonlinear simulation results show that the designed controllers contribute significantly to the damping of inter-area oscillations and the enhancement of small-signal stability.

Chapter 7

Mode Selective Damping of Electromechanical Oscillations for Very Large Power Systems

7.1 Introduction

Design of generator controls such as PSSs requires an external-system model. The large-scale power systems models, consisting of thousands of states, are impractical for control design without extensive order reduction. Lower-order state-space or transfer function model, sufficiently representative of the nominal system behavior, are prerequisite to the systematic design of control systems. Recent trends toward decentralized multivariable dynamic robust control through H_∞ optimization [55] further emphasize the critical need for accurate small-signal models with less than 20 states, irrespective of the size of the involved power system [56]. This chapter presents the extension of the scheme, proposed in Chapter 6, to realistic large-scale power systems by using system identification technique for deriving lower order state-space models suitable for control design. The complete, large-scale MIMO power system is directly used as the basis for building the required lower-order state-space or transfer function equivalent model. The lower-order model is identified by probing the network in open loop with low-energy pulses or random signals. The identification technique is then applied to signal responses, generated by time-domain simulations of the large-scale model, to obtain reduced-order model. Lower-order equivalent models, thus obtained, are used for the final

selection of suitable local and remote input signals, selection of suitable locations and design of the PSS controllers.

7.2 Lower-Order State-Space Model Identification

State-space identification aims at determining an equivalent lower-order state-space linear model of the system from time-domain simulation data. The form of the identified model is given as follows:

$$\dot{\mathbf{x}}(t) = \mathbf{A}\mathbf{x}(t) + \mathbf{B}\mathbf{u}(t) \tag{7.1}$$

$$\mathbf{y}(t) = \mathbf{C}\mathbf{x}(t) + \mathbf{D}\mathbf{u}(t) \tag{7.2}$$

where

$\mathbf{x}(t) \in R^{n\times 1}$ is the state vector,

$\mathbf{u}(t) \in R^{m\times 1}$ is the vector of input signals,

$\mathbf{y}(t) \in R^{p\times 1}$ is the vector of measured output signals,

$\mathbf{A} \in R^{n\times n}$, $\mathbf{B} \in R^{n\times m}$, $\mathbf{C} \in R^{p\times n}$ and $\mathbf{D} \in R^{p\times m}$ are constant matrices.

The time-domain response is obtained by applying a test excitation signal to the summing junction of the AVR of an excitation system. The measured time-domain response is then transformed into frequency domain. An identification algorithm is then applied to the frequency response data to obtain a linear dynamic model which accurately represents the system.

The frequency range for the electromechanical dynamic studies of power systems usually lies between 0.1 Hz and 10 Hz. Therefore, in this study, the input signal used to perturb the system is made over 0.1 to 10 Hz frequency range.

7.3 Application Results

7.3.1 Power System Simulation Model

Sixteen-machine, test power system, shown in Figure 7.1, is selected to apply the state-space model identification procedure, presented in Section 7.2, for finding the lower-order state-space model suitable for applying the control design approach presented in Section 6.4 and to illustrate the effectiveness of designed controllers for a separate better damping of specific inter-area modes. The test system consists of three strongly meshed areas, which are connected by long distance transmission lines. Therefore, the system experiences inter-area oscillations. The system has been developed based on characteristic parameters of the European interconnected electric power system, also known as UCTE/CENTREL [57], [58]. Moreover, for all simulation studies as well as for the PSS design, the structure of the i^{th}-generator together with an $n_{\text{ci}}^{\text{th}}$-order PSS controller in a multi-machine power system, presented in Chapter 4, Section 4.2.1 (Figure 4.1), is considered.

For illustrative purposes and from a sensitivity study, the damping ratio limit criterion for the test system, considered in this study, is defined as greater than 10% for all oscillatory modes and for all operating conditions. The profile of two most weakly damped rotor angle low-frequency electromechanical inter-area modes of oscillation, for the nominal power flow solution of the test system, is provided in Table 7.1. As there are two weakly damped inter-area modes in the considered test system, therefore, the decomposition strategy described in Chapter 6 (Section 6.2) suggests that there will be two PSS controllers for the considered test system.

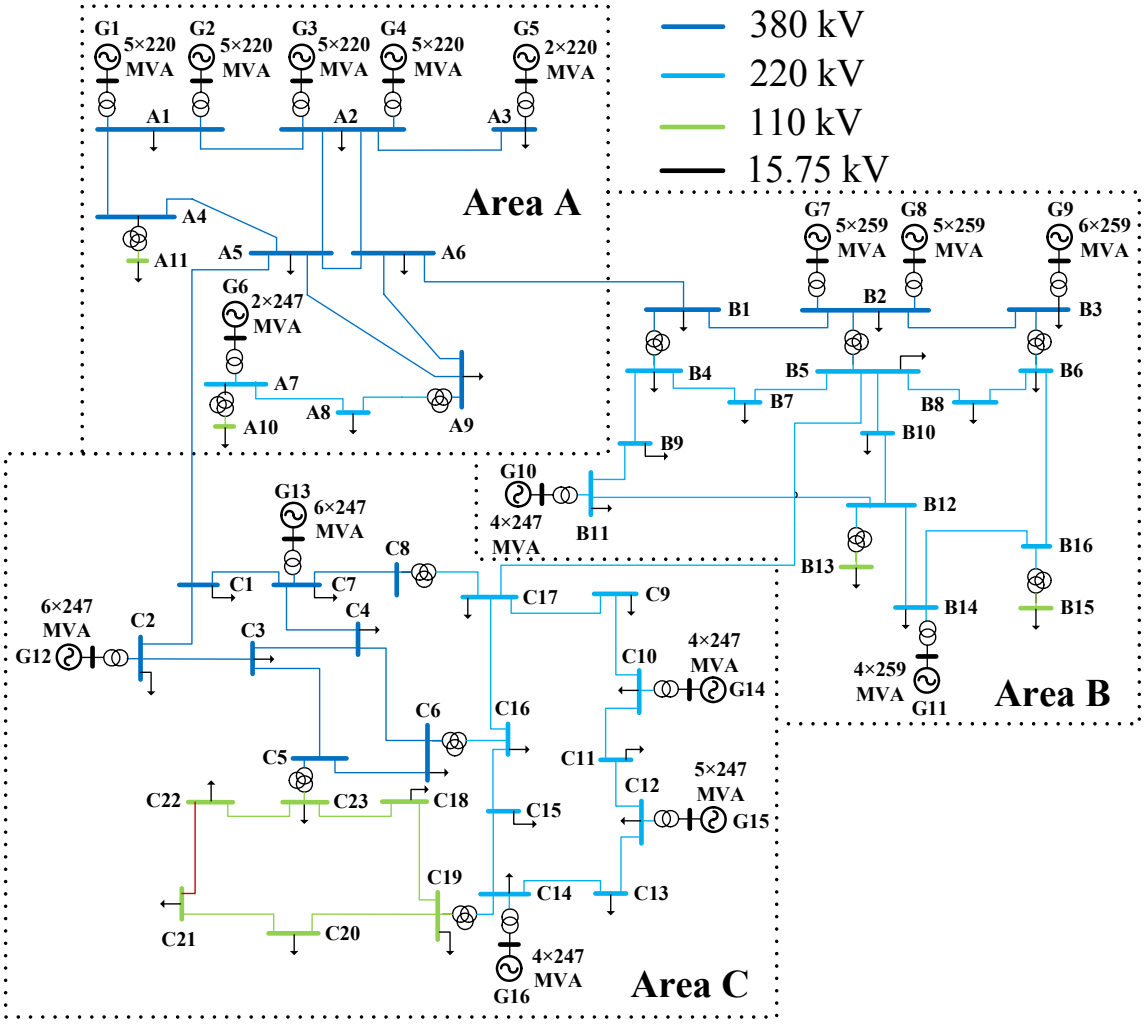

Figure 7.1 One line diagram of a test sixteen-machine, three-area power system

Table 7.1 Weakly damped inter-area modes of test system

Mode No.	Inter-area Modes	Damping Ratio (%)	Frequency (Hz)
1	-0.0793+3.8629	2.05	0.61
2	-0.5982+5.7031	10.43	0.91

7.3.2 Selection of Suitable Local and Remote Input Signals and Locations for PSS Controllers in the Test System

Following the procedure described in Chapter 6 (Section 6.3), the results for the selection of suitable local and supplementary remote signals and locations for the PSS controllers are given in the following sub-sections.

7.3.2.1 Engineering Pre-Selection of Features or Measurements

Following the procedure described in Chapter 6 (Section 6.3.1.1), the features selected are listed in Table 7.2.

Table 7.2 Features from the test system

#	Feature Description	Symbol	No.
1	Real power output of generators	P	16
2	Reactive power output of generators	Q	16
3	Real power over transmission lines	P	51
4	Reactive power over transmission lines	Q	51
5	Bus voltages	U	66
6	Bus voltage angles	θ_U	66
Total number of features			266

7.3.2.2 Feature Selection by k-Means Cluster Algorithm

Following the procedure described in Chapter 6 (Section 6.5.2.2), the data set, in this study, is clustered into three clusters for a short-circuit fault of 100 ms duration at all buses in the test system. Including engineering knowledge in the selection process, final pre-selected features obtained are as given in the Table 7.3.

Table 7.3 Final pre-selected features

#	**Final Pre-selected Features**
1	Real power through line between nodes A6 and B1 (P_{A6B1})
2	Voltage at node B2 (U_{B2})
3	Voltage Angle at node C1 (θ_{UC1})
4	Real power through line between nodes A5 and C1 (P_{A5C1})
5	Real power through line between nodes B5 and C17 (P_{B5C17})
6	Terminal Voltage of generator G1 (U_{G1})
7	Real power delivered by generator G4 (P_{G4})
8	Real power delivered by generator G15(P_{G15})
9	Reactive power supplied by generator G16 (Q_{G16})

7.3.2.3 Model Identification of the Test System

The probing signal (input signal) used to perturb the test system is applied to the AVR of the excitation system of generator G1 in the test system. The output signal (measured output) is taken as the real power through transmission line between nodes B5 and C17 (one of the final pre-selected features listed in Table 7.3). The system model is, therefore, single input and single output system. Following the procedure described in Section 7.2, 11^{th}-order identified system has been obtained.

For the identified model to be applicable for designing PSSs, its response in the frequency range associated with low frequency electromechanical oscillations must approximate that of the actual system. In particular, the frequency response in the neighborhood of the local and inter-area modes must be accurately represented. This is verified in Figure 7.2, which shows the frequency response of the identified system and the measured frequency response of the actual system in the 0.1 to 10 Hz frequency range. These plots show a good

match in the 0.3 to 10 Hz frequency range. In particular, both weakly damped inter-area modes of the test system have been clearly identified. Figure 7.3 shows the time-domain response of the identified system and the measured time-domain response of the actual system.

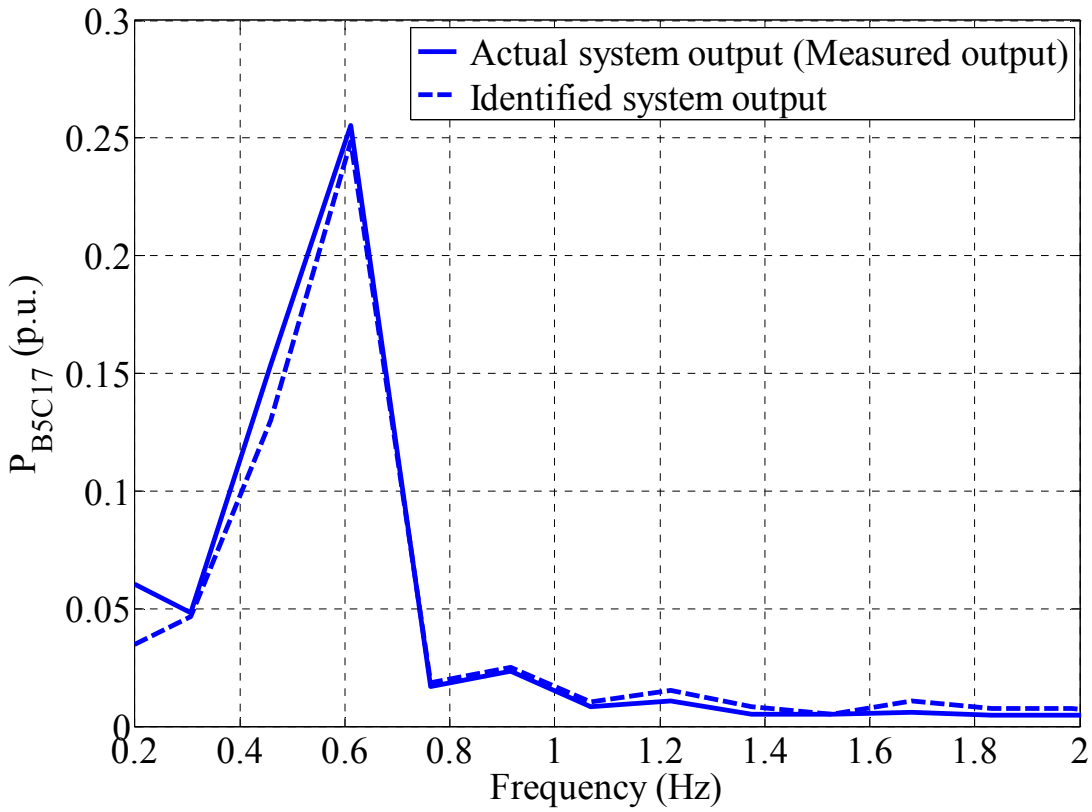

Fig. 7.2 Frequency response of the identified system and the measured frequency response of the actual system

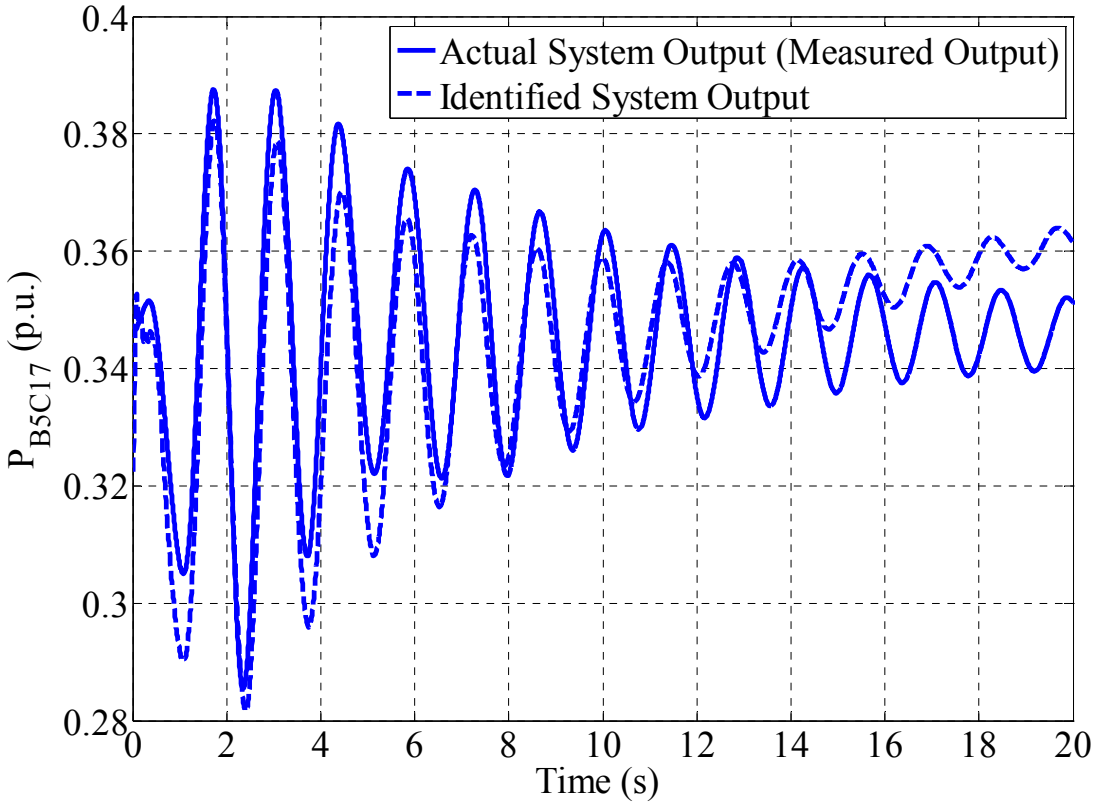

Fig. 7.3 Time-domain response of identified system and the measured time-domain response of actual system

For the probing signal applied to the AVR of generator G1 and the final pre-selected features listed in Table 7.3 taken as output signals (measured outputs), the system model is single input and nine outputs system. Following the procedure stated above, 11^{th}-order identified system has been obtained. The amplitude gains of frequency responses of final pre-selected features or measurements, listed in Table 7.3, obtained from the identified system, are shown in Figure 7.4. These frequency response curves exhibit resonance effects in the frequency bands of two weakly damped inter-area modes in the test system.

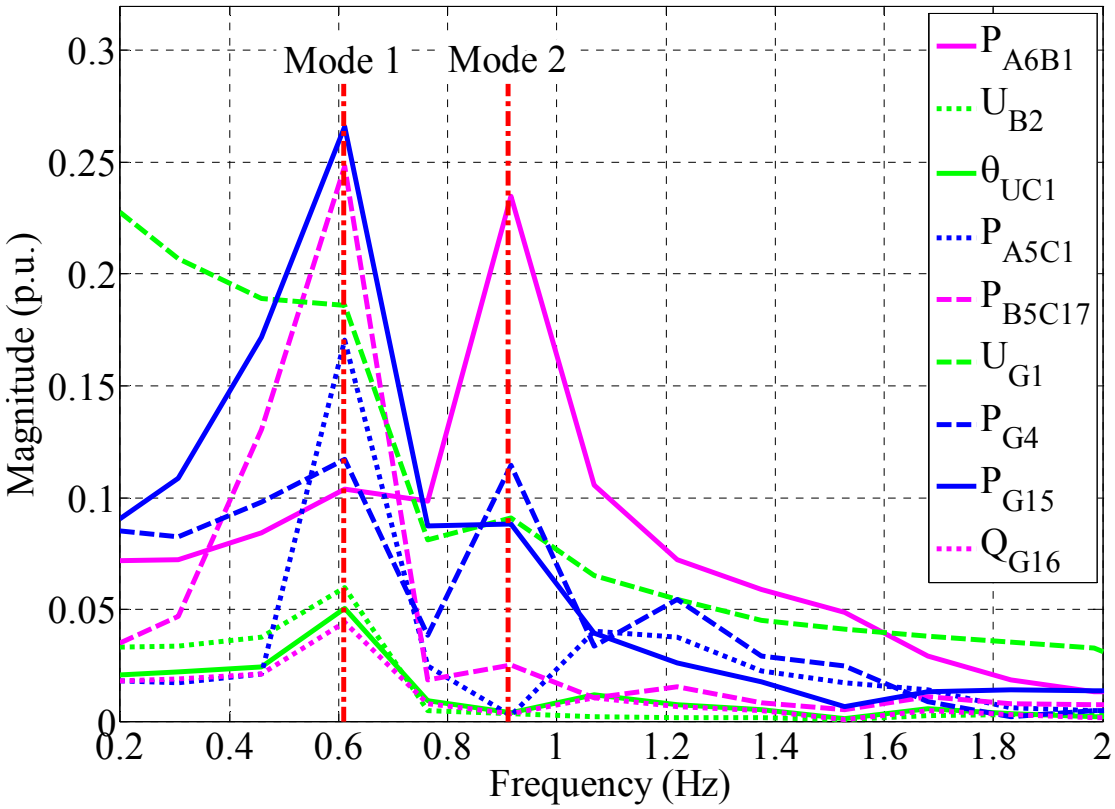

Figure 7.4 Frequency responses of pre-selected measurements

7.3.2.4 Selection of Suitable Locations for PSS Controllers in the Test System

The results shown in Figure 7.4 indicate that in the frequency bands of two most weakly damped inter-area modes in the test system, the frequency response curve for the electrical power output of generator G15 (P_{G15}) has maximum value out of frequency response curves for all other final pre-selected measurements (measurements obtained after the application of clustering technique). Therefore, according to the procedure described in Chapter 6 (Section 6.3.2), P_{G15} is considered as the best-suited measurement, whose frequency responses need to be obtained to the inputs at all generators in the test system for finding the suitable locations of two local decentralized PSS controllers in the test system.

For the probing signal applied to the AVR of all generators and P_{G15} taken as output signal (measured output), the system model is sixteen inputs and one output system. Following the procedure stated above, 11^{th}-order identified system has been obtained. The frequency responses of P_{G15} to the inputs at all generators, with no PSS controller located in the test system, are shown in Figure 7.5. These frequency response curves exhibit resonance effects in the frequency bands of the two weakly damped inter-area modes in test system. It is clear from the Figure 7.5 that for the inter-area mode 1 having the frequency 0.61 Hz, the frequency response curve of P_{G15} for an input to generator G15 has maximum value out of frequency response curves for inputs to all other generators. This indicates that the generator G15 is highly effective and suitable as the location of PSS controller to be designed to damp the inter-area mode 1. Figure 7.5 also shows that for the inter-area mode 2 having the frequency 0.91 Hz, the frequency response curve of P_{G15} for an input to generator G4 has maximum value out of frequency response curves for inputs to all other generators. This indicates that the generator G4 is highly effective and suitable as the location of PSS controller to be designed to damp the inter-area mode 2.

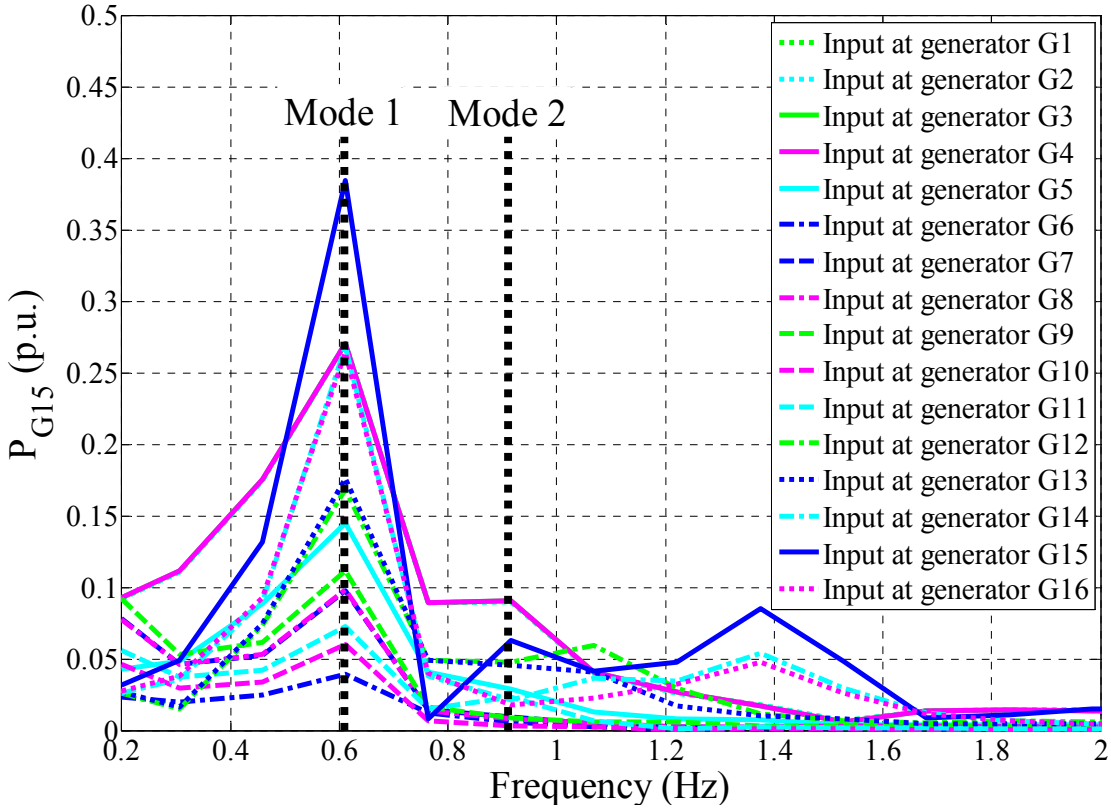

Figure 7.5 Frequency responses of P_{G15} for inputs at all generators in the test system with no PSS controller located in the test system

7.3.2.5 Final Selection of Suitable Local and Remote Input Signals

Final selection of local and remote signals is carried out, as described in Chapter 6 (Section 6.3.1.3), on basis of the amplitude gains of the frequency responses of final pre-selected features or measurements (Figure 7.4), i.e., the measurements obtained after the application of clustering technique. Figure 7.4 indicates that for the PSS controller, to be designed for inter-area mode 1, having suitable location G15, local signal is P_{G15} whereas the others are remote signals. Similarly, for the PSS controller, to be designed for inter-area mode 2, having suitable location G4, local signal is taken as P_{G4} whereas the others are remote signals.

The results shown in Figure 7.4 indicate that in the frequency band of the inter-area mode 1, the frequency response curve for the real power through transmission line between nodes B5 and C17 (P_{B5C17}) has maximum value out of frequency response curves for all other remote measurements. This indicates that P_{B5C17} is suitable as a supplementary remote feedback input signal for a local decentralized PSS controller to be designed to damp the inter-area mode 1. Figure 7.4 also shows that in the frequency band of the inter-area mode 2, the frequency response curve for the real power through transmission line between nodes A6 and B1 (P_{A6B1}) has maximum value out of frequency response curves for all other remote measurements. This indicates that P_{A6B1} is suitable as a supplementary remote feedback input signal for a local decentralized PSS controller to be designed to damp the inter-area mode 2. Table 7.4 summarizes the results for the selection of suitable local and remote input signals and locations of local decentralized PSS controllers, to be designed to damp out the two most weakly damped inter-area modes in the considered test system.

Table 7.4 Selected suitable local and remote input signals and locations for PSS controllers

Mode No.	Local Signals to Controllers	Remote Signals to Controllers	Locations of Controllers to be Designed
1	P_{G15}	P_{B5C17}	Generator G15
2	P_{G4}	P_{A6B1}	Generator G4

7.3.3 Design Results

During the design of robust H_∞-based PSS controller for the inter-area mode 1, P_{G15} and P_{B5C17} are used as its feedback input signals, i.e.,

$\mathbf{y}(t) = \begin{bmatrix} P_{\mathrm{G15}}(t) & P_{\mathrm{B5C17}}(t) \end{bmatrix}^{\mathrm{T}}$. The measured signals P_{G15} and P_{B5C17}, the output of the PSS (u_{sG15}) together with the terminal voltage error signals, which are the inputs to the regulator of the exciter, are used as regulated signals within this design framework, i.e., $\mathbf{z}(t) = \begin{bmatrix} P_{\mathrm{G15}}(t) & P_{\mathrm{B5C17}}(t) & u_{s\mathrm{G15}}(t) \end{bmatrix}^{\mathrm{T}}$. Similarly, during the design of robust H_∞-based PSS controller for the inter-area mode 2, P_{G4} and P_{A6B1} are used as its feedback input signals, i.e., $\mathbf{y}(t) = \begin{bmatrix} P_{\mathrm{G4}}(t) & P_{\mathrm{A6B1}}(t) \end{bmatrix}^{\mathrm{T}}$. The measured signals P_3 and P_{57}, the output of the PSS (u_{sG4}) together with the terminal voltage error signals, which are the inputs to the regulator of the exciter, are used as regulated signals within this design framework, i.e., $\mathbf{z}(t) = \begin{bmatrix} P_{G4}(t) & P_{\mathrm{A6B1}}(t) & u_{s\mathrm{G4}}(t) \end{bmatrix}^{\mathrm{T}}$. The design procedure described in Chapter 4 (Section 4.2.2) is used to design the dynamic controllers of the form of (4.7) and (4.8) such that minimum disturbance attenuation (from $\mathbf{w}(t)$ to $\mathbf{z}(t)$) is achieved. Balanced residualization technique [18] is used to reduce the order of controllers at each of the stages of design.

7.3.3.1 Sequential Design of PSS Controllers

As two PSS controllers need to be designed for the test system, the sequential design can, therefore, be performed in two different ways, depending on the sequence in which the controllers are designed. Table 7.5 provides description of the sequences for the design of controllers in the two possible sequential designs. Note that the first control loop consists of plant and the PSS controller, designed for inter-area mode 1, located at generator G15 and the second control loop consists of plant and the PSS controller, designed for inter-area mode 2, located at generator G4.

Table 7.5 Sequences for design of controllers in two possible sequential designs

Sequential Design No.	Sequences for the Design of Controllers
1	(i) PSS controller for the inter-area mode 1 is designed first with keeping the second control loop open; (ii) PSS controller for the inter-area mode 2 is then designed with keeping the first control loop closed, i.e., with the already designed PSS controller for the inter-area mode 1 located at generator G15 in the test system.
2	(i) PSS controller for the inter-area mode 2 is designed first with keeping the first control loop open; (ii) PSS controller for the inter-area mode 1 is then designed with keeping the second control loop closed, i.e., with the already designed PSS controller for the inter-area mode 2 located at generator G4 in the test system.

First Sequential Design

In the first sequential design, the PSS controller for the inter-area mode 1 is designed first with keeping the second control loop open in the test system. The H_∞-based PSS controller for the inter-area mode 1 obtained is:

$$\mathbf{C}_{11}(s) = \left[24.878 \frac{(1+s\,0.0314)(1+\ s3.9918)}{(1+s\,0.1984)(1+s\,0.2559)} \;\vdots\; 13.49 \frac{(1+s0\,.0159)(1+s\,2.6202)}{(1+s\,0.1984)(1+s\,0.2559)} \right]$$

Table 7.6 provides the profile of two most weakly damped inter-area modes of the test system with controller designed for inter-area mode 1, with controller designed for inter-area mode 1 and controller designed for inter-area mode 2. Figure 7.6 shows the frequency responses of P_{G15} and real power

flow through transmission line between nodes A6 and B1 (P_{A6B1}) with the controller designed for the inter-area mode 1 located at generator G15 in the test system. The results given in Table 7.6 and Figure 7.6 indicate that the damping of inter-area mode 1 has increased significantly whereas the damping of inter-area mode 2 has increased only slightly when the controller designed for mode 1 is incorporated in the test system.

Table 7.6 Weakly damped inter-area modes in test system

Mode No.	With Controller Designed for Mode 1			With Controllers Designed for Modes 1 and 2		
	Inter-area Modes	**ξ (%)**	**Freq. (Hz)**	**Inter-area Modes**	**ξ (%)**	**Freq. (Hz)**
1	-1.8334+3.7499	43.92	0.60	-1.4794+3.4207	43.70	0.54
2	-0.6258+5.7006	10.91	0.91	-1.2015+5.0564	23.12	0.80

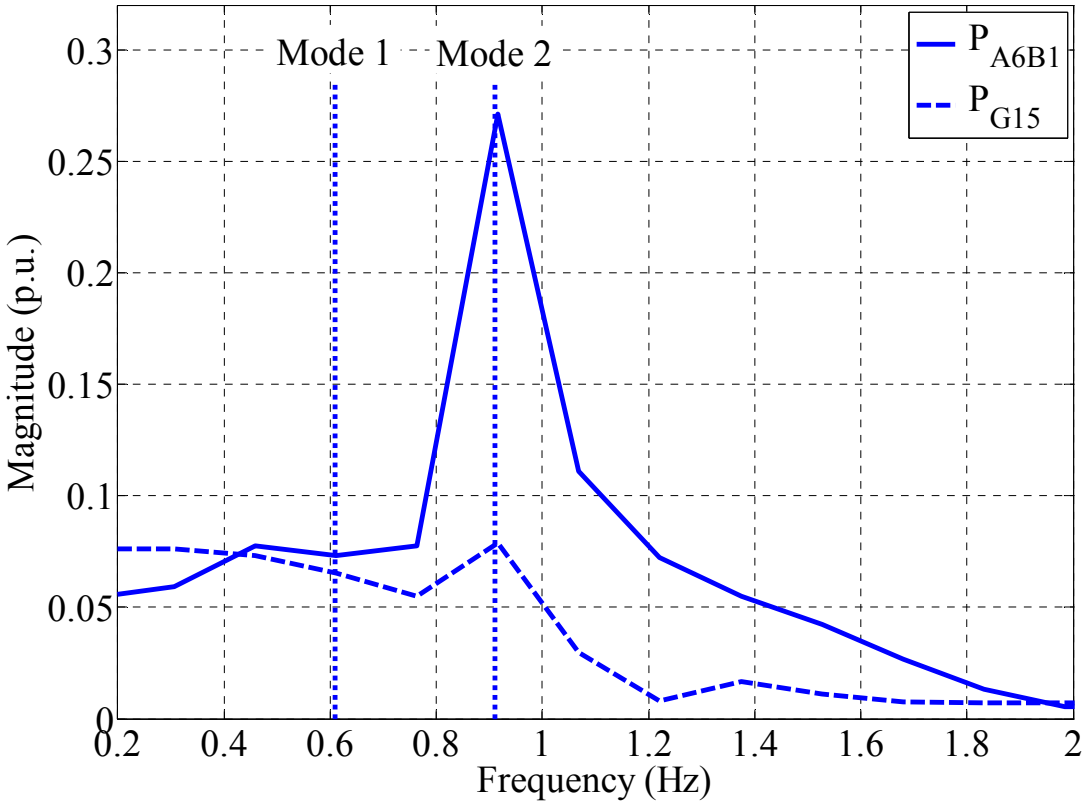

Figure 7.6 Frequency responses of P_{G15} and P_{A6B1} with the controller designed for inter-area mode 1 located in the test system

The PSS controller for the inter-area mode 2 is now designed with keeping the first control loop closed, i.e., with the already designed controller for the inter-area mode 1 located at G15 in the test system. The H_∞-based PSS controller for the inter-area mode 2 obtained is:

$$\mathbf{C}_{22}(s) = \left[2.30 \frac{(1+s\,0.2221)(1+s\,0.2701)}{(1+s\,0.5857)(1+s\,0.0185)} \;\vdots\; 3.5 \frac{(1+s\,0.011)(1+s\,1.055)}{(1+s\,0.5857)(1+s\,0.0185)} \right]$$

The frequency responses of P_{G15} and P_{A6B1} with the controllers designed for the inter-area modes 1 and 2 located at G15 and G4 respectively in the test system, are shown in Figure 7.7. The results given in Table 7.6 and Figure 7.7 indicate that the damping of inter-area mode 2 has increased significantly whereas the damping of inter-area mode 1 has changed slightly when the controller designed for inter-area mode 2 is incorporated at G4 in the test system which has already controller for inter-area mode 1 located in it at G15. This indicates that the controller designed for inter-area mode 2 has contributed significantly to the damping of inter-area mode 2.

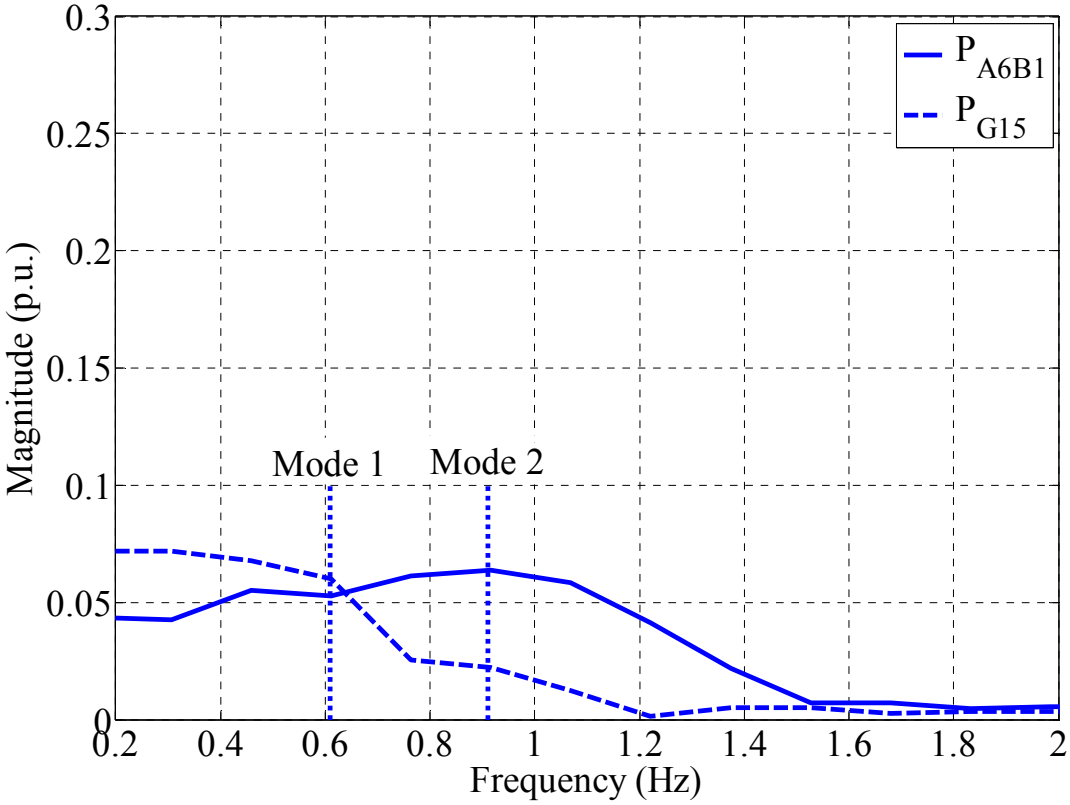

Figure 7.7 Frequency responses of P_{G15} and P_{A6B1} with the controllers designed for inter-area modes 1 and 2 located in the test system

Second Sequential Design

In the second sequential design, the PSS controller for the inter-area mode 2 is designed first with keeping the fist control loop open in the test system. The H_∞-based PSS controller for the inter-area mode 2 obtained is:

$$\mathbf{C}_{22}(s) = \left[2.5\frac{(1+s\,0.0121)(1+\ s0.1101)}{(1+s\,0.1877)(1+s\,0.1145)} \;\vdots\; 11.49\frac{(1+s0.0971)(1+s\,0.0255)}{(1+s\,0.1877)(1+s\,0.1145)} \right]$$

Table 7.7 provides the profile of two most weakly damped inter-area modes of the test system with the controller designed for the inter-area mode 2 and with the controller designed for inter-area mode 1 and the controller designed for inter-area mode 2. Figure 7.8 shows the frequency responses of P_{G15} and P_{A6B1} with the controller designed for the inter-area mode 2 located at G4 in the test system. The results given in Table 7.7 and Figure 7.8 indicate that the damp-

ing of inter-area modes 2 and 1 have increased slightly when the controller designed for mode 2 is incorporated in the test system.

Table 7.7 Weakly damped inter-area modes in test system

Mode No.	With Controller Designed for Mode 2			With Controllers Designed for Modes 2 and 1		
	Inter-area Modes	ξ (%)	Freq. (Hz)	Inter-area Modes	ξ (%)	Freq. (Hz)
1	-0.0824+3.8912	2.12	0.62	-2.6790+3.9003	56.62	0.62
2	-0.9577+ 5.6627	16.68	0.90	-1.0223+5.6975	17.66	0.91

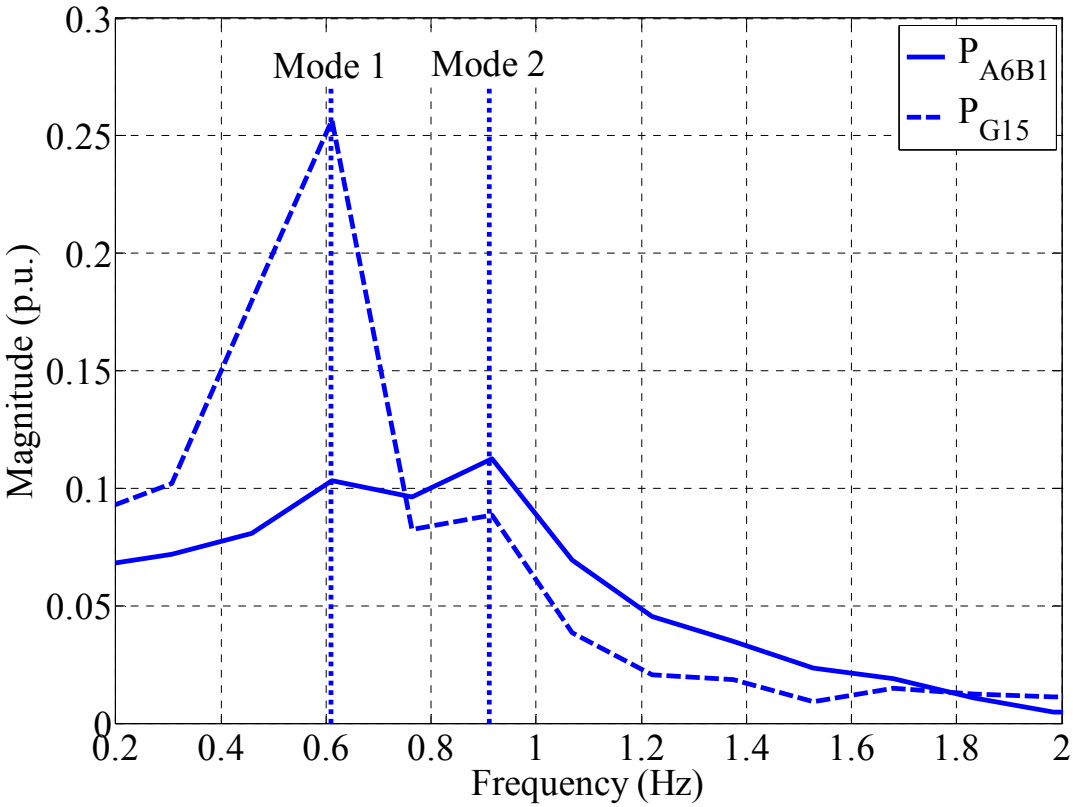

Figure 7.8 Frequency responses of P_{G15} and P_{A6B1} with the controller designed for inter-area mode 2 located in the test system

The PSS controller for the inter-area mode 1 is now designed with keeping the second control loop closed, i.e., with the already designed controller for

the inter-area mode 2 located at G4 in the test system. The H_∞-based PSS controller for the inter-area mode 1 obtained is:

$$\mathbf{C}_{11}(s) = \left[4.878 \frac{(1+s\,0.0314)(1+s\,1.9918)}{(1+s\,0.2984)(1+s\;0.2559)} \;\vdots\; 23.49 \frac{(1+s\,0.0159)(1+s\,3.6202)}{(1+s\,0.2984)(1+s\;0.2559)} \right]$$

The frequency responses of P_{G15} and P_{A6B1} with the controller designed for the inter-area modes 1 and 2 located at G15 and G4 respectively in the test system, are shown in Figure 7.9. The results given in Table 7.7 and Figure 7.9 show that the damping of inter-area mode 1 has increased significantly whereas the damping of inter-area mode 2 has increased slightly when the controller designed for mode 1 is incorporated in the test system which has already controller for inter-area mode 2 located in it. This indicates that the controller designed for mode 1 has contributed significantly to the damping of inter-area mode 1.

The results given in Table 7.7 and Figure 7.9 indicate that the inter-area mode 2 still needs damping improvement. The controller for the inter-area mode 2 is, therefore, designed again with keeping the first control loop closed, i.e., with the already designed controller for inter-area mode 1 located at generator G15 in the test system. It was found that, with the redesigned PSS controller for the inter-area mode 2 located at G4 and the controller designed for the inter-area mode 1 located at G15 in the test system, there was no damping improvement for the inter-area mode 2.

Comparison of results for the first and second sequential designs indicate that the damping of inter-area mode 1 has increased more than 40% in both the first and the second sequential designs whereas the damping of inter-area mode 2 has increased more in the first sequential design than in the second one. Therefore, it is concluded that the first sequential design is better than the second one.

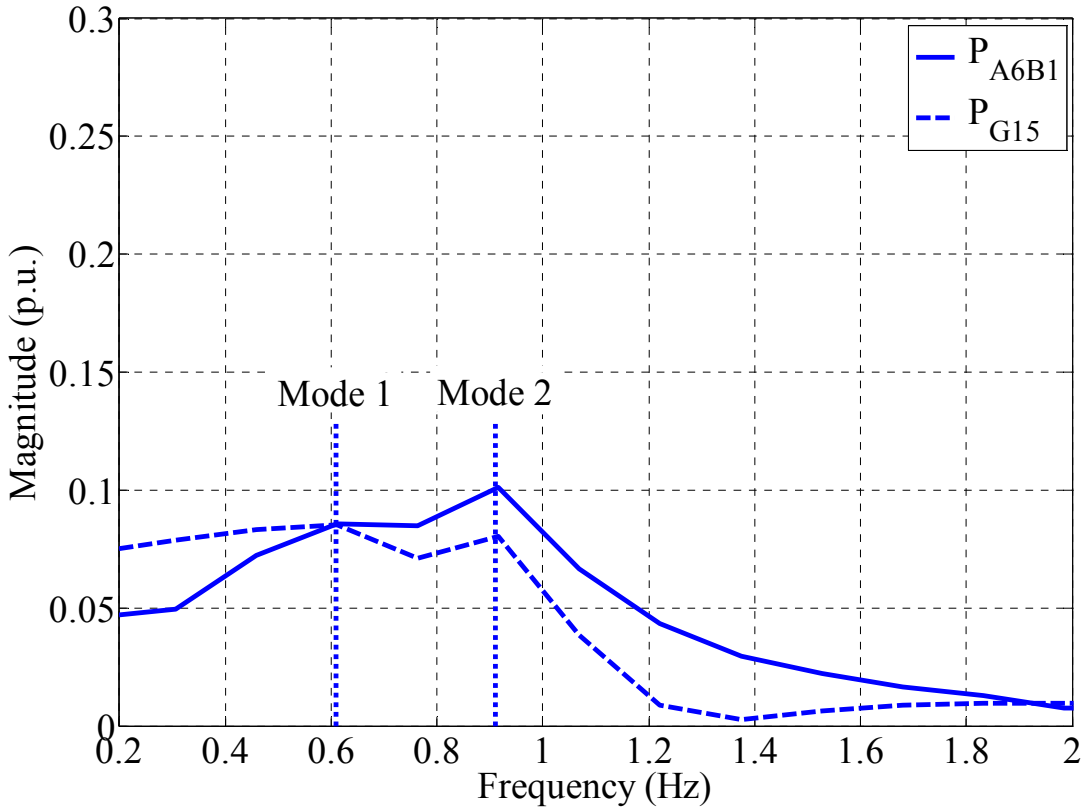

Figure 7.9 Frequency responses of P_{G15} and P_{A6B1} with the controllers designed for inter-area modes 1 and 2 in the test system

7.3.4 Time-Domain Simulation Results

In order to simulate the system behavior under large disturbance conditions, a balanced three-phase fault is applied at bus A2, for the duration of 100 ms, in the test system.

7.3.4.1 First Sequential Design of PSS Controllers

The behavior of deviation of real electrical power delivered by generator G3 ($\Delta P_{G3}(t)$) without PSS controllers, with the PSS controller designed for the inter-area mode 1, with the PSS controller designed for inter-area mode 1 and the PSS controller designed for inter-area mode 2 is shown in Figure 7.10. The simulation results shown in the figure clearly indicate that the behavior of

$\Delta P_{G3}(t)$ is better damped with the controller, designed for the inter-area mode 1, as compared to that without controllers. The results also indicate that the behavior of $\Delta P_{G3}(t)$ is better damped with the controllers, designed for the inter-area modes 1 and 2, as compared to that with the controller, designed for the inter-area mode 1.

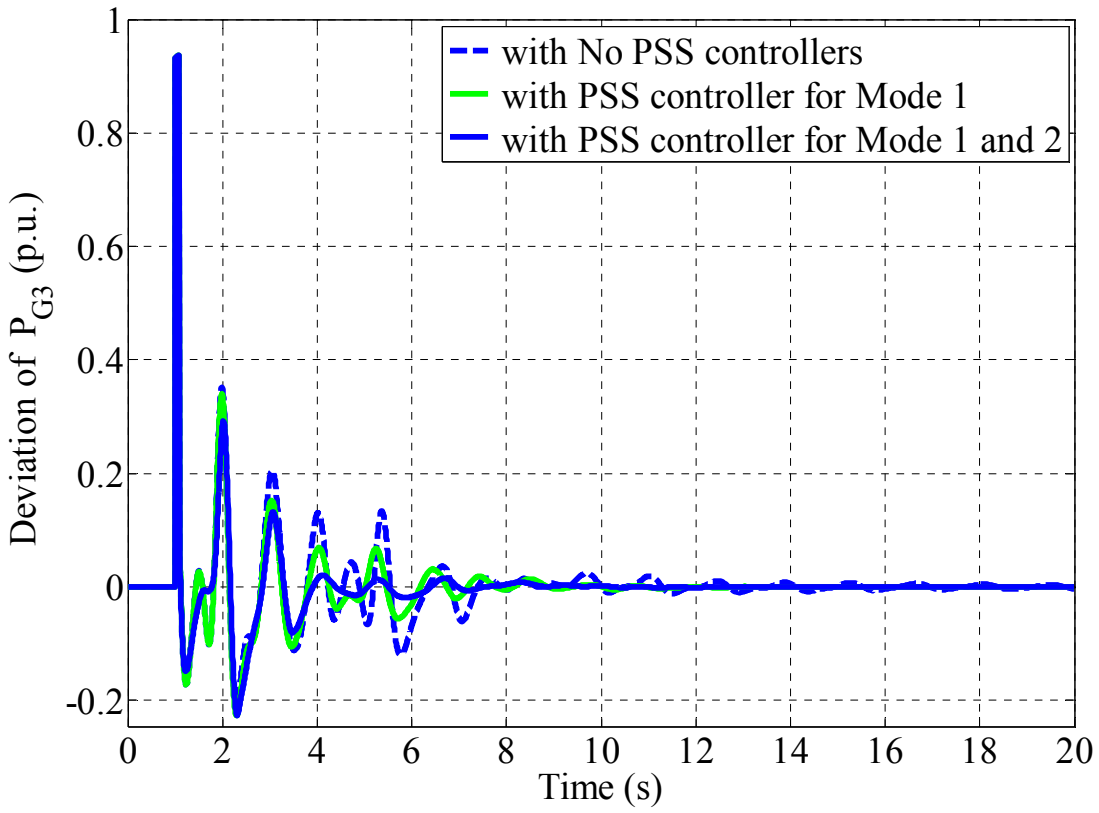

Fig. 7.10 Deviation of $P_{G3}(t)$ ($\Delta P_{G3}(t)$), following a three-phase fault at bus A2

7.4 Summary

The local decentralized control design approach for the separate damping of inter-area modes of interest, for very large power systems, proposed in this chapter, is applied on a sixteen-machine, three-area test power system. An identification technique is used to determine an equivalent lower-order state-

space linear model of the test system from time-domain simulation data. The time-domain response is obtained by applying a test probing signal (input signal), used to perturb the test system, to the AVR of the excitation system of the test system. The measured time-domain response is then transformed into frequency domain. An identification algorithm is then applied to the frequency response data to obtain a linear dynamic reduced order model which accurately represents the system. The frequency response of the identified test system and the measured frequency response of the actual test system show a good match in the 0.3 to 10 Hz frequency range. In particular, both weakly damped inter-area modes of the test system have been clearly identified.

Lower-order equivalent models have been used for the final selection of suitable local and remote input signals, selection of suitable locations and design of the PSS controllers. The nonlinear simulation results show that the designed controllers contribute significantly to the damping of inter-area oscillations and the enhancement of small-signal stability. Therefore, it is concluded that using system identification technique, mode selective damping approach can be applied to very large power systems.

Chapter 8

Conclusions and Future Work

8.1 Conclusions

The design of local H_∞-based PSS controller, which uses wide-area or global signals as additional measuring information from suitable remote network locations, where oscillations are well observable, is developed in this dissertation. The controllers, placed at suitably selected generators, provide control signals to the AVRs to damp out inter-area oscillations through the machines' excitation systems. The main contributions of this dissertation are as follows:

Robust H_∞-based PSS Controller Design using Supplementary Remote Signals

An H_∞-based dynamic output feedback PSS controller, using both local and remote signals, has been developed. An ARE approach has been used for the design of controller. The effectiveness of the designed controller is demonstrated through digital simulation studies on a test power system. The nonlinear simulation results have shown that the proposed controller is effective and robust in suppressing system oscillations for a wide range of system operating conditions under large disturbances in the system studied. The results also show that the proposed controller is effective when its remote input signal is lost.

Delayed-Input PSS using Supplementary Remote Signals

A local H_∞-based PSS controller, which uses wide area or global signals as additional measuring information, is designed considering time delay in the remote signals. Three methods for dealing with the effects of time delay are presented. First, time delay compensation method using lead/lag compensation along with gain scheduling for compensating effects of constant delay is presented. A delay compensator is designed and included with the controller, designed for the delay-free system, in the closed loop system in order to compensate the effects of considered constant time delay in the system. In the second method, Pade approximation approach is used to model time delay. The time delay model is then merged into delay-free power system model to obtain the delayed power system model. The controller is redesigned for the delayed-input system considering constant delay in the system.

Delay compensation and Pade approximation methods deal with constant delays and are not robust regarding time delays. Time delay uncertainty is, therefore, taken into account using LFT method. The controller is redesigned for the delayed-input system considering delay uncertainty in the system. The effectiveness of the resulting robust H_∞-based PSS controller is demonstrated through digital simulation studies conducted on a test power system. The nonlinear simulations results have shown that the proposed controller is effective and robust in suppressing system oscillations despite the uncertainty in delay.

Mode Selective Damping of Power System Electromechanical Oscillations using Supplementary Remote Signals

The design of local decentralized H_∞-based PSS controllers, using selected suitable remote signals coming from the whole system, as supplementary inputs, for a separate better damping of specific inter-area modes, has been developed. Each local PSS controller is designed separately for each of the inter-area modes of interest. The PSS controller uses only those local and remote input signals in which the assigned single inter-area mode is most observable and is located at a generator which is most effective in controlling that mode. The local PSS controller, designed for a particular single inter-area mode, also works mainly in a frequency band given by the natural frequency of the assigned mode. The locations of the local PSS controllers are obtained based on the amplitude gains of the frequency responses of the best-suited measurement to the inputs of all generators in the interconnected system. For the selection of suitable local and supplementary remote input signals, the features or measurements from the whole system are pre-selected first by engineering judgment and then using a clustering feature selection technique. Final selection of local and remote input signals is based on the degree of observability of the considered single mode in them.

The proposed approach is applied on a three-machine, three-area test power system. Two local decentralized robust H_∞-based PSS controllers have been designed for the two most weakly damped inter-area modes present in the test power system. Each of the two controllers, designed for the test power system, thus, uses only those local and remote feedback input signals in which the assigned inter-area mode is highly observable and is located at a generator which is highly effective in controlling the same assigned inter-area mode. The two PSS controllers for the test power system are designed in such a way

that each of them is effective only in a frequency band given by the natural frequency of the corresponding assigned mode. The two PSS controllers, therefore, damp only their corresponding assigned inter-area modes. The effectiveness of the resulting PSS controllers is demonstrated through digital simulation studies conducted on a three-machine, three-area test power system. The nonlinear simulation results show that the designed controllers contribute significantly to the damping of inter-area oscillations and the enhancement of small-signal stability.

Mode Selective Damping of Electromechanical Oscillations for Very Large Power Systems using Supplementary Remote Signals

The design of local decentralized PSS controllers, using selected suitable remote signals coming from the whole system, as supplementary inputs, for a separate better damping of specific inter-area modes in a large-scale power system, has been presented. The system identification technique is used for deriving lower order state-space models suitable for control design. The complete, large-scale MIMO power system is used directly as the basis for building the required lower-order state-space or transfer function equivalent model. The lower-order model is identified by probing the network in open loop with low-energy pulses or random signals. The identification technique is then applied to signal responses, generated by time-domain simulations of the large-scale model, to obtain reduced-order model. Lower-order equivalent models, thus obtained, are used for the final selection of suitable local and remote input signals for the PSS controllers, selection of suitable locations of the PSS controllers and design of the PSS controllers.

The proposed approach is applied on a sixteen-machine, three-area test power system. An identification technique is used to determine an equivalent low order state-space linear model of the test system from time-domain simulation data. The time-domain response is obtained by applying a test probing signal (input signal), used to perturb the test system, to the AVR of the excitation system of the test system. The measured time-domain response is then transformed into frequency domain. An identification algorithm is then applied to the frequency response data to obtain a linear dynamic reduced order model which accurately represents the system. The frequency response of the identified test system and the measured frequency response of the actual test system show a good match in the 0.3 to 10 Hz frequency range. In particular, both weakly damped inter-area modes of the test system have been clearly identified.

The local PSS controllers, in the proposed approach, use selected suitable remote signals from the whole system, as supplementary feedback inputs, to damp their corresponding assigned inter-area modes only. Lower-order equivalent models have been used for the final selection of suitable local and remote input signals for the PSS controllers, selection of suitable locations of the PSS controllers and design of the PSS controllers. The nonlinear simulation results show that the designed controllers contribute significantly to the damping of inter-area oscillations and the enhancement of small-signal stability. Therefore, using system identification technique, mode selective damping approach can be applied to very large power systems.

From the above discussion, it is concluded that the use of remote signals, as supplementary feedback inputs to the local PSS controllers, is appropriate for damping enhancement of electromechanical oscillations.

8.2 Future Work

The development of electric power industry follows closely the increase of the demand on electrical energy. Because of a lack on available investments, the development of transmission systems does not follow the increase in power demand. Hence, there is a gap between transmission capacity and actual power demand, which leads to technical problems in the overloaded transmission systems. Interconnection of separated grids in the developed countries can solve some of these problems, however, when the interconnections are heavily loaded due to an increasing power exchange, the reliability and availability of the transmission will be reduced. If systems have a large geographic extension and have to transmit large power over long distances, stability problems can arise.

Therefore, as the power demand increases due to increase in general consumption and new industry, the electrical power systems must be utilized more effectively, while considering geographical, economical and technical restrictions. Further, such increased utilization must not compromise the secure operation of the power system. Therefore, a strategy to allow increased utilization, while maintaining security of power supply is required. Methods for improved control of transmission systems are becoming increasingly important in meeting these objectives.

The authors have plans to design a robust coordinated Flexible AC Transmission Systems (FACTS) and PSS controllers (using global signals), for a better damping of power system oscillations. The coordinated use of FACTS controllers with the PSS controllers for a better damping of power system oscillations can play an important role for the safe and reliable transmission of active power. It can increase transmission transfer capabilities, improve sys-

tem stability and security of supply. Improvement in security of supply prevents blackouts and thus causes less expense due to blackouts. In this way, an improved transmission system operation with minimal infrastructure investment, environmental impact, and implementation time compared to the construction of new transmission lines can be achieved.

Improper locations of controllers may not enhance the damping of power system oscillations and hence leads to the loss of investment. The authors have plans to apply the approach presented in the paper to find the suitable locations for the proposed PSSs and FACTS controllers.

Appendices

Appendix A. Two-Machine Test System Data

Bus, line, generator and excitation data are given in this appendix.

A.1 Synchronous Machine Parameters:

S_r = 350.00 MVA; U_r = 15.75 kV; T_m = 7.00 s; r_a = 0.002 p.u.;

x_s = 0.19 p.u.; x_d = 2.49 p.u.; x_q = 2.49 p.u.; $x_d^{'}$ = 0.36 p.u.; $x_d^{''}$ = 0.24 p.u.;

$x_q^{'}$ = - ; $x_q^{''}$ = 0.24 p.u.; $T_d^{'}$ = 0.93 s; $T_d^{''}$ = 0.11 s; $T_q^{'}$ = - ; $T_q^{''}$ = 0.2 s

A.2 Transmission Line Parameters:

380 kV Single Line:

$\mathbf{Z}_{11}$= (0.0309 + j0.266) Ω/km; C_b = 0.0136 μF/km

A.3 Two Winding Transformer Parameters:

r_{ps} [%] = 0.246 ; z_{ps} [%] = 14.203

A.4 Exciter and classical AVR (Figure A.1) Parameters:

K_A = 264 ; T_A = 0.33 s; T_{F1}= 0.2 s; T_{F2} = 1.0 s; u_{rmax} = 7.0 p.u.;

u_{rmin} = -7.0 p.u.

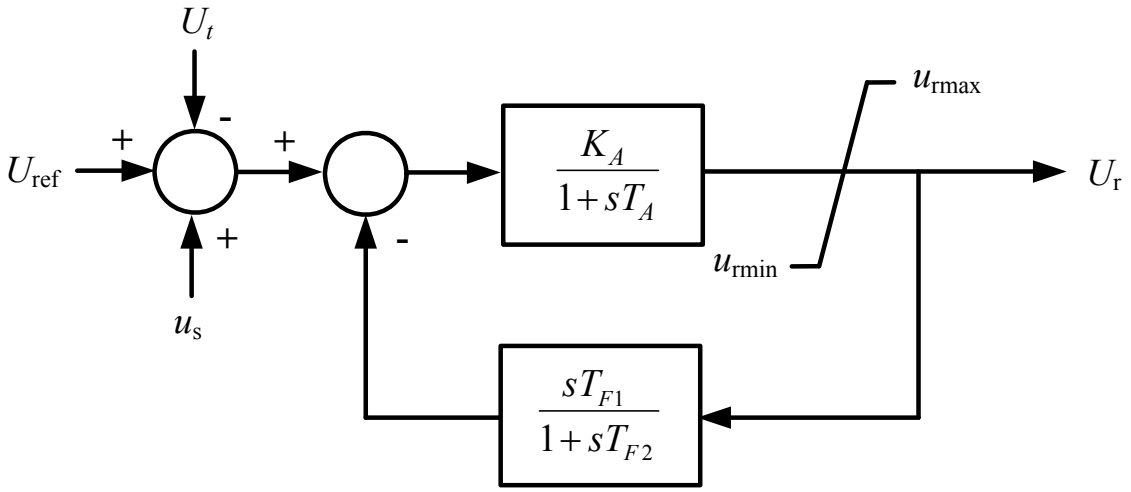

Figure A.1 Classical AVR

A.5 PSS Parameters:

T_{w1}= 0.05 s; T_{w2}= 0.1 s; T_{w3}= 0.05 s; T_{w4}= 0.01 s

A.6 Base Operating Conditions

The system is operating with generating units loaded as follows:

Generator 1 (G1):

P = 250 MW; Q = 7.57 MVAr; $\mathbf{U}_t$ = 15.75 kV $\angle$ - 23.06°

Generator 2 (G2):

P = 252.58 MW; Q = 2.83 MVAr; $\mathbf{U}_t$ = 15.75kV $\angle$ - 23.12°

Loads:

Load at bus 5: P_L = 500 MW, Q_L = 120 MVAr

Appendix B. Three-Machine, Three-Area Test System Data

Bus, line, generator and excitation data are given in this appendix.

B.1 Synchronous Machine Parameters:

Generator 1 (G1):

S_r = 6500.00 MVA; U_r = 15.75 kV; T_m = 11.00 s; r_a = 0.00 p.u.;

x_s = 0.195 p.u.; x_d = 1.880 p.u.; x_q = 1.240 p.u.; $x_d^{'}$ = 0.430 p.u.;

$x_d^{''}$ = 0.235 p.u.; $x_q^{'}$ = - ; $x_q^{''}$ = 0.27 p.u.; $T_d^{'}$ = 0.465 s; $T_d^{''}$ = 0.22 s;

$T_q^{'}$ = - ; $T_q^{''}$ = 0.288 s

Generator 2 (G2):

S_r = 6000.00 MVA; U_r = 15.75 kV; T_m = 12.50 s; r_a = 0.00 p.u.;

x_s = 0.156 p.u.; x_d = 1.97 p.u.; x_q = 1.97 p.u.; $x_d^{'}$ = 0.29 p.u.;

$x_d^{''}$ = 0.24 p.u.; $x_q^{'}$ = - ; $x_q^{''}$ = 0.28 p.u.; $T_d^{'}$ = 0.93 s; $T_d^{''}$ = 0.22 s; $T_q^{'}$ = - ;

$T_q^{''}$ = 0.289 s

Generator 3 (G3):

S_r = 5600.00 MVA; U_r = 15.75 kV; T_m = 10.00 s; r_a = 0.002 p.u.;

x_s = 0.19 p.u.; x_d = 2.49 p.u.; x_q = 2.49 p.u.; $x_d^{'}$ = 0.36 p.u.; $x_d^{''}$ = 0.24 p.u.;

$x_q^{'}$ = - ; $x_q^{''}$ = 0.28 p.u.; $T_d^{'}$ = 0.93 s; $T_d^{''}$ = 0.21 s; $T_q^{'}$ = - ; $T_q^{''}$ = 0.3 s

B.2 Transmission Line Parameters:

380 kV Double Line:

$\mathbf{Z}_{11}$= (0.0154 + j0.133) Ω/km; C_b = 0.0272 μF/km

B.3 Two Winding Transformer Parameters:

r_{ps} [%] = 0.246 ; z_{ps} [%] = 14.203

B.4 Exciter and Classical AVR (Figure A.1) Parameters:

K_A = 250; T_A = 0.22 s; T_{F1}= 0.38 s; T_{F2} = 1.84 s; u_{rmax} = 7.0 p.u.;
u_{rmin} = -7.0 p.u.

B.5 PSS Parameters:

PSS Located at Generator 2 (G2):

T_{w1}= 1.0 s; T_{w2}= 5.0 s; T_{w3}= 1.0 s; T_{w4}= 1.0 s

PSS Located at Generator 3 (G3):

T_{w1}= 1.0 s; T_{w2}= 1.0 s; T_{w3}= 1.0 s; T_{w4}= 10.0 s

B.6 Base Operating Conditions

The system is operating with generating units loaded as follows:

Generator 1 (G1):

P = 5080 MW; Q = 850.30 MVAr; $\mathbf{U}_t$ = 15.75 kV $\angle 6.679^o$

Generator 2 (G2):

P = 4725 MW; Q = 622.21 MVAr; $\mathbf{U}_t$ = 15.75kV $\angle 0.0^o$

Generator 3 (G3):

P = 4570 MW; Q = 413.80 MVAr; $\mathbf{U}_t$ = 15.75kV $\angle 4.567^o$

Loads:

Load at bus 4: P_L = 5000 MW, Q_L = 500 MVAr

Load at bus 5: P_L = 1050 MW, Q_L = 300 MVAr

Load at bus 6: P_L = 4500 MW, Q_L = 500 MVAr

Load at bus 7: P_L = 3800 MW, Q_L = 600 MVAr

References

[1] P. Kundur, *Power System Stability and Control*, McGraw-Hill, 1994.

[2] Kamwa, R. Grondin and Y. Hebert, "Wide-area measurement based stabilizing control of large power system-a decentralized/hierarchical approach," *IEEE Transaction on Power Systems*, vol. 16, no. 1, pp. 136-153, Feb. 2001.

[3] Kamwa, L. Gérin Lajoie, "State-space system identification-toward MIMO models for modal analysis and optimization of bulk power systems," *IEEE Trans. on Power Systems*, vol. 15, no. 1, pp. 326-335, Feb. 2000.

[4] C. W. Taylor, D. C. Erickson, K. E. Martin, R. E. Wilson and V. Venkatasubramanian, "WACS-wide area stability and voltage control system: R & D and Online Demonstartion," *Proceedings of IEEE*, vol. 93, no. 5, pp. 892-906, May 2005.

[5] J. F. Hauer, W. A. Mittelstadt, R. Adapa, W. H. Litzenberger, and M. K. Donnelly, "Chapter 11: Power System Dynamics and Stability. Section 8: Direct Analysis of Wide Area Dynamics," *CRC Electric Power Engineering Handbook* (L. L. Grigsby ed.), CRC Press, and IEEE press, Boca Raton, FL, 2001, pp. 11-82 through 11-120.

[6] N. Martins, A. A. Barbosa, J. C. R. Feraz, M. G. dos Santos, A. L. B. Bergarno, C. S. Yung, V. R. Oliveria, N. J. P. Macedo, "Retuning the stabilizers for the North-South Brazilian Interconnection," *IEEE PES summer Meeting*, Vol.1, pp. 58-67, 18-22 July 1999.

[7] H. Breulmann, E. Grebe, M. Lösing, W. Winter, R. Witzmann, P. Dupuis, M. P. Houry, T. Margotin, J. Zerenyi, J. Dudzik, J. Machowski, L. Martin, J. M. Rodriguez, E. Urretavizcaya, "Analysis and Damping of Inter-Area Oscillations in the UCTE/CENTREL Power System," *CIGRE*, pp. 38-113, Paris, 2000.

[8] U.S.-Canada Power System Outage Task Force, Final Report on the August 14, 2003 Blackout in the United States and Canada (on line): http://www.pserc.wisc.edu/BlackoutFinal-Web.pdf

[9] Aaron F. Snyder, Dan Ivanescu, Nouredine HadjSaid, Didier Geroges and Thibault Margotin, "Delay-input Wide-area Stability Control with Synchronized Phasor Measurements," *Proceedings of IEEE PES Summer Meeting,* vol. 2, pp. 1009-1014, 2000.

[10] G. T. Heydt, C. C. Liu, A. G. Phadke, and V. Vittal, "Solutions for the crisis in electric power supply," *IEEE. Computer Applications in Power*, vol. 14, Issue 3, pp. 22-30, July 2001.

[11] M. E. Aboul-Ela, A. A. Sallam, J. D. McCalley and A. A. Fouad, "Damping controller design for power system oscillations using global signals," *IEEE Transactions on Power Systems*, vol. 11, pp. 767-773, May 1996.

[12] U. Bachmann, I. Erlich, "Untersuchung von Netzpendelungen mittels Modalanalyse," 4. *Tagung Netzregelung,* Berlin, Germany, VDI-Berichte 1329, pp. 85-99, 1997.

[13] F. P. DeMello and C. Concordia, "Concepts of synchronous machine stability as affected by excitation control," *IEEE Transactions on Power Apparatus and Systems*, vol. PAS-88, pp. 316-329, April 1969.

[14] E. V. Larsen, D. A. Swann, "Applying Power System Stabilizers,parts I-III," *IEEE Trans. on Power Apparatus and Systems*, vol. PAS-100, pp. 3017-3046, 1981.

[15] E. V. Larsen and D. A. Swann, "Applying power system stabilizers part-i: General concepts," *IEEE Trans. on Power Apparatus and Systems*, vol. PAS-100, no. 6, pp. 3017-3024, June 1981.

[16] E. V. Larsen and D. A. Swann, "Applying power system stabilizers part-ii: General concepts," *IEEE Trans. on Power Apparatus and Systems*, vol. PAS-100, no. 6, pp. 3025-3033, June 1981.

[17] K. Zhou, J. C. Doyle, "*Essentials of robust control*", Prentice Hall, 1998.

[18] Sigurd Skogestad, Ian Postlethwaite, *Multivariable feedback control*, Willey, 2005.

[19] M. E. Aboul-Ela, A. A. Fouad, J. D. McCalley, A. A. Sallam, "Damping Controller Design for Power System Oscillations using Global Signals," *IEEE Trans. on Power Systems*, vol. 11, pp. 767 - 773, May 1996.

[20] C. P. Steinmetz, "Power control and stability of electric generating stations," *AIEE Trans.*, vol. XXXIX, Part II, pp. 1215–1287, July 1920.

[21] AIEE Subcommittee on Interconnections and Stability Factors, "First report of power system stability," *AIEE Trans.*, pp. 51-80, 1926.

[22] G. S. Vassell, "Northeast blackout of 1965," *IEEE Power Engineering Review*, pp. 4-8, Jan. 1991.

[23] P. Kundur, J. Paserba, et al., "Definition and Classification of Power System Stability," *IEEE Transactions on Power Systems*, vol. 19, no.2. May 2004, pp. 1387-1401.

[24] CIGRE Task Force 38.01.07 on Power System Oscillations, "Analysis and control of power system oscillations," *CIGRE Technical Brochure*, no. 111, Dec. 1996.

[25] IEEE PES Working Group on System Oscillations, "Power System Oscillations," *IEEE Special Publication 95-TP-101*, 1995.

[26] J. Bucciero, and M. Terbrueggen, "Interconnected power systems dynamic tutorial," *Electric Power Research Institute Tutorial TR-107726-R1*, 1998.

[27] T. Van Cutsem and C. Vournas, *Voltage Stability of Electric Power Systems*, Norwell, MA: Kluwer, 1998.

[28] CIGRE Task Force 38.02.14 Rep., Analysis and Modeling Needs of Power Systems Under Major Frequency Disturbances, Jan. 1999.

[29] P. Kundur, D. C. Lee, J. P. Bayne, and P. L. Dandeno, "Impact of turbine generator controls on unit performance under system disturbance conditions," *IEEE Trans. Power Apparatus and Systems*, vol. PAS-104, pp. 1262-1267, June 1985.

[30] Q. B. Chow, P. Kundur, P. N. Acchione, and B. Lautsch, "Improving nuclear generating station response for electrical grid islanding," *IEEE Trans. Energy Conversion*, vol. EC-4, pp. 406–413, Sept. 1989.

[31] P. Kundur, "A survey of utility experiences with power plant response during partial load rejections and system disturbances," *IEEE Transaction Power Apparatus and Systems*, vol. PAS-100, pp. 2471–2475, May 1981.

[32] F. Aboytes, F. Sanchez, A. I. Murcia Cabra, and J. E. Gomez Castro, "Dynamic stability analysis of the interconnected Colombia-Venezuela Power System", *IEEE Transactions on Power Systems*, vol. 15, no. 1, Feb. 2000, pp. 376-381.

[33] G. C. verghese, I. J. Perez-Arriaga, and F. C. Schweppe, "Selective modal analysis with application to electric power systems, Part I: Heuristic Introduction, Part II: The dynamic stability problem," *IEEE Trans*., vol., PAS-101,No. 9, pp. 3117-3134, September 1982.

[34] I. Erlich, *Analyse und Simulation des dynamischen Verhaltens von Elektro energiesystemen*, Habilitation Dissertation, Technical University of Dresden, 1995.

[35] I. Erlich, H. Pundt and S. Djumenta, "A new synchronous generator model for power system stability analysis," *12th PSCC Proceedings*, vol.2, Dresden, Germany, pp.1062 - 1068, 1996, August 19-23.

[36] J. H. Chow (ed), *Time-Scale modelling of dynamic networks with applications to power systems*, vol. 46, Springer-Verlag, NY, 1982.

[37] P. Kokotovic, H. K. Khalil and J. O'Reilly, *Singular perturbation methods in control: analysis and design*, Orland, FL Academic Press, 1986.

[38] J. H. Chow, J. R. Winkelman, M. A. Pai and P. Sauer, "Application of singular perturbations theory to power system modelling and stability analysis," *Proc. Am. Control Conf*., 1985.

[39] G. K. Befekadu, *Robust Decentralized Control of Power Systems: A Matrix Inequalities Approach*, Dissertation, University Duisburg-Essen, 2006.

[40] G. K. Befekadu and I. Erlich, "Robust Decentralized Controller Design for Power Systems Using Matrix Inequalities Approaches," *IEEE Power Engineering Society General Meeting*, Conference Proceedings, Montreal, QC, Canada, June 18-22, 2006.

[41] S. H. Wang and E. J. Davidson, "On stabilization of decentralized control systems," *IEEE Transactions on Automatic Control*, vol. 18, no. 5, pp. 473-478, 1973.

[42] P. Gahinet and P. Apkarian, "A linear matrix inequality approach to H_∞ control," *International Journal of Robust and Nonlinear control*, vol. 4, pp. 421-448, 1994.

[43] P. Gahinet, *Reliable computation of H_∞ central controllers near the optimum*, Research report of Institut National de Recherche en Informatique et en Automatique (INRIA), France, pp. 1-16, 1992.

[44] H. Cabannes, *Pade approximations method and its applications to mechanics*, Springer-Verlag, New York, 1976.

[45] V. B. Kolmanovskii, S. I. Niculescu, and K. Gu, "Delay effects on stability: a survey," *38th IEEE Conference on Decision and Control*, pp. 1993-1998, 1999.

[46] Wu Hongxia, Ni Hui, and G. T. Heydt, "The impact of time delay on robust control design in power systems," *IEEE Power Engineering Society Winter Meeting,* vol. 2, pp. 1511-1516, 2002.

[47] '*Cluster Analysis*', in 'IMSL Fortran 90 MP Library Help, Stat/Library', (Visual Numerics, Inc., volume 2)

[48] J. C. C. De Castro, ,and S. De Araujo, "Frequency domain analysis of oscillatory modes in decentralized control systems," *Automatica*, vol, 34, pp. 1647-1649, December 1998.

[49] E. Z. Zhou, O. P Malik, and G. S. Hope, "Theory and Method for Selection of Power System Stabilizer Location," *IEEE Transactions on Energy Conversion*, vol. 6, no. 1, pp. 170-176, March 1991.

[50] H. F. Wang, F. J. Swift, and M. Li, "Indices for selecting the best location of PSSs or FACTS-based stabilisers in multi-machine power systems: a comparative study," *IEE Proceedings Generation, Transmission and Distribution,* vol. 144, no. 2, pp. 155-159, March 1997.

[51] Morten Hovd, and Sigurd Skogestad, "Sequential design of decentralized controllers," *Automatica*, vol. 30, no. 10, pp. 1601-1607, 1994.

[52] T. C. Yang, "Applying a sequential loop-closure method to power system stabilizer design," *Control Eng. Practice*, vol. 4, no. 10, pp. 1371-1380, 1996.

[53] M. S. Chiu, and Y. Arkun, "A methodology for sequential design of robust decentralized control systems," *Automatica*, vol. 28, no. 5, pp. 997-1001, 1992.

[54] G. Amico, R. Molina, and V. Sinagra, "Rules for determining transmission limits in the power grid of Argentina," *Proceedings of the CIGRE* XII Iberian-American Regional Meeting, 2007.

[55] P. Kundur, at all, *Investigation of Low Frequency Inter-Area Oscillation Problems in Large Interconnected Power Systems*, Canadian Electrical Association Report, CEA 294 T 622, Dec. 1993.

[56] C. E. Grund, J. J. Paserba, J. F. Hauer, S. Nilsson, "Comparison of Prony Analysis and Eigenanalysis for Power System Control Design," *IEEE Trans.,* PWRS- vol. 8, no. 3, pp. 964-971, August 1993.

[57] S. P. Teeuwsen, I. Erlich, M. A. El-Sharkawi, "Neural Network based Classification Method for Small-Signal Stability Assessment," *IEEE PowerTech*, Bologna, Italy, June, 2003.

[58] S. P. Teeuwsen, I. Erlich, M. A. El-Sharkawi, and U. Bachmann, "Genetic Algorithm and Decision Tree based Oscillatory Stability Assessment," *IEEE PowerTech*, Bologna, Italy, June, 2003.

Acronyms

ARE	Algebraic Ricatti Equation
AVR	Automatic Voltage Regulator
cd	constant delay
DD	Different Delays
df	delay free
LFT	Linear Fractional Transformation
MD	Mean Delay
MIMO	Multi-Input, Multi-Output
MISO	Multi-Input, Single-Output
PMU	Phasor Measurement Unit
PSS	Power System Stabilizer
WAM	Wide Area Measurement
PSD	Power System Dynamics
FACTS	Flexible AC Transmission Systems
SVC	Static Var Compensators
ud	uncertain delay

Curriculum Vitae

Personal Data:

Name Ashfaque Ahmed Hashmani

Nationality Pakistani

Date of birth September 15, 1968

Working Experience:

2004-To date
Assistant Professor
Department of Electrical Engineering
Mehran University of Engg. & Tech. (M.U.E.T.)
Jamshoro-Sindh, Pakistan

1996-2004
Lecturer
Department of Electrical Engineering
Mehran University of Engg. & Tech. (M.U.E.T.)
Jamshoro-Sindh, Pakistan

1993-1996
Assistant Lecturer
Department of Electrical Engineering
Mehran University of Engg. & Tech. (M.U.E.T.)
Jamshoro-Sindh, Pakistan

Education and Qualifications:

2006-2010
Dr. Ing. degree in Electrical Engineering,
Institute of Electrical Power Systems (EAN)
University of Duisburg-Essen, Germany
Dissertation: "Damping of Electromechanical Oscillations in Power Systems using Wide Area Control"

1999-2000
M. E. degree in Electrical Engineering,
Division of Power Engineering,
Nanyang Technological University, Singapore

	Dissertation: "A Nonlinear Coordinated Excitation and TCPS Controller for Transient Stability Enhancement in Power Systems"
1987-1993	B. E. degree in Electrical Engineering, Department of Electrical Engineering, Mehran University of Engg. & Tech. (M.U.E.T.) Jamshoro-Sindh, Pakistan
1984-1986	Higher Secondary Certificate Examination (Intermediate) of the Board of Intermediate & Secondary Education, Hyderabad-Sindh, Pakistan Government Muslim Science College, Hyderabad-Sindh, Pakistan
1980-1984	Secondary School Certificate Examination of the Board of Intermediate & Secondary Education, Hyderabad-Sindh, Pakistan Government High School, Matiari-Sindh, Pakistan
1976-1980	Primary School Certificate Government Nationalized Primary Muslim School, Matiari-Sindh, Pakistan

List of Publications

Journal Papers

[1] Ashfaque A. Hashmani, I. Erlich, "Mode selective damping of power system electromechanical oscillations using supplementary remote signals," *IET Generation, Transmission & Distribution*, UK, accepted for publication.

[2] Ashfaque A. Hashmani, I. Erlich, "Mode selective damping of power system electromechanical oscillations for large power systems using supplementary remote signals," *International Journal of Electrical Power and Energy Systems*, UK, submitted for publication.

[3] Ashfaque Ahmed Hashmani, Muhammad Aslam Uqaili and Muhammad Rafique Abro, "A Thyristor Controlled Phase Shifter Controller for Transient Stability Enhancement in Power Systems," *Mehran University Research Journal of Engineering and Technology*, Pakistan, vol. 24, no. 2 pp. 169- 174, April 2005.

[4] Ashfaque Ahmed Hashmani, Youyi Wang and Tek Tjing, "Design and Application of A Nonlinear Coordinated Excitation and TCPS Controller in Power Systems," *International Journal of Control, Automation, and Systems*, Korea, vol. 3, no. 2, pp. 346-354, June 2005.

[5] Ashfaque A. Hashmani, Youyi Wang and T. T. Lie, "Enhancement of Power System Transient Stability Using A Nonlinear Coordinated Excitation and TCPS Controller," *International Journal of Electrical Power and Energy Systems*, UK, vol. 24, no. 3, pp. 201-214, 2002.

[6] Y. Wang, Ashfaque A. Hashmani and T. T. Lie, "A Nonlinear Coordinated Excitation and TCPS Controller for Multimachine Power System Transient Stability Enhancement," *Institution of Electrical Engineers (IEE) Proceedings-Generation, Transmission, and Distribution*, UK, vol. 148, no. 2, pp. 133-141, 2001.

Conference Proceedings

[1] A. A. Hashmani, I. Erlich, "Delayed-input power system stabilizer using supplementary remote signals," *Proceedings of International Federation of Automatic Control* (*IFAC*) *Symposium on Power Plants and Power Systems Control* (*PP & PSC),* Tampere, Finland, 05-08 July 2009.

[2] A. A. Hashmani, I. Erlich, "Power system stabilizer by using supplementary remote signals," *Proceedings of 16th PSCC,* Glasgow, paper No. 131, 14-18 July 2008.

[3] Ashfaque A. Hashmani, Y. Wang and T. T. Lie, "Design of A Nonlinear Coordinated Excitation and TCPS Controller for Transient Stability Enhancement in Power Systems," *Proceedings of International Power Engineering Conference* (*IPEC*), Singapore, vol. 2, pp. 483-488, 17-19 May 2001.

[4] Y. Wang, Ashfaque A. Hashmani and T. T. Lie, "A Nonlinear Coordinated Excitation and TCPS Controller for Transient Stability Enhancement in Power Systems," *Proceedings of AUPEC Conference on Innovation for Secure Power*, Brisbane, Australia, pp. 9-14, September 2000.